SNC·LAVALIN

TECHNICAL JOURNAL

Engineering excellence around the globe

Volume 4 | Issue 2 | 2022

SNC·LAVALIN

CHRIS HENDY

Editor-in-Chief SNC-Lavalin Technical Journal

Atkins Fellow, Professional Head of Bridge Engineering and Transportation Technical Director, Engineering Services

Foreword

Welcome to the eighth edition of our SNC-Lavalin Technical Journal, established to showcase the fantastic depth and breadth of our engineering expertise across a wide range of disciplines and domains and to demonstrate that technical excellence is at the heart of everything we do. This edition highlights the impressive work we have been doing preserving the environment and reducing the carbon impact of new and existing infrastructure whilst adapting for climate resilience and designing new signature infrastructure.

In preserving our environment, we have addressed propeller scar impacts in St. Joseph Bay Aquatic Preserve (AP) in the Florida panhandle using high resolution aerial imagery to target restoration. Through our City Simulator resilience modelling tool and a connected digital twin, we have also helped the North Carolina Department of Transportation (NCDOT) assess vulnerabilities to flood, travel, heat impact, economics, asset lifecycle maintenance, and sea level rise along the 190-mile US74 corridor. We have also led ice river management at Muskrat Falls, mitigating the risk of flooding from high backwater levels. And we have conducted ground investigation (GI) and installed monitoring equipment for a culvert to understand the cause of settlement and produced recommendations for improved backfill selection for future culvert design.

In tackling climate change, we have used the Atkins Rail Carbon Tool and the principles of PAS 2080 to make recommendations for reducing the whole life impact of rail schemes, citing the Soham Station Redevelopment case study as an example. We have also carried out a feasibility study for hydrogen-based low carbon steel production which proposes transition from hydrogen production from natural gas combustion to a green hydrogen supply system based on electrolysis with a power supply mix of renewables and nuclear energy.

In assuring rail safety, we have simulated the performance of new rolling stock to inform quantitative risk assessments looking at the probability and magnitude of “hyper-acceleration” events and we have produced recommendations for the upgrading of existing buffer stops.

Finally, as an example of balancing optimal use of materials with demanding aesthetic requirements of a truly signature project, we have carried out the design and construction supervision of the marina cable stayed foot bridge (FB01) as part of the Port City Colombo development in Sri Lanka.

The above examples provide only a small insight into the wealth of innovation that SNC-Lavalin creates day to day.

I hope you enjoy the selection of technical papers included in this edition as much as we have enjoyed compiling them.

Editor-in-chief

Chris Hendy
FREng MA (Cantab)
CEng FICE Eur Ing
Technical Director,
Atkins Fellow, Professional
Head of Bridge Engineering
Engineering Services
– Transportation UK
Epsom, UK

2022 Editorial Board Members

Ramy Azar
PhD Ing.
Vice-President, Engineering & Chief Technology Officer – Power Grids
Engineering Services Canada
– Power & Renewables
Montreal, Canada

Vinod Batta
PhD P.Eng.
Vice President & General Manager, Power Solutions - Western Canada
Chief Technical Officer - Hydro
Engineering Services Canada
– Power & Renewables
Vancouver, Canada

Donna Huey
GISP
Atkins Fellow & Sr. Vice President, Chief Digital Officer
Engineering Services USA
– Business Development, Digital
Orlando, FL, USA

Jill Hayden
PhD FIET
Technical Director, Atkins Fellow (Intelligent Mobility & Smart Technologies)
Engineering Services
– Transportation UK
Manchester, UK

Tracey Radford
BSc MSc CGeol FGS
Practice Manager, Geotech Network Chair
Engineering Services
– Infrastructure UK
Epsom, UK

Dr. Santhosh Kumar M
PhD CEng MIET
Technical Director, GDC and Atkins Fellow of Digital
Engineering Services – Global Technology Center
Bangalore, India

Production Team

Dorothy Gartner
MLIS
Librarian
Project Performance
and Risk Oversight
Montreal, Canada

Samantha Morley
CAPM
Project Controls Analyst I
Engineering Services USA
– Operational Services
Omaha, NE, USA

Cheryl Law
MEng CEng MICE
Associate Director
Engineering Services
– Infrastructure UK
Epsom, UK

2022 Editorial Board Members

Dr. Navil Shetty
PhD DIC FIAM
Atkins Fellow and Technical Chair for Asset Management
Leader, Centre of Excellence for Asset Management & Operations (AMOCE)
Bangalore, India

Patrick Sikka
P.Eng.
Vice-President
Engineering Services - Mining & Metallurgy – North America
Toronto, Canada

Richard Moura
P.Eng.
Vice-President,
Major Projects O&M
Capital and O&M
Toronto, Canada

Tim Milner
CSci CChem MRSC
Atkins Fellow and Chief Technology Officer
Nuclear
Columbia, SC, USA

Roger Cruickshank
BEng
Senior Director, Strategic Transport Planning, Atkins Fellow
Engineering, Design and Consultancy Services
Engineering Services – Middle East
Dubai, UAE

Kan Pang
BEng CEng
Senior Technical Director
Engineering
Services Asia – Transportation
Hong Kong, China

Samuel Fradd
Technology Manager
Engineering Services
– Transportation UK
Epsom, UK

About the Cover

Completed marina cable stayed foot bridge (FB01) as part of the Port City Colombo development in Sri Lanka

Contents

David Loy
Sr Scientist II
Engineering Services – TPO EcoSciences
Tampa, FL, USA

Renee Price
Sr Scientist I
Engineering Services – TPO EcoSciences
Tampa, FL, USA

Donald Deis
Principal Technical Professional
Engineering Services – TPO Sciences
Melbourne, FL, USA

Shayne Paynter
Sr Technical Manager I
Engineering Services – TPO Water
Tampa, FL, USA

Jonathan Brucker
Florida Department of Environmental Protection Central Panhandle Aquatic Preserves
Eastpoint, FL, USA

Scott Zengel
Research Planning Inc.
Columbia, SC, USA

01: St. Joseph Bay Seagrass Restoration: Drone Guided Seagrass Restoration Planning and Implementation in St. Joseph Bay Aquatic Preserve, Florida

Abstract

Recreational boating in turtle-grass *(Thalassia testudinum)* dominant bays has resulted in high density areas of propeller scarring, potentially compromising marine habitat and ecosystem services. Given turtle-grass growth habits, recruitment of substantial prop scars may take up to 10 years to reach normal density. Assessment by aerial photointerpretation coupled with installation of biodegradable sediment tubes can facilitate restoration of impacted turtle-grass beds. Atkins teamed with the Florida Department of Environmental Protection (FDEP) Central Panhandle Aquatic Preserve staff to complete a multi-phase restoration project to assess, map, quantify sediment loss, and develop/implement a restoration strategy to address propeller scar impacts in St. Joseph Bay Aquatic Preserve (AP) in the Florida panhandle. Prop scar assessment was based on high resolution aerial imagery of seagrass beds within the AP acquired by small Unmanned Aerial Vehicles (UAVs). Resultant imagery was analyzed with photointerpretation and semi-automated feature extraction software to create prop scar maps that were verified by extensive field-based signature development, ground control, and spatial and thematic assessment. Hot spot analysis, quantification, and classification results were utilized to identify areas of the highest scarring density for potential restoration. Analyses identified 789 potential candidate scars totaling 1 hectare within 11 targeted areas located in the AP. The AP restoration concluded with deployment of 43,954 sediment tubes in 379 prop scars, equating to nearly 40 kilometers or 0.8 hectare of restored prop scars.

KEYWORDS
Seagrass restoration; Marine habitat; Propeller scarring; Aerial photointerpretation; Sediment tubes

1. Introduction

Seagrasses (submerged flowering plants) form extensive meadows in shallow coastal waters worldwide, providing important ecosystem services such as shoreline stabilization, maintenance of water quality and provision of food and habitat to many marine organisms (Barbier et al., 2011; Lefcheck et al., 2019). Despite growing recognition of the global importance of these coastal ecosystems, particularly as a major carbon sink (Prentice et al., 2019; Berger et al., 2020), seagrasses are in global decline due to stressors such as increased sediment loading, coastal eutrophication, mechanical disturbance, and climate change (Orth et al., 2006; Waycott et al., 2009; Unsworth et al., 2019). With 40% of the world's human population living in coastal areas, the magnitude of human pressure on seagrasses is increasing. Coastal development and nutrient enrichment have historically been responsible for global seagrass declines (Fraser and Kendrick, 2017), as shown by a 29% global loss in seagrass coverage since the 1980s (Waycott et al., 2009; Short et al., 2011), and seagrasses continue to be lost at a rate of 1.4% per year (Short et al., 2011).

In Florida, eutrophication has been linked to an increase in anthropogenic disturbances to seagrass meadows (Tomasko et al. 2005) and seagrasses there remain vulnerable to nuisance algal blooms that reduce light availability (Han et al., 2016; Hughes et al., 2018; Rasmusson et al., 2020). Additionally, physical factors such as substratum, wave scour, and biological interactions such as grazing by herbivores influence the growth and distribution of seagrass in Florida. This habitat degradation in Florida has many sources (e.g., pollution, dredge and fill), but an increasingly common cause of habitat degradation is the scarring of seagrasses (Sargent, et al. 1995). Seagrass beds can be scarred by many activities, but scars are most commonly made when a boat's propeller tears and cuts up roots, stems, and leaves of seagrasses, producing a long, narrow furrow devoid of seagrasses. Boats operating in shallow waters are severely scarring, and sometimes completely denuding, seagrass beds throughout the state (Sargent, et al. 1995).

St. Joseph Bay Aquatic Preserve in Port St. Joe, Florida is one area that has experienced extensive propeller scarring due, in part, to high levels of recreational boating traffic and relatively shallow depths. Seagrass injuries from propeller damage can result from a combination of impacts including but not limited to propeller scars, berms, and blowholes (Sargent et al. 1995, Uhrin et al. 2011). Propeller scars are formed by the dredging effect of the turning propeller as a boat travels over a shallow seagrass bed.

The severity (width and depth) of propeller scars varies depending on many factors including the size of the vessel, the extent to which the propeller is forced into the seagrass bed, and the depth of the water column at the time of impact. A widely accepted seagrass stabilization technique involves the placement of biodegradable fabric mesh tubes filled with sand (sediment tubes) inside of the propeller scar trench (Hall et al. 2006). Sediment tubes have been identified as being effective in reducing erosion rates in propeller scar injuries while supporting conditions suitable for natural re-colonization of the injured area by neighboring seagrasses through filling in with growth across the scar.

Propeller scar damage assessment and restoration of excavated sediments in seagrass beds has eclipsed the "research" phase (McNeese et al. 2006). Members of the Atkins team have executed projects throughout Florida generally following the methods and protocols developed by the National Oceanic Atmospheric Administration (NOAA) and the State of Florida (Kenworthy et al. 2018). The prolific vegetative growth pattern and high rates of asexual reproduction of *Halodule wrightii* allows the apical meristems, rhizomes and roots to rapidly recolonize propeller scars if there are no additional severe disturbances (e.g., a hurricane, see Kenworthy et al. 2002, Whitfield et al. 2002). Our work throughout Florida has shown that propeller-scarring in areas with pioneering species such as *H. wrightii,* and even *Syringodium filiforme,* recover quickly if scarring is not severe (i.e., if deep, long scars and blow-outs are not present) (Kenworthy et al. 2002). However, recovery of *Thalassia testudinum* can require 5 to over 10 years (Kenworthy et al. 2002, Uhrin et al. 2011).

The shallow bathymetric conditions in St. Joseph Bay in conjunction with a dramatic tide cycle create susceptible conditions for scarring, resulting in numerous unintended propeller scars throughout the *T. testudinum* seagrass beds in the Aquatic Preserve (AP). To resolve, Atkins partnered with the Florida Department of Environmental Protection (FDEP) and designed and implemented a sediment tube-based seagrass restoration effort in the AP located in Gulf County in the northern panhandle of Florida (Figures 1 and 2).

FIGURE 1

Project location map

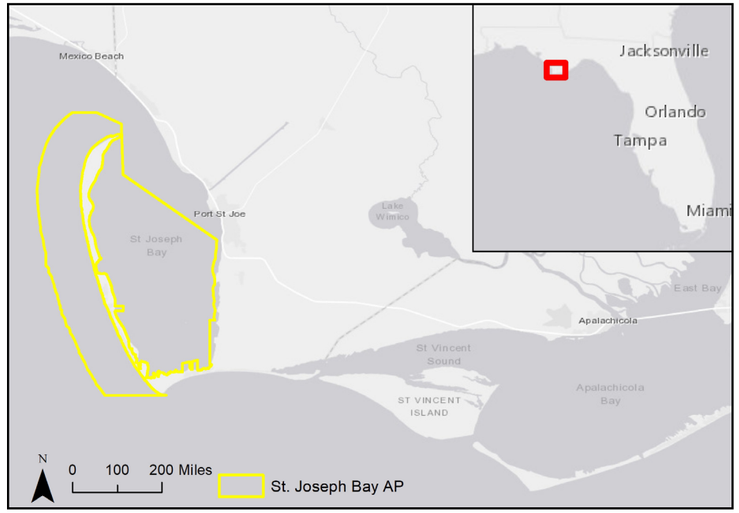

FIGURE 2

Representative propeller scar within *Thalassia testudinum* meadow with newly installed sediment tube (left) and one year post-installation with recruitment (right)

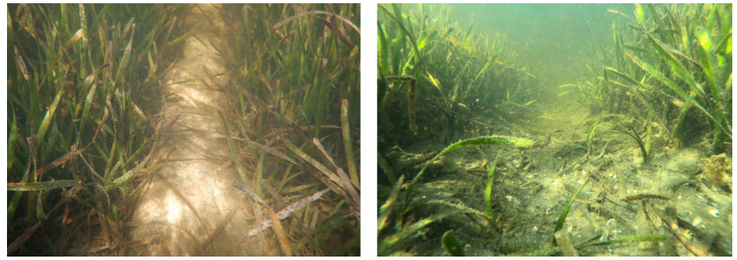

The AP is 222 square kilometers of state-owned sovereign submerged lands and is bounded to the east by Port St. Joe and the St. Joseph Bay Buffer Preserve and to the west by St. Joseph Peninsula (FDEP 2022). The seagrass meadows within the AP are of the most diverse and abundant in north Florida and are a popular destination for tourists and recreational fishers.

The objective of this project was to restore 0.8 hectares or approximately 40 kilometers (km) of propeller scars within *T. testudinum* meadows of the AP. Specifically, our goals were to:

1. Assess, map, and quantify seagrass loss in areas where propeller scar damage from boating traffic has occurred in seagrass habitat;
2. Design a restoration plan tailored to the unique needs and conditions of the AP; and
3. Implement seagrass restoration of 0.8 hectares of propeller scars.

2. Methods

2.1. MAPPING AND QUANTIFICATION EFFORT

2.1.1 AERIAL IMAGERY COLLECTION

Surveying and Mapping, LLC (SAM) was contracted by FDEP to provide Small Unmanned Aerial Vehicle (sUAV) services for the purpose of developing high resolution aerial photographs of potential seagrass restoration areas in St. Joseph Bay AP. The sUAV system utilized the BirdseyeView Aerobotics FireFly6 Pro carrying a Sony α6000 Digital Single Lens Reflex camera with a 24.3-megapixel sensor and a fixed 16-millimeter (mm) lens and was paired with FireFly Planner for mission control. The resulting orthophotos were used in support of seagrass propeller scarring identification and mapping.

2.1.2 IMAGERY ANALYSIS, MAPPING, AND QUANTIFICATION

Aerial imagery acquired by SAM and publicly available aerial imagery were reviewed to identify areas of potential propeller scarring. To initiate assessment of propeller scars in St. Joseph Bay AP, three categories of impact were defined:

- Type I damage: Scarring in which propeller damage is limited to the partial loss of shoot biomass (e.g. trimming), without impacts to the rhizosphere or surrounding sediment;
- Type II damage: Scarring with complete loss of above ground biomass and little to no damage to the rhizosphere; and
- Type III damage: Scarring with complete loss of seagrass and loss of sediment below the rhizosphere, including removal of the rhizosphere.

Aerial desktop analysis perspective revealed that Type I and Type II damages can be similarly represented and therefore, were typically lumped together. Type III damage was a more defined aerial signature with an exposed estuarine sediment characteristic.

To create draft propeller scar coverage, ESRI's ArcGIS spatial statistics toolset and a combination of geoprocessing tools was used to distinguish areas of significant clustering of prop scars (Figure 3).

One-acre polygonal grid cells were created across the project area. A spatial join was then performed between the grid cells and the prop scar occurrences to count the number of scars in each grid cell, which became the analysis features.

The scar count was used as the analysis field in the spatial statistic. Grid cells with a count of 0 were clipped out prior to further analysis. The Getis-Ord Gi* spatial statistics tool in the Mapping Clusters toolset was utilized to quantify prop scar hot spots centered on moderate or high intensity scarred areas. The hot spots were used to generate areas of interest, referred to as potential seagrass restoration areas (PSR's) polygons, for subsequent ground truthing and signature development. PSR's and their corresponding mapped propeller scars were loaded into a handheld GPS unit with sub-meter spatial capabilities for navigation during latter ground-truthing and potential signature development efforts.

FIGURE 3

Aerial interpreted propeller scars and PSRs in St. Joseph AP

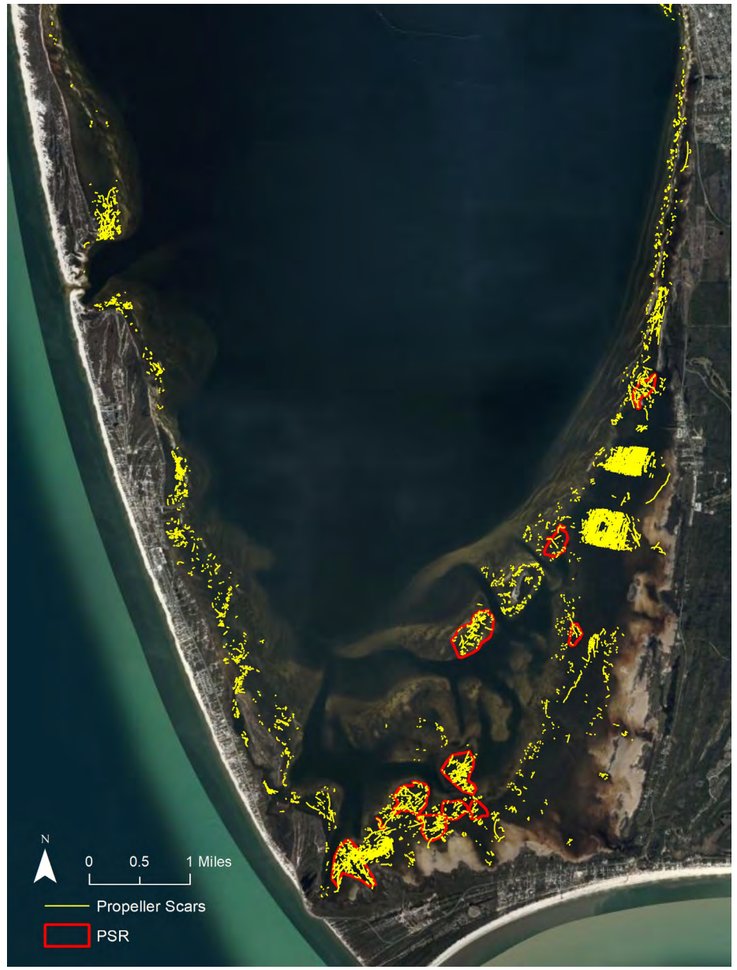

2.1.3 GROUND TRUTHING

In some cases, tidal currents can interact with large seagrass canopy heights to produce seemingly linear features in undisturbed seagrass beds. Such hydrodynamically induced patterns can be misinterpreted during analysis of the aerial images. Epiphytic loads (including cyanobacteria) and species composition of seagrass can also create a mosaic of spectral differences that mimic propeller scarring. To address potential misinterpretations, the total number of mapped propeller scars were randomly subset for field verification using ESRI ArcGIS software random point generator. Field verification of the propeller scars identified in the mapping effort was accomplished using the results of the aerial image analyses and guided by Trimble Geo-XT 6000 series handheld GPS units. Accuracy of each randomly selected mapped scar was assessed on two fronts:

1. Spatial accuracy, which included whether the length and orientation of the propeller scar was accurately delineated using the high-resolution aerial imagery; and
2. Thematic accuracy, which included determining whether the feature was accurately classified as a propeller scar in-lieu of other confounding features (potential sources of error).

Following the systematic assessment, mapping, and ground-truthing of prop scars throughout the St. Joseph Bay AP, quantification of the scars and associated scar area was performed (Sargent et al. 1995, Fonseca et al. 1998). Once these polygons were established for the areas of intersecting prop scars, the intensity of scarring for each polygon was categorized based on the Comparison Chart for Visual Estimation of Percent Composition (Sargent et al. 1995, Figure 4). According to this methodology, polygons designated as light intensity were areas where less than 5 percent of the seagrasses were scarred, moderate polygons contained areas with from 5 percent to 20 percent scarring, and severe polygons delineated areas with more than 20 percent scarring.

FIGURE 4

Diagram representative of categories of propeller scarring intensity (Sargent et al., 1995)

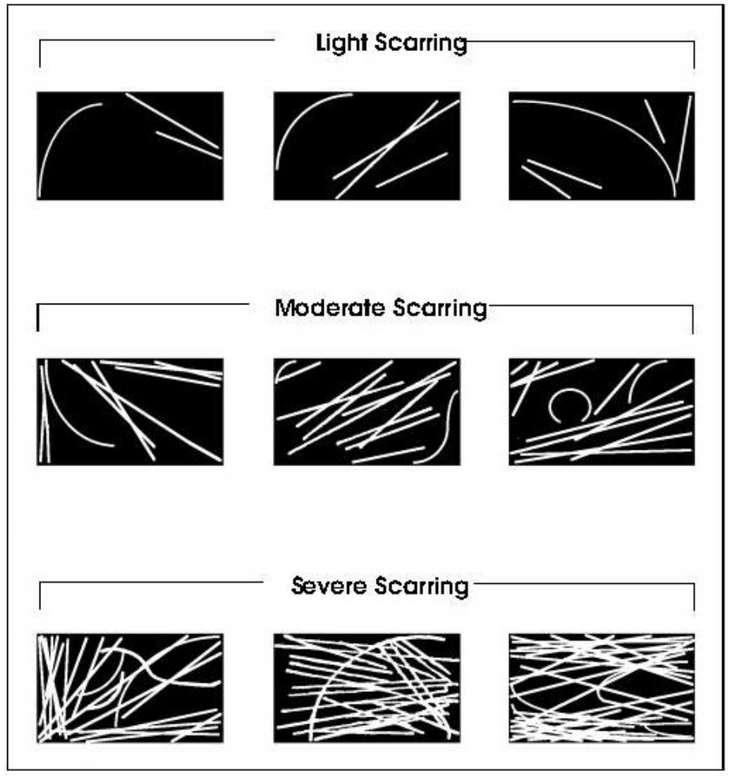

2.2 RESTORATION PLAN

2.2.1 IN-SITU DATA COLLECTION

In-situ data were collected from a stratified random subset of 10% of the total ground-truthed scars to characterize the various areas of scarring and determine ultimately what PSRs and associated scars were conducive to restoration. Atkins scientists navigated to each subset area using a Trimble R1 GPs receiver with submeter accuracy and ESRI Collector. The high aerial imagery resolution allowed scientists to navigate to individual mapped scars and verify their presence and suitability for restoration. Once the PSRs and individual scars of interest were identified, measurements were taken of water depth, scar depth and scar width.

Representative sediment cores were collected within the northernmost PSR (PSR 1), a central-southern PSR (PSR9), and the PSR in the southern-most extent of the restoration area (PSR 11).

Cores were taken from depths that included both the surficial sediments as well as sediments below the rhizosphere. Sediment samples were placed in labeled plastic Nalgene bottles. Environmental and Geotechnical Specialists (EGS) performed granulometry using a laser diffraction instrument (Coulter 1994) and data from the 93 size distribution channels were consolidated into 26 channels corresponding with the Wentworth scale of half phi sizes with standard percent sand-silt-clay designations (Folk 1974).

2.2.2 PRIORITY DEVELOPMENT

Project restoration priorities were developed based on methods and protocols developed by the National Oceanic Atmospheric Administration (NOAA) and the State of Florida (Kenworthy et al. 2018; McNeese et al. 2006) as well as in-situ data collection results. Linear seagrass propeller scars greater than 1m in length were proposed for restoration. Circular blowout features that are often associated with the terminus of the linear feature were excluded from restoration. Type III damage propeller scars were proposed for restoration, with a no action alternative selected for Type I and II scars, for scars with signs of new seagrass growth meeting at least five percent cover, and/or for scars surrounded by colonizing seagrass species (e.g., *H. wrightii*) (Fonseca et al. 1985, Kenworthy et al. 2002, Uhrin et al. 2011). As part of the prioritization, focus was on propeller scars that were greater than 7.5cm in depth to ensure seagrass would not have the ability to self-recruit back into the scar (Sargent et. al 1995).

2.2.3 PERMITTING

The restoration project required state and federal permitting and agency coordination prior to initiation of the implementation phase of the project.

2.2.4 RESTORATION IMPLEMENTATION

The restoration project utilized biodegradable sediment tubes manufactured by a third-party supplier. Sediment tubes were manufactured to a size that is suitable for the average scar dimensions. Typically, these sediment tubes were fabricated at either 23 centimeters (cm) by 91cm or 20cm by 91cm. Once filled with sand the width reduced to approximately 18 to 20cm wide.

The sediment tubes used a 5-ply Jute cord for drawstring and were manufactured with Tex 60 natural cotton, five thread construction, and were rated to hold up to around 75 lbs. weight. All the materials being used were made with natural processes without any chemicals and were designed to biodegrade within six months.

Sediment tubes were filled on site and the resultant thickness was adjusted as necessary to match the depths of the propeller scars and to ensure that ambient grade was met. Pallets of filled sediment tubes were loaded onto vessels and transported to each PSR. Potentially suitable propeller scars were examined in water to ensure they meet all applicable criteria (e.g., appropriate width, depth, and length) and marked with a poly vinyl chloride (PVC) pipe and flagging. Most of the sediment tube deployments were comprised of placing sediment tubes end to end along the length of the propeller scar. Wider or deeper scars required multiple tubes being placed side-by-side within the propeller scar. Following installation, restored propeller scars were reviewed for quality control, spatially documented with a centroid geopoint and polyline extending the complete length of the scar, and visually documented with representative photos.

2.2.5 MONITORING PLAN

Per the FDEP's State of Florida's Monitoring Plan for Deepwater Horizon Natural Resource Damage Assessment Early Restoration Phase III Project: Florida Seagrass Recovery Project, restored (treated) propeller scars will be monitored annually. Treated propeller scars that do not naturally revegetate to a minimum 25 to 50% coverage after two growing seasons (approximately 18 to 24 months) after restoration, will be supplemented with plantings. By year 3 (36 months) post sediment tube installation, treated propeller scars are estimated to revegetate to a minimum 50 to 75% coverage in scarred areas at the completion of the project.

3. Results

3.1. MAPPING EFFORT

During the quantification process, 11 PSRs were established which were geographically or spatially distributed throughout the eastern side of the St. Joseph Bay AP (Figure 3). PSR's 1 and 2 were in the northern extent of the total map scarred areas, PSR's 3, 4, 6, and 7 were established in the central area, with PSR's 5, 8, 9, 10, and 11 occurred within the southernmost extent of the mapped areas.

Propeller scars identified during the imagery analysis included 18% of PSRs classified as having light scarring, 46% of PSRs classified as being moderately scarred and the remaining 36% of PSRs classified as heavily scarred (Table 1). A total of 789 propeller scars were identified, totaling 1 hectare for restoration. The total average prop scar width for the PSR's was 33.5cm and the total average prop scar length was 42 meters (m).

TABLE 1:

Propeller scar restoration area scar area based on aerial interpretation and ground truthing

Propeller Scar Restoration Area	Scarring Severity	Total Number Of Scars	Total Average Length of Scars (m)	Restoration Area (hectares)	Propeller Scar (hectares)
1	Moderate	58	35.00	8.42	0.07
2	Light	19	41.25	10.69	0.03
3	Moderate	19	32.20	4.66	0.02
4	Moderate	114	39.63	28.87	0.16
5	Moderate	31	32.99	9.35	0.03
6	Heavy	119	50.61	22.31	0.22
7	Moderate	10	39.30	5.71	0.01
8	Heavy	80	54.60	21.01	0.16
9	Heavy	79	33.20	13.72	0.09
10	Light	4	97.41	0.36	0.01
11	Heavy	256	40.85	27.65	0.20
Total	NA	789	497.04	152.75	1.00

3.2 RESTORATION PLAN

Initial ground truthing of 77 propeller scars with the PSRs revealed depths ranging from 2.5 to 15cm, with an average depth of 8cm. Propeller scar widths ranged from 15 to 68.5cm, with an average of 48cm. Total propeller scar lengths ranged from 1 to 91m.

Fully and partially filled prototype sediment tubes were placed in propeller scars of PSRs. The full sediment tube measured 76cm in length by 15cm in width and 12cm in height. The partially filled sediment tube measured 81cm in length by 20cm in width and 8cm in height. It was determined that partially filled sediment tubes ambient optimal grade conditions for most scars, with the option to double stack for deeper scars.

Native and local mine material was analyzed for size, percent visual shell inclusion, and color. Grain size analysis of three samples from the AP were compared to eight sands from local mines. The source suitability threshold was set at no greater than a 20% deviation from native material.

3.3 PERMITTING

The project was deemed clearly in the public interest as it is a habitat restoration project that will positively affect the fish or recreational values and marine productivity in the area and therefore, an Environmental Resource Permit (ERP) was granted. Additionally, the project is located on sovereignty submerged lands owned by the State of Florida. Therefore, state permitting also required authorization from the Board of Trustees of the Internal Improvement Trust Fund (Board of Trustees).

Through coordination with the U.S. Army Corps of Engineers (USACOE) it was determined that the proposed project satisfied the conditions of a Nationwide Permit (NWP) 27 which are for activities in waters of the United States associated with the restoration, enhancement, and establishment of tidal and non-tidal wetlands and riparian areas, the restoration and enhancement of non-tidal streams and other non-tidal open waters, and the rehabilitation or enhancement of tidal streams, tidal wetlands, and tidal open waters, provided those activities result in net increases in aquatic resource functions and services.

Additionally, as part of the USACE permit, coordination regarding potential cultural resources was required. As part of the permit, it was required that no structure or work shall adversely affect impact or disturb properties listed in the National Register of Historic Places (NRHP) or those eligible for inclusion in the NRHP.

If during the ground disturbing activities and construction work within the permit area, there were archaeological/cultural materials encountered which were not the subject of a previous cultural resources assessment survey (and which included, but not be limited to: pottery, modified shell, flora, fauna, human remains, ceramics, stone tools or metal implements, dugout canoes, evidence of structures or any other physical remains that could be associated with Native American cultures or early colonial or American settlement), that Atkins would immediately stop all work and ground-disturbing activities within a 100-meter diameter of the discovery and notify USACE within the same business day (8 hours).

The project also was subject to Project Design Criteria (PDC) outlined in the Jacksonville District Biological Opinion (JAXBO). These PDC's included requirements regarding the use of vessels in and near navigable channels, requirements to address requirements pursuant to Section 7, Endangered Species Act (ESA), as well as turbidity control measures and best management practices (BMP's). Finally, the PDC's required that any fill to restore natural contours or improve water quality, including the fill of scars or ruts caused by vessel groundings or similar activities must match the surrounding natural elevation at the conclusion of the restoration activities.

3.4 RESTORATION IMPLEMENTATION

The total restoration effort included 379 propeller scars with 43,954 sediment tubes installed, for a total of 0.84 hectares of restored propeller scars (Figure 5; Table 2). Per PSR, the quantity of scars restored ranged from three in PSR 9 to 77 in PSR 6, which total 0.002 and 0.217 hectares restored, respectively. Of all restored scars, the shortest was 1.8m in length and the longest was 1.20km, with an average restored scar length of 106m. Depth of restored scars ranged from 7 to 26cm.

FIGURE 5

PSRs with treated propeller scars (to same scale)

TABLE 2:

Treated propeller scars, sediment tubes, and area per PSR

PSR	Total Scars Restored	Sediment Tubes Installed	Hectares
1	59	4,788	0.089
2	47	3,500	0.065
3	10	478	0.009
4	62	3,686	0.068
5	8	2,620	0.049
6	77	11,678	0.217
7	5	594	0.011
8	53	8,062	0.150
9	3	102	0.002
10	21	3,461	0.064
11	34	4,985	0.093
TOTAL	379	43,954	0.817

3.5 MONITORING

Baseline monitoring was conducted approximately one year after implementation. Monitoring is ongoing and 74% of the restored scars had been surveyed to date. 62% of surveyed scars were scored a "1" or higher on the Braun-Blanquet scars and 14% scored "3" or higher, which fulfill success criteria for the restoration effort.

4. Discussion

Preliminary sediment tube degradation and seagrass recruitment was observed in propeller scars treated at the beginning of the implementation by the completion of the effort (approximately 5 months). Year one post installation monitoring results further demonstrate successful *T. testudinum* recruitment in treated propeller scars, with minimal pioneering species competition. Generally, treated propeller scars within sandy substrate appear to be recruiting more rapidly than mucky substrates. Unanticipated confounding factors include seagrass denuding by sea urchins.

Sediment tubes appear to be stabilizing seagrass meadows amid challenging situations. The restoration implementation occurred between July and November 2020, a notably active hurricane season for the AP. Despite atypical conditions, the installed sediment tubes remained in place throughout the storm events. Furthermore, installed sediment tubes remained largely unimpacted during periods of heavy boating traffic (e.g., scallop season). This can likely be attributed to the sediment tubes low profile within the substrate as well as deliberate placement outside of established channels and popular fishing destinations. This innovative method of seagrass restoration has advantages over other methods in terms of costs and predictive success and contributes to the goal of mitigating seagrass loss worldwide. In addition to the restoration implementation, continued attention to public education is needed to inform both residents and visitors of the effects of vessel groundings on this important resource.

References

- Coulter Electronics Ltd., Luton, England. 1994. Industrial and Scientific Bibliography
- Folk RL. 1974 The petrology of sedimentary rocks. Austin, Texas, Hemphill Publishing Co., 182 pp.
- Fonseca MS, Kenworthy WJ, Thayer GW, Heller DY, Cheap KM. 1985. Transplanting of the seagrass Zostera marina and Halodule wrightii for sediment stabilization and habitat development on the East Coast of the United States. U.S. Army Engineer Waterways Experiment Station Technical Report EL-85-9, Mississippi.
- Fonseca MS, Kenworthy WJ, Thayer GW. 1998. Guidelines for the Conservation and Restoration of Seagrasses in the United States and Adjacent Waters. NOAA Coastal Ocean Program Decision Analysis Series 12, Maryland.
- Hall MO, Merello M, Kenworthy WJ, Berns D, Ferenc K, Kunzelman J, Hall F, and Hyniova J. 2006. Developing Techniques to Enhance the Recovery Rates of Propeller Scars in Turtlegrass (Thalassia Testudinum) Meadows. Florida Fish and Wildlife Conservation Commission Final Report, Florida.
- Kenworthy WJ, Fonseca MS, Whitfield PE, Hammerstrom K. 2002. Analysis of seagrass recovery in experimental excavations and propeller-scar disturbances in the Florida Keys National Marine Sanctuary. Journal of Coastal Research 37:75-85
- Kenworthy WJ, Hall MO, Hammerstrom KK, Merello M, Schwartzchild AC. 2018. Restoration of tropical seagrass beds using wild bird fertilization and sediment regrading. Ecological Engineering 112:72-81.
- McNeese PL, Kruer CR, Kenworthy WJ, Schwarzchild AC, P Wells, Hobbs J. 2006. Topographic restoration of boat grounding damage at the Ligumvitae Submerged Land Management Area. Proceedings of a habitat restoration conference held at Mote Marine Laboratory, Sarasota, Florida.
- Sargent FJ, Leary TJ, Crewz DW, and Kruer CR. 1995. Scarring of Florida's seagrasses: Assessment and Management Options. Florida Marine Research Institute Technical Report TR-1, Florida.
- Uhrin, AV, Kenworthy WJ, and Fonseca MS. 2011. Understanding uncertainty in seagrass injury recovery: an information-theoretic approach. Ecological Applications 21:1365-1379.

Nick Rothwell
Senior Sustainability Consultant
Engineering Services – Infrastructure UK
London, UK

Hector Lyons
Assistant Sustainability and Carbon Consultant
Engineering Services – Infrastructure UK
London, UK

Dr. Mohammad Safari Baghsorkhi
Principal Engineer
Engineering Services – Infrastructure UK
London, UK

02: Whole Life Carbon Management in the Rail Industry

Abstract

Meeting Net Zero emissions targets is fundamental to the avoidance of further impacts and discontinuing the visible environmental deterioration that the world is currently witnessing. With the transport industry responsible for over a quarter of the UK's greenhouse gases, the importance of decarbonisation continues to expand. Currently 40% of the UK's rail fleets are already electric and as the electrification further heightens the Department of Transport continues to focus on achieving net zero greenhouse gas emissions by 2030 along with the removal of all diesel-only trains from the rail network by 2040. As operational energy is actively being reduced, the importance of reducing whole life carbon emissions within the rail industry continues to rise. Following the guidance of the PAS 2080 principles, a common framework for the full supply chain can be achieved, encouraging the correct approaches to deliver reduced carbon emissions and cost. Carbon can be reduced at any point of a project, understanding the carbon reduction hierarchy shows that the earlier the whole life carbon emissions are reduced the greater the potential to reduce total emissions. PAS 2080 provides quantification requirements allowing carbon tools such as the Rail Carbon Tool to carry out carbon calculations. The Soham Station Redevelopment case study explores the principles of PAS 2080 to make low carbon decisions that are quantified for a carbon assessment using the rail carbon tool.

KEYWORDS

Carbon management; Whole life carbon management; Net Zero; Greenhouse gas emissions; Decarbonising transport; Electrification

1. Introduction

Climate change, accelerated by anthropogenic greenhouse gas (GHG) emissions, is one of the critical global issues within today's society. The effects of climate change are already visible, from rising sea levels to long-term shifts in weather patterns and increased temperatures. Meeting net zero emissions targets is therefore paramount to avoiding further impacts and potentially reversing the changes that we are already seeing around the world.

The transport sector represents around 27% of the UK's GHG emissions[1]. Traditionally, the focus of carbon reduction efforts in the transport industry has been on operational emissions from fuel combustion in vehicles; however, as the net zero agenda grows in prominence and vehicles decarbonise through electrification, whole life carbon of transport infrastructure is becoming increasingly important.

Whole life carbon is the sum of total greenhouse gas emissions that occur throughout the lifecycle of a project, from the emissions released during the extraction of raw materials and manufacturing of products, the transport of products to the construction site and emissions released during the construction process, as well as operation and maintenance, and, finally, end-of-life emissions, as demonstrated in Figure 1.

FIGURE 1

End-to-end emissions sources across the whole life of a construction project

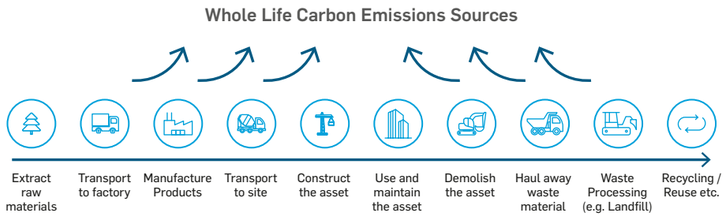

This article explores whole life carbon management for the rail industry in the context of the wider net zero agenda. It aims to demystify carbon management and quantification to help people in the rail industry embed sustainability best practice. Guidance is provided for effective use of carbon calculators such as the RSSB Rail Carbon Tool[2] supported by a case study of an example of Atkins' experience in managing carbon on a rail infrastructure project and quantifying the benefits using the Rail Carbon Tool.

2. UK Net Zero Targets

Responding to the threat of catastrophic climate change requires coordinated action to reduce greenhouse gas (GHG) emissions in order to meet targets set out in the Paris Agreement of 2015. These targets aim to keep global temperature rise this century below 2°C (above pre-industrial levels) and encourage efforts to limit the temperature increase even further to 1.5°C[3]. In response, the UK statutory target for reducing GHG emissions was strengthened in May 2019 to focus on achieving Net Zero by 2050[4].

The Committee on Climate Change (CCC) defines "Net-Zero" emissions as the point when the "total of active removals of carbon from the atmosphere offsets any remaining emissions from the rest of the economy"[5]. In practice, this means that to achieve net zero, emissions must be reduced as far as possible, with any remaining emissions being offset by active removals (e.g., land use change to forests, grassland, etc.). Understanding how to identify carbon emissions sources and then how to effectively manage those sources to create carbon reductions is therefore paramount to achieving net zero.

2.1. GHG EMISSIONS IN THE RAIL INDUSTRY

Rail is one of the lowest carbon forms of transport, accounting for just 1.4% of the UK's domestic transport emissions in 2019, despite 9% of transport being carried out on the UK's railways[6].

Over 40% of the UK's railways are already electrified, enabling the transport of passengers and goods with minimal GHG emissions being released. As electrification of the rail network extends, and the National Grid continues to decarbonise, this mode of transport is becoming even less carbon intensive.

The Department for Transport's top priorities from the Rail Environment Policy Statement are:

- Achieve net zero GHG emissions from rail by 2050 (including whole life carbon emissions).
- Remove all diesel-only trains from the rail network by 2040.
- Sustainable, deliverable programme of electrification that delivers a higher performing, net zero railway.

In order to achieve these ambitions, and as operational emissions are actively being reduced across the rail network, reducing whole life emissions associated with rail infrastructure is becoming even more important. Emissions associated with the construction and maintenance of rail infrastructure will become the main source of emissions once trains are fully electrified and the grid decarbonises.

The Department for Transport's plan, "Decarbonising transport: a greener, better Britain,"[7] recognises this, stating that a joined-up approach across the supply chain to managing whole life emissions will be critical to achieving net zero across the non-traction elements of UK railways.

The rail industry's 2021 proposal for a cleaner and greener future[8] states that whole life carbon reductions will be achieved by including carbon reduction targets within rail management contracts and investing in zero carbon infrastructure along with providing Great British Railways with responsibility for carbon monitoring.

Furthermore, Network Rail's Environmental & Social Minimum Requirements[9] call for a capital carbon assessment to be carried out for all projects with a capital value of over £1million. These assessments must use the RSSB Rail Carbon Tool (RCT) to develop a baseline and identify opportunities for whole life carbon reduction[10].

Processes for quantifying and managing carbon in rail infrastructure therefore need to be defined, understood, and implemented to enable effective reductions of whole life carbon.

2.2. MANAGING WHOLE LIFE CARBON IN RAIL INFRASTRUCTURE

The key technical standard that provides guidance for management of whole life carbon in the infrastructure industry is PAS 2080[11]. PAS 2080 is a voluntary standard and aims to improve the management of carbon throughout the supply chain, allowing evidence-based decisions to be made and the identification of carbon reduction opportunities[12]. PAS 2080 provides a common framework for the whole supply chain, encouraging the right behaviours and approaches to deliver reduced carbon and cost.

The key requirements of an effective carbon management system, as defined by PAS 2080 are:

- **Show clear leadership:** Set an organisational strategy for carbon management and assign roles and responsibilities to individuals/teams so they understand the part they play in reducing carbon.
- **Embrace a culture of challenge and change:** Communicate the importance of carbon management to project teams and the supply chain and encourage challenging of the status quo.
- **Set bold targets:** Set challenging carbon reduction targets against a defined baseline and establish KPIs to monitor emissions during project delivery.
- **Develop a carbon management process integrated within standard project delivery:** Ensure carbon information feeds into decision making from the earliest project stages.
- **Engage the value chain early:** Collaborate with the whole value chain from the earliest project stages to share carbon objectives and identify innovative low carbon solutions, removing any constraints to collaboration.
- **Establish an accurate carbon accounting procedure:** Use relevant tools and processes to quantify and report carbon throughout project delivery to feed into decision making.
- **Promote continual improvement of the process:** Seek the input of the whole supply chain to improving the carbon management process.

Following the principles of PAS 2080 on rail infrastructure projects will allow for innovation, carbon, and cost reduction. It ensures consistency within infrastructure delivery, making carbon visible across the supply chain, and will ultimately lead to low carbon solutions. Developing a carbon management system for projects, aligned with PAS 2080, is therefore strongly recommended. Tools, such as the Rail Carbon Tool, can be used to support carbon management throughout project delivery and chapter 7 of PAS 2080 provides a methodology for effective use of such tools.

3. Integrating Carbon Management into Project Delivery

To ensure that carbon is considered at all project decision points alongside other key factors, such as cost and programme, carbon must be embedded within the delivery of a project from the earliest stages. The 2013 Infrastructure Carbon Review[13] illustrates this importance through the infrastructure carbon reduction hierarchy, as set out in Figure 2.

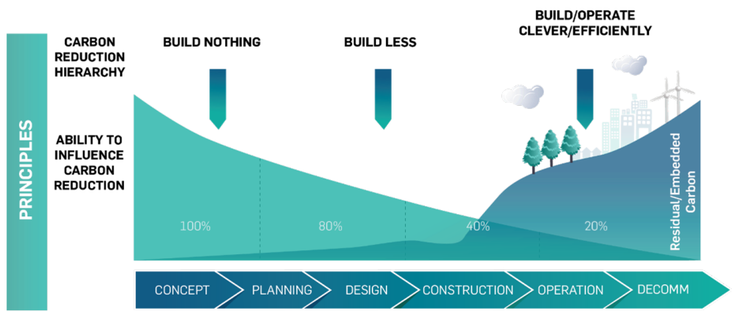

FIGURE 2

The carbon reduction hierarchy (Source: Infrastructure Carbon Review – 2013)

Carbon can be reduced at any point during project delivery but the proportion of emissions that can be reduced decreases over time. The earlier that whole life carbon is considered in project decision making, the greater the potential to reduce emissions. The carbon reduction hierarchy forms the basis of effective management of whole life carbon within the delivery of assets or programmes of work.

In practice, the carbon reduction hierarchy provides a framework for decision making that will result in innovation and low carbon results:

- **Build Nothing:** Evaluate the basic need for an asset and/or programme of works and explore alternative solutions to achieve stated project aims.
- **Build Less:** Evaluate the potential for reusing and/or refurbishing existing assets to reduce the extent of new construction required.
- **Build Clever:** Consider the use of innovative approaches or low carbon solutions to minimise resource consumption during construction operation and use, and build infrastructure that has been designed for easy decommissioning and reuse/recycling.
- **Build Efficiently:** Use technologies that reduce resource consumption during construction, operation, and end of life[14].

Working closely with stakeholders, including clients, project teams, and the supply chain, is essential to embedding the carbon reduction hierarchy into all areas of project planning and delivery. This can be achieved through in-depth discussions and holding workshops that allow for supply chain collaboration where all parties can gain an understanding and contribute ideas.

Using the carbon reduction hierarchy as the framework to these conversations, and as general principles to follow during design and construction, helps to instil a challenge culture throughout project delivery where carbon reduction is considered at every stage.

By embedding the principles of PAS 2080 and the carbon reduction hierarchy within project delivery, substantial carbon reduction opportunities are unlocked. These opportunities can be explored, options can be compared, and whole project reporting can be carried out by assessing carbon using carbon calculation tools, such as the Rail Carbon Tool.

3.1. WHOLE LIFE CARBON ASSESSMENT

3.1.1. FUNDAMENTALS

Calculating whole life carbon emissions is often perceived as being a complicated process; however, the basic calculation is very simple. At its core, carbon calculation is simply multiplying project activity data (e.g., a quantity of material) by a relevant carbon factor. A carbon factor is a coefficient representing the average emissions associated with a single unit of a specific source (e.g., the average emissions associated with the production of 1 tonne of concrete). Carbon factors are provided by various carbon factor libraries and cover all processes across the project lifecycle including products/materials, vehicle transport, construction processes, fuel, energy and water use as well as end of life processes. Carbon factors are produced according to specific technical standards, such as BS EN 15804[15], to ensure consistency and accuracy.

In some instances, product manufacturers may provide a carbon factor that has been calculated for a specific product and is reported in an Environmental Product Declaration (EPD). EPDs are the most accurate form of carbon factor and therefore should be prioritised wherever possible.

Carbon emissions factors and calculated emissions from project activities are expressed in carbon dioxide equivalents (CO_2e) per unit (e.g., per tonne). CO_2e represents the global warming potential of all GHGs released by an activity, put in the context of carbon emissions to enable easy comparison.

3.1.2. CARBON MODELLING AND CARBON TOOLS

To carry out a robust carbon assessment of a project or a project option, there are a number of technical components that must be in place and understood, including:

- A thorough understanding of the life cycle of the project/asset, and where the measurable emissions sources exist.
- Data sources, including project-specific input data as well as appropriate carbon emissions factors.
- A robust assessment methodology that is aligned with relevant technical standards (e.g., PAS 2080).
- A defined system boundary, outlining the physical and geographical boundaries to be included in the assessment as well as all inclusions and exclusions within that boundary.
- A reference study period, which defines the time-period for the assessment, and consequently the range of operational activities for which emissions will be accounted for (e.g., energy required during operational lifetime, maintenance/ replacement requirements).

3.1.3. BENEFITS OF QUANTIFYING EMISSIONS

A wealth of benefits arises from calculating whole life carbon emissions within projects. Carbon calculation is most effective when feeding into the optioneering process of project development. Understanding the whole life carbon impact of each project option enables teams to make sustainable decisions.

Calculating emissions also enables project teams to fully understand where the majority of carbon is occurring within a project or option, often referred to as the carbon hotspots. Efforts can then be focussed on reducing these large emissions sources where the potential for reduction is greatest.

Carbon quantification can also be particularly useful when making a business case for more sustainable solutions; if a sustainable product has greater upfront costs, then understanding the potential emissions savings helps to make a case for the additional upfront capital expenditure.

Similarly, calculating whole life carbon ensures that the lifetime of a product/asset is considered, and therefore may enable teams to select options that have greater upfront costs but will save money over the lifetime of the project as they last longer or require less maintenance.

3.1.4. LEVELS OF QUANTIFICATION

There are varying levels of carbon quantification that can be followed; depending on the size and budget of the project and the project stage, certain approaches are likely to be more relevant than others.

For larger projects (e.g., Network Rail projects with a capital value of over £1 million) it is likely that a fully quantified carbon model is required and from early stages of the project lifecycle covering the whole life of the project and comparing emissions reductions against an agreed project baseline.

In some instances, in particular when feeding into particular decisions within project delivery, it may be appropriate to carry out a more targeted assessment. This may be a quantified carbon model covering only certain stages of the assets' life cycles that are likely to have a material impact on the results of a comparison between options. For example, when comparing the carbon associated with two options with the same expected lifespan and maintenance requirements, it may only be necessary to quantify the impact of the materials, transport, and construction to understand which will have the larger whole life carbon impact.

Projects at very early stages or smaller projects may not require a quantified carbon model in order to make low-carbon decisions. In these instances, qualitative data may be utilized. This may take the form of discussions regarding the project options and which ones will use the most materials, have the shortest lifespan or will take the longest to build. Discussions may also be focussed on a single option, framed around the carbon reduction hierarchy and identifying ways to make assets smaller, or use alternative materials. Whenever a qualitative approach is taken, the whole life impact should still be considered to ensure that all aspects that will make a material impact are accounted for. Such discussions are most effective when they are collaborative and involve supply chain stakeholders and are often aided by the presence of a carbon management expert; however, this is not a necessity as long as the principles of the carbon reduction hierarchy are followed and the whole life impact is considered.

Regardless of whether a quantitative or qualitative approach is followed, it is important to track decisions that are made so the processes and resulting carbon savings can be documented. Furthermore, when data is limited at early project stages, if documented, these early decisions may be quantified at later stages when data is more available so the total emissions reduction can be reported.

3.1.5. GATHERING DATA

When carrying out a quantitative assessment, data should be gathered from all potential emissions sources as per Figure 1. Ensuring that the various disciplines within project teams know they are required to provide data, in what format it should be provided, and when it will be required streamlines the process and ensures consistency.

Whilst some data may be difficult to acquire and may require teams to make assumptions based on experience and technical judgement, often a lot of the data required is already captured as part of traditional project delivery. For example, bills of quantities, costing exercises, and construction programmes all create usable datasets that feed into carbon calculation. Planning data sources and working with teams to understand what data will be available is therefore an important exercise.

Accurate whole life data is most effectively sourced through collaboration between supply chain stakeholders, each providing data relevant to their particular specialist area (e.g., contractors providing fuel/energy use data for the construction process). Again, it is important for stakeholders to understand that they will be required to provide data and in what format to make the process as streamlined as possible.

At very early project stages, it may not be possible to gather project-specific data across the whole life cycle of the project. In these cases, previous project examples may be utilised, in combination with assumptions made through expert technical judgement or standard data provided by technical standards or industry best-practice. Where this is the case, this data should be updated at the next iteration of assessment by project-specific data where possible, and the baseline adjusted where necessary.

4. The Rail Carbon Tool

The RSSB Rail Carbon tool (RCT) is a freely available, web-based, carbon assessment tool for the rail industry, hosted and provided by RSSB and originally developed by Atkins. Premium carbon factor libraries for the infrastructure industry, including the Inventory of Carbon & Energy (ICE) database[16], are embedded within the RCT, enabling the assessment of whole life carbon for rail projects. The RCT is simple to use and enables all levels of carbon quantification to be carried out, from small scale targeted assessments to holistic whole life assessment for whole project reporting. When the correct methodology is followed, the Rail Carbon Tool can be used to carry out carbon calculations that adhere to the quantification requirements of PAS 2080.

For further information and training regarding use of the RCT, please refer to the RSSB website[17].

5. Case Study: Soham Station Redevelopment

5.1. A CARBON ASSESSMENT USING THE RAIL CARBON TOOL

5.1.1. SITUATION

Soham Station in Ely, Cambridgeshire, previously operated on the Ipswich to Ely line serving the town of Soham, until its closure in the 1960s. Following a long campaign to rebuild it, the station was reopened in December 2021. The new station reconnects the local community to the rail network supporting further investment as part of Cambridgeshire & Peterborough Combined Authority's vision for the wider area[18].

Atkins was involved in project design optioneering and used the principles of PAS 2080 to make low-carbon decisions and then quantified carbon in the Rail Carbon Tool, feeding into the wider options appraisal.

5.1.2. CLIENT ISSUES

The client, Network Rail, needed to decide what type of platform should be built at the station as well as understand the carbon benefits of design decisions that were made. An appraisal of five platform options was required considering cost, constructability, and carbon, and a full project assessment was required to quantify the carbon benefit of design changes throughout options appraisal stage.

5.1.3. ATKINS SOLUTIONS AND ADDED VALUE

Atkins' carbon experts and engineering design team worked in collaboration to gather life cycle inventory data of the five platform options to feed into a targeted carbon assessment using the Rail Carbon Tool, comparing each option. The options included:

1. Red brick, crosswall and plank platform
2. Steel modular platform
3. Glass Reinforced Plastic (GRP) modular platform
4. Polystyrene modular platform
5. Concrete modular platform

The results of the assessment fed into a wider options appraisal considering various factors including cost, constructability, and sustainability.

Additional to the platform assessment, Atkins' sustainability team worked with the designers to identify sustainable, low-carbon solutions within all aspects of the overall design by integrating the principles of the carbon reduction hierarchy and by carrying out carbon reduction workshops.

At later stages, once the preferred platform option had been chosen, a full carbon model was developed covering the whole station, including the station footbridge, access road and car park, shelters, signalling structures and the platform. The intention of the full model was to demonstrate how carbon had been reduced throughout the options appraisal stage.

Atkins' carbon specialists also used the assessment to identify carbon hotspots within the overall station design and worked with the design team to identify further opportunities to reduce carbon associated with those hotspots in later stages.

5.1.4. METHODOLOGY

The carbon assessments carried out throughout project delivery were conducted using the Rail Carbon Tool, in line with Network Rail's environment standard (NR/L2/ENV/015). The assessment methodology followed the principles set out in section 7 of PAS 2080: Carbon Management in Infrastructure on whole life carbon quantification.

5.1.5. FINDINGS

Atkins identified through the targeted platforms assessment that the polystyrene modular solution had the lowest associated carbon emissions, as illustrated in Figure 3.

FIGURE 3

Platform options carbon assessment comparison

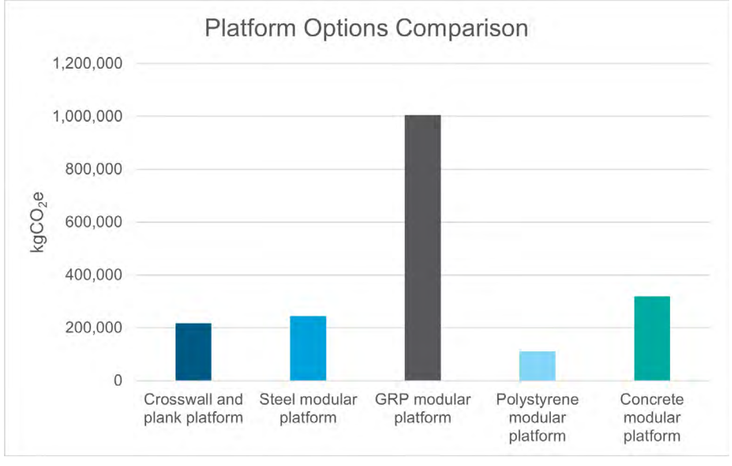

5.1.6. KEY BENEFITS AND SUCCESS FACTORS

- The carbon assessments provided the information necessary to enable design decisions that were significantly more informed and justifiable from a sustainability perspective. A key factor in this was the transparent assessment methodology, using direct project and supplier data.
- Atkins used the Rail Carbon Tool to quantify carbon between different platform components, demonstrating to the client that the most carbon efficient solution (polystyrene modular) delivered a carbon reduction of 49% against the baseline option (crosswall and plank).
- Based on the results of the platforms carbon assessment and the wider aspects of the options appraisal, the client chose the lowest carbon platform solution, polystyrene modular, which contributed a significant amount to the overall carbon reduction of the station design.

- Through embedding the principles of the carbon reduction hierarchy into the design decision making process, Atkins were able to achieve further carbon reductions across the whole station design.
- An overall carbon reduction of 18% was achieved throughout the options selection stage, when compared to the baseline design from the previous stage.

From the in-depth comparison between options and the identification of carbon hotspots within the design, Atkins' carbon experts were able to make the following recommendations to the project team:

- Consideration should be given to potential opportunities to reduce the volumes of materials in the design option taken forward, aligning with the "Build Less" principle of the carbon reduction hierarchy.
- Consideration of opportunities to transport materials by rail, wherever possible, as rail transport has a lower carbon intensity than road.
- Seek to identify alternative materials with a lower carbon intensity, wherever possible, aligning with the "Build Clever" principle of the carbon reduction hierarchy. Opportunities may exist to utilise recycled or site won materials in the design which would reduce the overall carbon impact.
- Explore opportunities to optimise the construction process by reducing the plant machinery and vehicles required and/or their time on site, aligning with the "Build Efficiently" principle of the carbon reduction hierarchy. Choosing electric plant machinery and vehicles and using renewable energy wherever possible on site should also be considered.
- A large opportunity exists to reduce carbon emissions if materials are recycled at their end-of-life. Implementing project components so they are as recyclable as possible will therefore increase the opportunity to minimise carbon through recycling at end-of-life.

6. Atkins' Approach to Whole Life Carbon Management

As part of the SNC-Lavalin group, Atkins made a commitment in May 2021 to achieve net zero by 2030. Our approach to whole life carbon management forms part of our contribution to SNC-Lavalin's vision to "create sustainable solutions that connect people, data and technology to design, deliver and operate the most complex projects."

Our approach is a core part of our Engineering Net Zero[19] initiative, with a vision of "embedding sustainability in everything we do, progressing attitudes within the industry and aspiring to make all schemes in which we are involved net zero by 2030."

We are committed to offering our clients ambitious design options and advice that are fully compatible with Net Zero outcomes. We aim to design out carbon at every opportunity, with our methodology focused on driving engagement, collaboration, and innovation amongst all our project partners, including asset owners, designers, construction teams, operators, and materials suppliers. At every project stage, we strive to challenge carbon intensive materials and methods and push the boundaries of innovation to enable our clients to develop solutions that deliver long-term positive change. We channel our low-carbon engineering experience into pioneering solutions for faster decarbonisation of businesses, sectors, and regions at scale to deliver sustainable economic growth.

Acknowledgements

This paper was originally published as: ROTHWELL, N., LYONS, H., SAFARI BAGHSORKHI, M. (2022) Whole Life Carbon Management in the Rail Industry. The PWI Journal, Vol 140 PT 2, Permanent Way Institution, April 2022, Pages 30-35. ISSN 2057-2425.

References

1. Transport and Environment Statistics 2021 Annual report (2021). [online] Available at: https://assets.publishing.service.gov.uk/government/uploads/system/uploads/attachment_data/file/984685/transport-and-environment-statistics-2021.pdf (Accessed: 10 January 2022)
2. Rail Safety and Standards Board, Rail Carbon Tool (2021). [online] Available at: https://www.rssb.co.uk/en/sustainability/rail-carbon-tool (Accessed: 10 January 2022)
3. Intergovernmental Panel on Climate Change, Global Warming of 1.5 ºC (2018). [online] Available at: https://www.ipcc.ch/sr15/ (Accessed: 10 January 2022)
4. The Climate Change Act 2008 (2050 Target Amendment) Order 2019 (2019). [online] Available at: http://www.legislation.gov.uk/ukdsi/2019/9780111187654 (Accessed: 10 January 2022)
5. Climate Change Committee, Net Zero Repots (2019). [online] Available at: https://www.theccc.org.uk/publication/net-zero-the-uks-contribution-to-stopping-global-warming/ (Accessed: 10 January 2022)
6. Department for Transport, Rail Environment Policy Statement (2021). [online] Available at: https://assets.publishing.service.gov.uk/government/uploads/system/uploads/attachment_data/file/1002166/rail-environment-policy-statement.pdf (Accessed: 10 January 2022)
7. Department for Transport, Decarbonising Transport (2021). [online] Available at: https://assets.publishing.service.gov.uk/government/uploads/system/uploads/attachment_data/file/1009448/decarbonising-transport-a-better-greener-britain.pdf (Accessed: 10 January 2022)
8. Local Government Association, The importance of rail in meeting the UK's net zero ambitions. [online] Available at: https://www.local.gov.uk/andy-bagnall-rail-net-zero (Accessed: 10 January 2022)
9. Network Rail, Environment & Social Minimum Requirements – Deliverables (NR/GN/ESD36) (2020) [online] Available at: https://safety.networkrail.co.uk/wp-content/uploads/2020/02/NR_GN_ESD36-Environmental-and-Social-Minimum-Requirements-Deliverables.pdf (Accessed: 10 January 2022)
10. Network Rail NR/L2/ENV/015 ISSUE 9 (Clause 6.4.2) - Environment and Social Minimum Requirements for Projects - Design and Construction - Compliance Date: 4 September 2021.
11. British Standards Institution, PAS 2080: Carbon management in infrastructure (2016). [online] Available at: https://shop.bsigroup.com/products/carbon-management-in-infrastructure/standard (Accessed: 10 January 2022)
12. The Green Construction Board, Guidance Document for PAS 2080 (2016). [online] Available at: Guidance-Document-for-PAS2080_vFinal.pdf (constructionleadershipcouncil.co.uk) (Accessed: 10 January 2022)
13. HM Treasury, Infrastructure Carbon Review (2013). [online] Available at: https://assets.publishing.service.gov.uk/government/uploads/system/uploads/attachment_data/file/260710/infrastructure_carbon_review_251113.pdf (Accessed: 10 January 2022)
14. Procurement Requirements for Carbon Reduction in Infrastructure Construction Projects - An International Case Study (2019). [online] Available at: https://www.diva-portal.org/smash/get/diva2:1324140/FULLTEXT01.pdf (Accessed: 10 January 2022)
15. British Standards Institution. BS EN 15804 - Sustainability of construction works. Environmental product declarations. Core rules for the product category of construction products. [online] Available at: https://shop.bsigroup.com/products/sustainability-of-construction-works-environmental-product-declarations-core-rules-for-the-product-category-of-construction-products/standard (Accessed: 04 February 2022)
16. Embodied Carbon - The ICE Database. [online] Available at: https://circularecology.com/embodied-carbon-footprint-database.html (Accessed: 10 January 2022)
17. RSSB Rail Carbon Tool Training. [online] Available at: https://www.rssb.co.uk/en/services-and-resources/training/rssb-rail-carbon-tool-training (Accessed: 10 January 2022)
18. Network Rail, Reconnecting Soham. [online] Available at: https://www.networkrail.co.uk/running-the-railway/our-routes/anglia/improving-the-railway-in-anglia/reconnecting-soham/ (Accessed: 04 February 2022)
19. SNC-Lavalin, Engineering Net Zero [online] Available at: https://www.engineeringnetzero.com/sectors-services/ (Accessed: 10 January 2022)

Gareth Richardson
Low Carbon Technology Lead
Nuclear
Bristol, UK

Peter Appleby
Senior Engineer
Nuclear
Glasgow, UK

Ross Cooper
Assistant Process Engineer
Nuclear
Bristol, UK

03: Clean Hydrogen for Steel Production

Abstract

Decarbonization of the steel sector is currently receiving significant attention in many countries, mostly focusing on the direct reduction of iron using hydrogen. However, unless green hydrogen from renewable energy sources becomes available in sufficient quantities and at an economical cost, the overall decarbonization of steelmaking remains a challenge. The current paper covers the learnings from a recent feasibility study completed for the conversions of a direct reduction iron (DRI) and associated electric arc furnace (EAF) plant to a green steel plant. The feasibility study centered on the transition from hydrogen, produced by natural gas combustion, to a green hydrogen supply system, based on electrolysis with a power supply mix of renewables and nuclear energy. Four areas of interest are laid out in the paper: a) Electricity source and its impact on the levelized cost of hydrogen, b) Electrolyser plant types and suitability for integration, c) Value stacking through electrical load management and benefits for plants with electric arc furnaces, d) Impact of high purity hydrogen on the DRI plant and the necessary adjustments to be made. The identified benefits include producing minimized carbon dioxide during the production of the steel, possible increased DRI capacity, mitigation of EAF impact on grids, and tuneable carbon content of the DRI.

KEYWORDS

Green Hydrogen; Steelmaking; Carbon footprint; CO_2-emission

1. Introduction

Decarbonization of the steel sector is big task and is currently receiving significant attention globally, with many decarbonization pathways being proposed and some in the initial testing phase. There are some relatively quick wins that can be made through increased recycling, replacement of steam methane reformers on DRI plants, and injection of hydrogen in blast furnaces.

If we look at the drivers for decarbonization, we have the Net Zero pledges from most of the steel producing countries, carbon border adjustments, and carbon taxes. It is not just regulation driving the change, there is a growing demand from car manufacturers and end customers. The IEA has stated that the steel industry needs to get to 0.6 tonne of CO_2 per tonne of steel by 2050. This is a huge build out of new technologies and new clean source of energy with 100TWh of new clean energy required to meet the IEA forecast for hydrogen alone.

However, unless clean hydrogen becomes available in sufficient quantities and at an economical cost, the overall decarbonization of steelmaking remains a challenge. This paper covers the learnings from recent studies in hydrogen production and for the conversions of a direct reduction iron (DRI) and associated electric arc furnace (EAF) plant to a green steel plant.

Currently, the majority of the global steel production is via one of the two process pathways: the integrated Blast Furnace – Basic Oxygen Furnace (BF-BOF) or the Direct Reduced Iron – Electric Arc Furnace (DRI-EAF). DRI-EAF plants can utilize coal in the rotary kiln process route or natural gas (NG) in the shaft or fluidized bed process routes. The NG-DRI pathway has relatively low specific carbon emissions of <1.4tCO_2/t_{steel} compared to the BF pathway at ~1.9tCO_2/t_{steel}[1]. There are two main technology suppliers for the NG-DRI process route, namely, MIDREX and ENERGION with ~60% and 12.4% market shares in 2020, respectively[2]. In both technologies, the NG can be reformed separately using Steam Methane Reforming (SMR) or via an integrated reforming process. This case study focuses on the replacement of an SMR by a water electrolyser feeding an Energion DRI plant. Figure 1 shows a block flow diagram (BFD) of the process in which NG is reformed to a syngas in a SMR unit; the gas is composed primarily of CO (~15 Vol%) and H_2 (~73 Vol%), providing both reductants and carbon for carburization of the iron.

FIGURE 1

BFD of the original process, NG reformed in a SMR unit

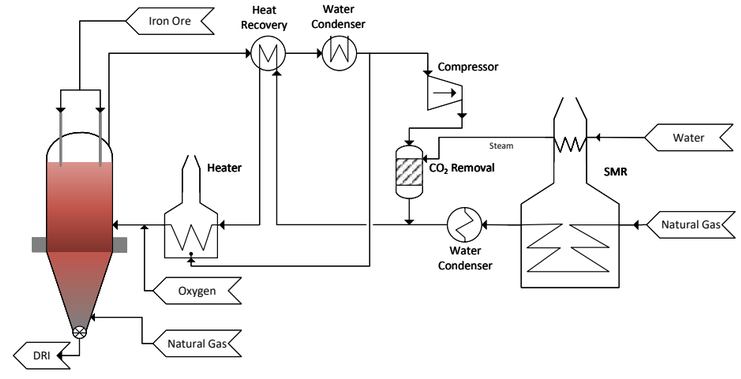

The reformer syngas is then blended with a recycle stream from the reactor containing CO_2, then passes through heat recovery, and fired in the furnace using tail gas and NG to reach a temperature in excess of 900°C. To increase the temperature to above 1,000°C for improved reaction kinetics, O_2 is added to combust some of the methane and hydrogen from the SMR.

The aim of the conducted feasibility study was to replace the SMR with hydrogen, produced via water electrolysis, changing the block flow diagram to what is shown in Figure 2.

FIGURE 2

BFD of the modified flowsheet, water electrolysis process

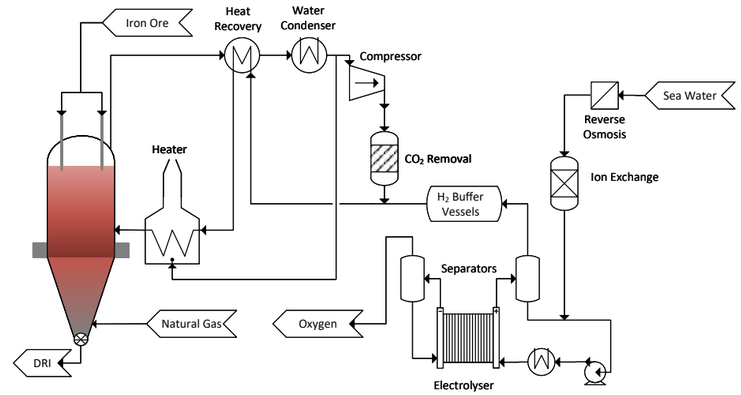

2. Electrolyser Types and Suitability for Integration with DRI

2.1. ELECTROLYSER TYPES

The global electrolyser market is currently at an inflection point and may well be entering a hockey-stick moment of demand with supply struggling to keep up. SNC-Lavalin is actively supporting electrolyser manufacturers with scaling up their stack and module manufacturing operations and resolving engineering issues from the stack level to the module and beyond. These interactions have given a unique insight into the industry, with manufacturer's struggling to meet demand. As such, securing electrolyser manufacturing capacity with the optimum technology is one of the key areas to project success. Proper due diligence should be made of each electrolyser technology vendor to ensure not only system performance but the manufacturability and manufacturing process alongside supply chain are able to meet project requirements.

Electrolyser technology is developing rapidly with increasing numbers of patents filed year on year from ~2000 in 2010 to >30,000 by 2021. Developments in cell operation in terms of temperature, pressure, and cell structure will continue to improve overall economics in the coming years. Improvements in electrocatalyst materials and separators offer the possibility of upgrading operating plant performance be it in electrical efficiency or stack degradation within the plant lifetime.

2.1.1. ALKALINE ELECTROLYSIS

Alkaline electrolysis is the most-established water electrolysis technology and has been used for industrial-scale applications since 1920 and is commercially available from multiple vendors (Thyssenkrupp, Nel Hydrogen, Asahi Kasei, MHI, Next Hydrogen etc.). Alkaline electrolysis delivery pressure varies depending on manufacturer with MW scale packages ranging from atmospheric pressure to 15.5 bar with up to 32 bar in development.

Originally used to produce hydrogen for ammonia, competition from steam methane reforming of natural gas in the 1970s led to the decline of installed alkaline capacity. The recent energy transition has led to a resurgence in the technology. Large-scale plants have been installed up to a capacity of 3,000kgH_2/h or ~162MW(e) input; however, recently, scale of Alkaline hydrogen projects is in the 1-10MW(e) range.

Alkaline electrolysers offer up a level of assurance above other current technologies in terms of the known operating performance over time and have been shown to be scalable.

There are many developments occurring in the Alkaline electrolyser space that attempt to overcome some of the limitations and issues, including new cell architectures to allow higher current density and improve response time from mins to seconds. In addition, developments in separator materials and design are leading to longer life, improved response times, and improvements in electrical efficiency.

2.1.2. POLYMER ELECTROLYTE MEMBRANE (PEM)

Polymer electrolyte membrane, also known as proton exchange membrane (PEM) technology, is a more recently developed method of hydrogen production than alkaline electrolysis. PEM electrolysis is a mature technology that is commercially available from multiple vendors (Plug Power, ITM Power, Siemens, Swiss Hydrogen, Nel, etc.). However, it is yet to be established at the same scale as alkaline electrolysis on a system level with current world scale facility capacity of 20MW, surpassing the previous of 10MW. In terms of physical differences, the PEM cell is made up of a solid electrolyte, so removes the need for using electrolyte solutions such as potassium hydroxide. The advantages of PEM technology relative to Alkaline is often noted as having a fast response capability, as well as a wide dynamic operating range of 0-100%. PEM operates at higher current densities than Alkaline as such it has more compact stacks which allow for a smaller footprint and higher operating pressures with some on the market operating at 40 Bar. In addition, PEM has a lower gas crossover which has safety benefits and aids overall system performance.

As with Alkaline, there are many developments occurring in the PEM electrolyser space. These are focused on reducing cost through vertically scaling the cell architecture and reducing the levels of expensive metals such as platinum in the Cathode and Iridium in the Anode. There are also developments in efficiency with the current market leading PEM systems having beginning-of-life specific electrical consumption rates of ~49kWh/kg.

2.1.3. SOLID OXIDE ELECTROLYSER CELL (SOEC)

Unlike low temperature electrolysis technologies such as Alkaline or PEM, Solid Oxide Electrolyser Cell (SOEC) technology is a high temperature process fed by saturated steam. The required input steam conditions can vary between vendors, from around 120-700+°C. However, the most reported feed steam data indicates 150°C. Heat is then recovered from the outlet cell flows and a final electric trim heater is used to reach the operating temperature in excess of 600°C depending on the electrical operating point of the cell. While SOEC systems are commercially available at MW(e) scale, operation at this capacity in an industrial setting has only occurred recently. Current SOEC have been demonstrated at 720kW(e) and are planned to be demonstrated at 2.4MW(e) in 2022 with 20-50MW scale projects in 2023 and >100MW from 2024 onwards.

FIGURE 3

Electrolyser Efficiency for PEM, Alkaline and SOEC modified from Ceres Power SOEC Teach-in, July 1st, 2001 [8].

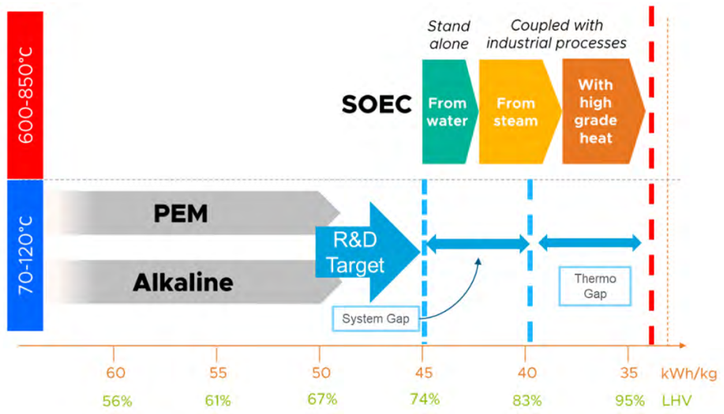

SOEC offers significant overall efficiency benefits when integrated with industrial applications such as steel or ammonia production. Due to the exothermic nature of the ammonia synthesis, it produces enough energy to supply >60% of the hydrogen needed for a facility if produced via SOEC. The efficiency gain vs. PEM/Alkaline is >30%, which is a major benefit when constrained by electricity, see Figure 3. In terms of capital expenditure, it is close to PEM/Alkaline electrolysis on a CAPEX $/kg of hydrogen. SOEC has a shorter stack life of 4-6 years vs. 8-10 years, so has a slightly higher maintenance burden equating to ~5-15% of original electrolyser module CAPEX. Also, unlike Alkaline, it has not been demonstrated at large capacities >100MW and has not yet generated operational experience yet. Despite this, the technology at the stack level is fundamentally the same as solid oxide fuel cells that have been in the market for a long time.

The developments occurring in the SOEC electrolyser space are focused on increasing cell life from 40,000 hours to >60,000 hours and reducing cost through improved cell architecture and materials. There are new SOEC technologies coming to the market in the mid-2020's using metal supported catalyst instead of ceramic supported, which have lower capital costs, better manufacturability, and improved cell life.

A useful comparison of electrical efficiency, which is one of the key parameters for lowering hydrogen production cost, is shown below:

TABLE 1:

Comparison of three main electrolyser technologies

Type	Specific System Energy	Stack Operating Life	Discharge Pressure	Ramp Rate	Specific CAPEX 2021	LCOH* In 2021 @30$/MWhe
Units	kWhe/kg	hours	Bar	Sec	USD/kgH2/h	USD/kg
Alkaline	50-60	80,000-100000	1-30	~30	~50,547	2.57
PEM	50-58	80,000	1-40	<2	~57,275	2.69
SOEC (Integrated)	38-41	40,000-60,000	0-2	>60	~33,014	1.78
SOEC (Elec. only)	44-46				~56,100	2.01

*LCOH stands for Levelized Cost of Hydrogen Production

The key outcomes of the comparison in Table 1 is that Alkaline and PEM electrolysers are close in performance and Levelised Cost of Hydrogen (LCOH). PEM provides the greatest flexibility in terms of ramp rates with a comparable specific energy to that of Alkaline. The specific electrical consumption of SOEC is ~30% lower when steam can be supplied. SOEC can be operated with an electric heater in the feed, which adds the latent heat of vaporization if no steam is available. This leads to an increase in specific energy consumption, which brings the LCOH more in line with Alkaline and PEM. It should be noted that the lowest cost electrolysers on the market are currently from China, reaching values as low as 30,400USD/kgH_2/h, which can lower LCOH to 2.25USD/kg.

2.2 INTEGRATION OF ELECTROLYSERS

There are many factors to consider when integrating an electrolyser into a brownfield site, including utility requirements, footprint, heat integration, and reliability.

Utilities: There are five key utilities to be considered:

- **Steam** – The loss of steam produced by the Steam Methane Reformer (SMR) will require consideration and will likely require the replacement of several pump/compressor turbine drives with electric motors.
- **Nitrogen** - Required for vent stack, the safe shutdown, and purging of the electrolyser plant, which can be supplied from the site or a new liquid N_2 storage and evaporation system.
- **Compressed Air** - The majority of the automated valves will be air operated due to the flammability risk of hydrogen.
- **Cooling Water** - As the electrolysers are not 100% efficient at low temperatures, significant amounts of heat may be discharged, typically 20-30% of the electrical load, depending on the amount of degradation of the electrolyser stack. Low-temperature electrolysers typically run at between 50-90°C, with a cooling water inlet of ~20-30°C. High-temperature electolysers, SOEC, have a much lower system cooling requirements due to the higher efficiency and heat recovery in the system which intrinsically requires heat input.
- **Feed Water** – Deionised and demineralized water purity grade is required for electroylser feedwater; therefore, water treatment is dependent on the source of water. In this case, a seawater reverse osmosis (RO) plant is utilized with the second pass of the RO plant feeding a mixed bed ion exchange (MBIX) or electro-deionization (EDI) plant to achieve the required demineralized grade water.

2.3 FOOTPRINT

The footprint of an electrolyser facility is primarily dependent on the technology selected. Table 2 shows the indicative sizes for different technologies based on the complete plant, single level, and a capacity of 100,000 tonnes per annum (TPA) of hydrogen.

TABLE 2:

Indicative required size for different technologies

Technology	Power Required MWDC	Power Density m2/MWDC	Footprint Hectares
Alkaline	647	101	6.5
PEM	647	69	4.5
SOEC (Steam)	459	100	4.6
SOEC (Elec)	541	101	5.5

A number of electrolyser plants are being designed to be housed in multistory buildings, allowing the footprint to be significantly reduced (e.g., by 25-30% for a two-story design).

2.4 HEAT INTEGRATION

Heat integration is only of benefit for SOEC-based electrolyser plants. Significant modifications are required to a brownfield DRI plant for full integration, allowing the highest electrical efficiency through the utilization of high-grade heat. As DRI plants are typically integrated with EAFs, it is possible to recover waste heat from the EAF off-gas system. The batch operation of the EAF requires a thermal buffer system. If there is more than one EAF onsite, then a single thermal store can be used to reduce the CAPEX and increase steam availability to the continuous level that is required for SOEC. A steam generator is then used to create a continuous supply of saturated steam at a temperature suitable for the SOEC system, typically saturated steam at 5 bar is required. As such, a single 150-tonne EAF could supply ~51tonnes/h of steam, depending on EAF operation. SNC-Lavalins' experience indicates that a system CAPEX of ~$20-25 million per EAF can be assumed for a waste heat boiler and accumulator system. An SOEC system typically has a steam-to-hydrogen ratio of 9-12kgSteam/kgH_2, with the ratio depending on the SOEC system design. Assuming a ratio of 9kgSteam/kgH_2, then a total hydrogen production from SOEC of ~5700kg/h can be realized from a single EAF. The hydrogen requirement for DRI production is between 47-68kgH_2/tonneDRI, assuming a value of 57.5kgH_2/tonneDRI, which is just above the stoichiometric amount required for hematite of 54kgH_2/tonneDRI[3], it is equivalent to 100tonne/h of steel or 0.88 million TPA.

2.5 RELIABILITY

A DRI plant requires a high level of reliability from the hydrogen supply. Electrolysers are inherently modular, and the cell stacks can range in size from a few kW to multi-MW. Hence, a hydrogen plant will be formed using 100's of cell stacks. Manufactures are increasing the size of the stacks to reduce CAPEX, with some of the largest single stacks being above 2MW.

The cell stacks degrade over time with degradation rates of between 0.5-2% per year, leading to increased specific energy consumption. However, SOEC has the ability to recover energy as heat giving virtually no increase in plant electrical consumption. As such, electrolyser plants can be designed with a small amount of additional capacity to allow isolation of either individual cell stacks or modules without impacting the production rate. Large-scale plants will typically utilise combined balances of plant supplying the electrolyser modules. The redundancy of cooling tower cells, pumps and valves, compressors, and transformers can be sufficient to allow for continuous hydrogen production in the event of a failure of one of these components. The highly modular nature of the electrolyser facilities and limited common modes of failure should yield an improvement in reliability over the traditional SMR.

2.6 EFFECT OF ELECTRICITY COST ON LCOH

The specific energy consumption and the specific CAPEX are the two critical parameters in determining LCOH. As shown in Figure 4, specific energy consumption is most impactful at electrical costs above 20USD/MWh. Higher electricity prices increase the benefits of higher efficiency as you can see SOEC has a lower LCOH than Chinese manufactured Alkaline systems. It should be noted that 100% utilization of the electrolysers is considered in developing this sensitivity analysis and no possible benefits from the utilization of oxygen or providing grid services have been considered.

FIGURE 4

LCOH of Technologies vs. Cost of Electricity

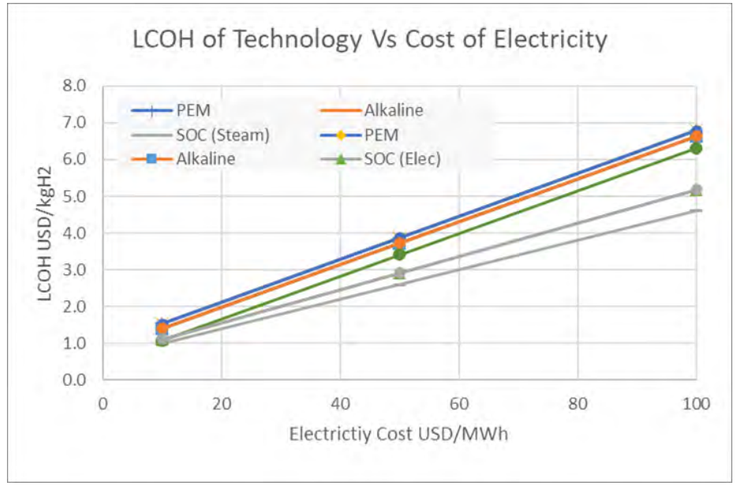

2.7 EFFECT OF CAPACITY FACTOR

A key contributor to the cost of hydrogen production is the availability of input electricity. Should a hydrogen production plant be fed purely by renewable power, assuming no electrical storage, it must be significantly oversized, and hydrogen storage utilized to accommodate the low-capacity factor. Table 3 shows an assessment of the effect of the power supply capacity factor on LCOH with three scenarios.

TABLE 3:

Effect of power supply capacity on LCOH

Case	Capacity factor	Required plant nameplate capacity MW for 100kTPA H_2
Solar PV	33%	303
Solar PV & Wind	68%	147
Renewables & Nuclear	100%	100

The effect of capacity factor on overall LCOH, without inclusion of hydrogen storage costs, is illustrated in Figure 5. It is evident that even when considering the lower electrical cost for Solar PV ($15/MWh) and Solar PV/Wind ($22/MWh) scenarios over the 100% capacity scenario ($28/MWh), significant savings can be obtained from maximizing capacity factor of the plant.

FIGURE 5

Effect of capacity factor on LCOH

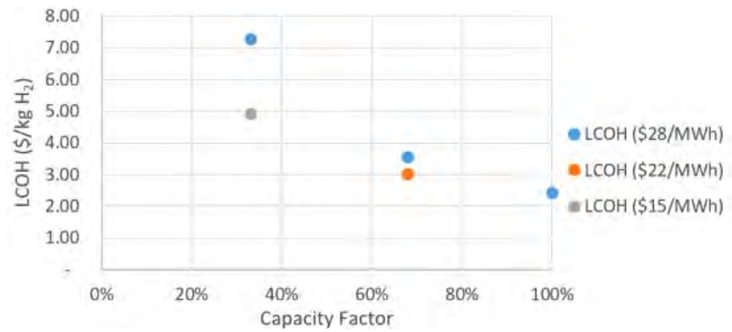

3. Value Stacking through Electrical Load Management and Benefits for Plants with Electric Arc Furnaces

Steel facilities operating EAF will have significant fluctuation in electricity demand, resulting from the intermittent operation of the EAFs. Electrolysers can alter production rates to offset these sudden fluctuations in steel facility power demand. Where electorlysers are used to provide grid support, additional electrolyser capacity is required. This allows the electroysers to cope with the additional production necessary to offset the largest steel plant drop in power consumption. To maintain continuous hydrogen supply to the steel plant, hydrogen storage is required.

Assessment of the benefits of electrolysers for a steel plant case with 100MW baseload electricity requirement and 100MW variable load, resulting from EAF intermittent operation, is examined in Table 4. Three cases were considered, each with the requirement for 100kTPA hydrogen fed to the steel plant. For these scenarios, the total EAF cycle time has been assumed to be 50 minutes with a 40-minute EAF operation time and 10 minutes shut down, prior to the start of the next cycle. The electricity price has been assumed to be $35/MWh.

TABLE 4:

Benefits of the electrolyser for a steel plant with 100MW base load and 100MW variable load in three different scenarios

	Base	Grid Support – no overload	Grid support -5% overload
Name plate electrolyser capacity (MW)	647	718	689
H_2 Storage Capacity (t)	–	5.1	5.1
Overall additional cost over 20 years (MM$)	-	43.9	28.2

4. Impact of using near 100% Green Hydrogen on the DRI Plant and the Necessary Adjustments Required

4.1 HYDROGEN FEED AND IT'S REACTION EFFECTS

DRI plants run with H_2 in the feed from 50-80 Vol%, depending on the vendor and plant set up. SNC-Lavalin's experience is that DRI plants with non-integrated reformers have the highest levels of hydrogen in feed, typically >70 Vol%. The metallization degree of the DRI has been found to be equivalent to the NG-DRI process route[4]. The thermodynamics and kinetics behaviors of iron oxide reduction with hydrogen have been examined by others[5], showing that hydrogen reduction has much faster reaction kinetics. At the operating temperatures of the reactor under study, both CO and H_2 gases have the same reduction potential. However, H_2 has a much higher effective diffusion rate of $5.835\times10^{4}m^2/s$ at 900°C vs. carbon monoxides diffusion rate of $0.124\times10^{4}m^2/s$. The diffusion rate difference is driven by the smaller molecular size of H_2 and the lower viscosity this allows reduction to occur quicker and at lower temperatures.

It is expected that the improved reactor kinetics from using green hydrogen will make it possible to increase reactor throughput. In the case study under investigation, an increase of approximately 10% may be achievable.

There are, however, issues with having no carbon in the DRI reactor. Firstly, steel is an alloy of carbon; Secondly, EAFs inject oxygen to remove carbon in the DRI this produces an energy input which is very efficient at heating the DRI to melting point. As such, no carbon in DRI will result in increased electrical energy consumption. There are other impacts and a good write up can be found in an article by Midrex[7].

4.2 EFFECT ON PLANT EQUIPMENT

The composition of the recycled gas from the reactor will change. Producing a composition at the outlet of hydrogen, water and some CO_2, depending on any NG injection in the reactor cone. The change in composition results in a much lower molecular weight gas at the compressor inlet leading to an increase in recycle compressor energy demand. As the compressor will typically be turbine driven from steam generated in the natural gas reformer then this will also need to be changed to an electrical motor drive.

The reduced level or possible elimination of CO_2 in the recycle gas will mean the CO_2 absorption system will either not be required or will have a reduced load. If there is a suitable location to sequester CO_2, then it is possible to have an increased carbon content in the DRI through injection of natural gas in the cone and reducing gas while still being able to achieve very low levels of CO_2 emissions.

Hydrogen temperature from the electrolysers will be dependent on the operating temperature, compression needs, and the amount of water that can be allowed in the feed to the reactor. The typical operating temperature is >1,000°C. However, with the improved reaction kinetics from using a high proportion of hydrogen, the operating temperature can be slightly lower ~900°C. Reducing gas temperature is therefore significantly above low-temperature electrolysis outlet temperatures which are <100°C. It is possible to reuse the recycled gas furnace that currently uses natural gas to boost the temperature. However, to mitigate the emissions, this would need conversion to burn some of the recycled hydrogen from the reactor or the installation of a new electric resistance heater. The use of SOEC technology for all or part of the hydrogen demand can reduce or eliminate the need for a preheater. There are ongoing studies at the University of California Irvine funded by the US Department of Energy[6] in this area of research.

5. Conclusion

Electrolysers can be effectively integrated into existing brownfield steel plants. The cost of electricity has a significant effect on project economics along with the capacity factor of the electricity supply, so both should be considered carefully.

Three major electrolyser types that are currently available in the market are Alkaline, PEM, and SOEC. A mixture of PEM and Alkaline offers the benefit of PEM quick response times and corresponding grid integration along with Alkaline technology maturity. As we approach 2030, SOEC is highly likely to take a larger market share as the technology matures and the significant efficiency benefits can be realized.

Higher hydrogen concentrations, provided by electrolysis, inside the DRI reactor improve reaction kinetics and allow the plant to operate at lower temperatures. These improved kinetics could also yield 10% additional DRI production.

When integrating an electrolyser plant into a brownfield steel facility, the key issues that need to be considered are reduction in steam production, impact on EAF operation, EAF heat recovery options, and utility requirements.

SNC-Lavalin has successfully completed a feasibility study for clean hydrogen supply to a world scale DRI production facility using hydrogen produced from electrolysis. As the findings in this paper show, SNC-Lavalin has excellent insight into the subject and is helping lead the way in the decarbonization of key industries.

References

1. EPRS, “Carbon-free steel Production”, [Online]. Available: https://www.europarl.europa.eu/thinktank/en/document/EPRS_STU(2021)690008
2. Midrex, “2020 World Direct Reduction Statistics”, [Online]. Available: https://www.midrex.com/wp-content/uploads/Midrex-STATSbookprint-2020.Final_.pdf
3. Fabrice Patisson & Olivier Mirgaux, “Hydrogen Ironmaking: How It Works”, Metals 2020, 10(7), 922; https://doi.org/10.3390/met10070922
4. Dario Pauluzzi et al., “CFD Study of an Energiron Reactor Fed With Different Concentrations of Hydrogen”, [Online]. Available: https://www.energiron.com/wp-content/uploads/2021/09/MARCH-2021_AIST-IRON-STEEL-TECHNOLOGY.pdf
5. Hai-bin Zuo et al., “Reduction kinetics of iron oxide pellets with H2 and CO mixtures”, [Online]. Available: https://www.researchgate.net/publication/282499310_Reduction_kinetics_of_iron_oxide_pellets_with_H2_and_CO_mixtures
6. DOE, “CX-101959: Solid Oxide Electrolysis Cells (SOEC) Integrated with Direct Reduced Iron (DRI) Plants for Producing Green Steel” [Online]. https://www.energy.gov/nepa/downloads/cx-101959-solid-oxide-electrolysis-cells-soec-integrated-direct-reduced-iron-dri
7. Midrex, “Impact of Hydrogen DRI on EAF Steelmaking” [Online] https://www.midrex.com/tech-article/impact-of-hydrogen-dri-on-eaf-steelmaking/
8. Ceres, “Electrolyser Teach In” [Online] https://wp-ceres-2022.s3.eu-west-2.amazonaws.com/media/2021/07/SOEC-Teach-in_FINAL-.pdf

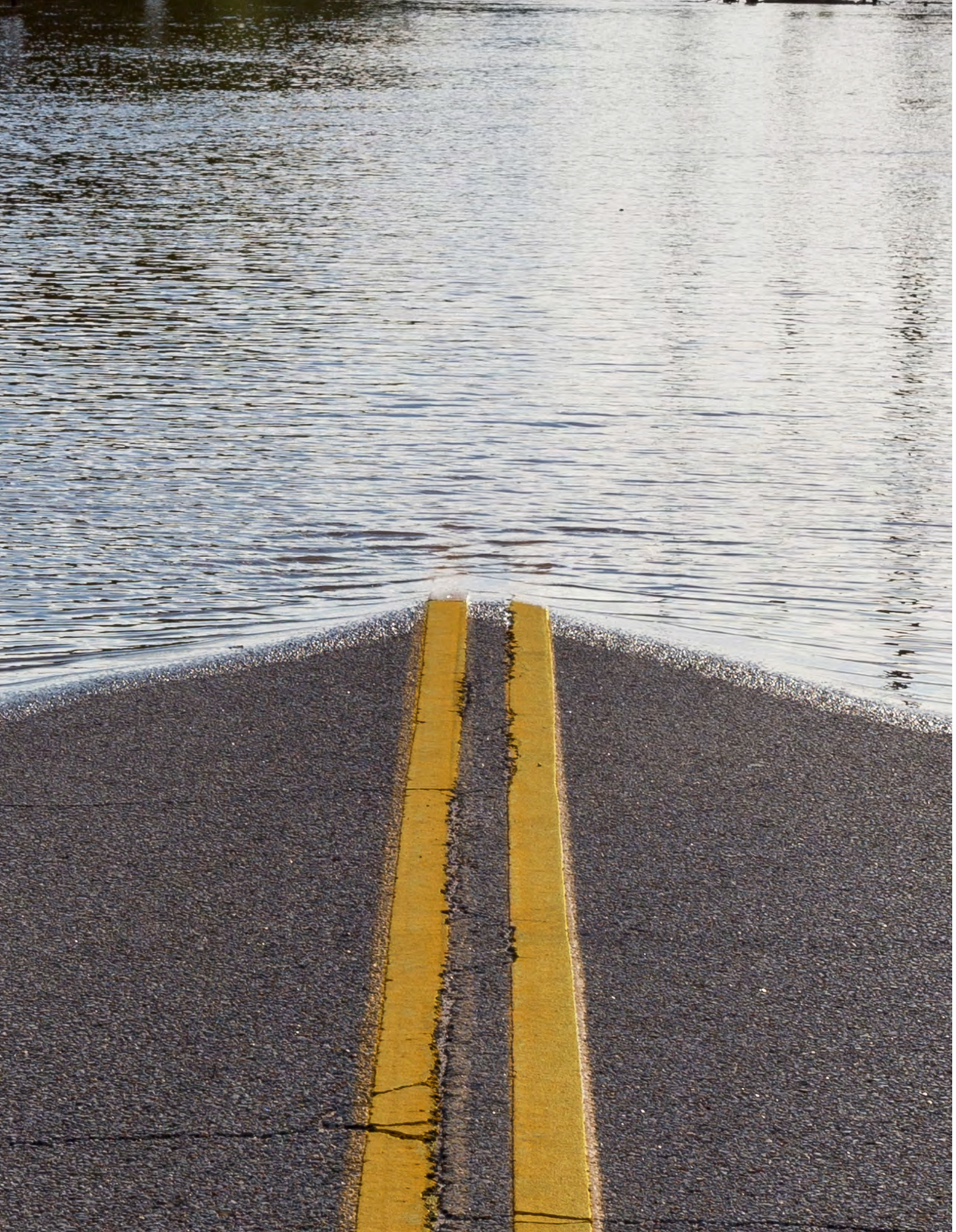

Stephen Bourne
Atkins Fellow, Project Director
Engineering Services USA
Rome, GA, USA

Amit Sachan
Sr. Project Director
Engineering Services USA
Raleigh, NC, USA

Environment, Carbon Reduction and Climate Resilience

04: The Digital Transportation Corridor – Quantifying Climate Change Impacts on the Transportation Corridor of Tomorrow

Abstract

As avenues for commuters, national freight arteries, recreational pathways, and critical means of egress during emergencies, transportation corridors provide invaluable support to today's businesses and travelers. Through Atkins' City Simulator resilience modeling tool, an Atkins team recently helped the North Carolina Department of Transportation (NCDOT) assess vulnerabilities along the 190-mile US74 corridor. The process consisted of creating a digital twin of the corridor, including all people, buildings, land parcels, roads, bridges, culverts, drainpipes, and other assets in the transportation system. Once created, the team simulated the digital corridor evolving from 2020-2060, including growth of buildings, infrastructure, population, and travel, as well as climate change influenced events like hurricanes, heat waves, and sea level rise. The result was a quantification of future vulnerabilities across the corridor at the level of each transportation asset. Leveraging the integrated discipline modeling, which blended flood, travel, heat impact, economics, asset lifecycle maintenance, and sea level rise into one model, key performance metrics like freight disrupted, commute trips disrupted, productivity lost, capital expenditures, and economic storm damage were all evaluated. A key set of metrics concerned disadvantaged populations, which are high poverty and minority groups that largely live in the rural areas along the corridor. Metrics related to their access to sustenance facilities (gas stations, emergency care, emergency shelters) were assessed and included in the results.

The results provided a unique foundation on which to try adaptation and mitigation measures like elevating bridges, hardening rail crossings, and enhancing road design methods to increase robustness. Corridor-wide scenarios were created and simulated with these measures in place. The result was a report, live web app, and online story map that will help NCDOT stakeholders reach consensus on actions they will take to increase corridor resilience in the future.

KEYWORDS
Climate Change; Resiliency; Transportation; Sea Level Rise; Equity

1. Introduction

Described as a "hurricane magnet" by NCDOT lead engineers and planners, US74 stretches 190 miles from Wilmington to Charlotte NC. It intersects with I-95 at the halfway point, a major north south interstate highway servicing 65,000 trips per day and millions of tons of freight. Experiencing two major hurricanes in the last five years – Matthew and Florence – this area is forecasted to experience even more intense and frequent hurricane activity in the coming decades (NCA4). An Atkins team recently used Atkins City Simulator resilience modeling tool to assist the North Carolina Department of Transportation (NCDOT) with assessing future vulnerabilities and explore adaptation and mitigation options. City Simulator was used to create a digital twin of the 20-mi wide corridor that included people, buildings, land parcels, roads, bridges, culverts, and drainpipes. It was then used to simulate future growth and climate change influenced disasters from present day to mid-century. Study questions focused on where future flooding will be most damaging to infrastructure, productivity, and freight; sea-level rise impacts; how future climate may impact disadvantaged populations; and what actions will both save on system operation costs and reduce downtime.

2. Methodoloy

The Atkins City Simulator tools is an Esri ArcMap extension. It implements an agent-based approach that simulates climate change impacts at the level of the corridor resident. The following sections describe the two primary steps of using City Simulator, creating the digital twin and conducting the simulation.

FIGURE 1

Simulation proceeds in a nest loop with annual growth happening once per year and daily storm, travel, commerce, and recreation happening once per day.

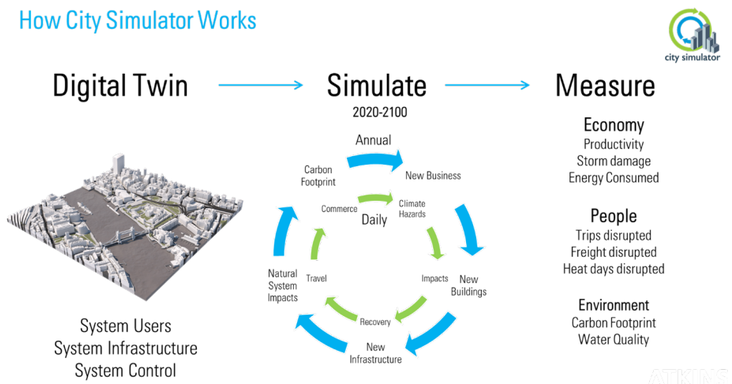

2.1. CREATING THE DIGITAL TWIN

As shown in Figure 2, the corridor digital twin includes system users, systems infrastructure, and system control. Starting with system infrastructure, the parcels, buildings, roads, utility systems, stormwater infrastructure (bridges, culverts, drainpipes), and hydrography (rivers, streams, waterbodies), and elevation data are loaded to a specially designed Esri City Simulator geodatabase.

To simulate how these digital twin elements will respond when heatwaves and floods happen, City Simulator leverages existing models. This not only speeds up the process of creating the digital twin, but it results in a significant reduction in project costs. A flood response curve is extracted from the existing flood model results to depict for each individual building or transportation asset the level of flooding that occurs for a range of storm sizes. During simulation, these curves are then used to estimate flooding levels as storm events occur.

The flood models used in the US74 study included:

- Riverine 1D HEC-RAS models from the Federal Emergency Management Agency (FEMA),
- 2D HEC-RAS Rain-on-Grid (ROG) models from NC Floodplain Mapping Program,
- Telemac2D pluvial rain models from Atkins (Kipp, 2016), and
- ADvanced CIRCulation (ADCIRC) plus Wave Height Analysis for Flood Insurance Studies (WHAFIS) models for coastal surge and wave action modeling.

System users are people, or agents. Using census block group level statistics of population, jobs, households, and commute times as well as travel demand models from NCDOT and corridor municipal planning organizations (MPOs) with the same information, a digital population of avatars was allocated to buildings in the corridor (Figure 1). The allocation gives each agent a home, workplace, and commute path through the road network.

System control constitutes rules governing build out of the digital twin in the future. Zoning rules, building codes, and existing policies are included.

FIGURE 2

The US74 Digital Twin

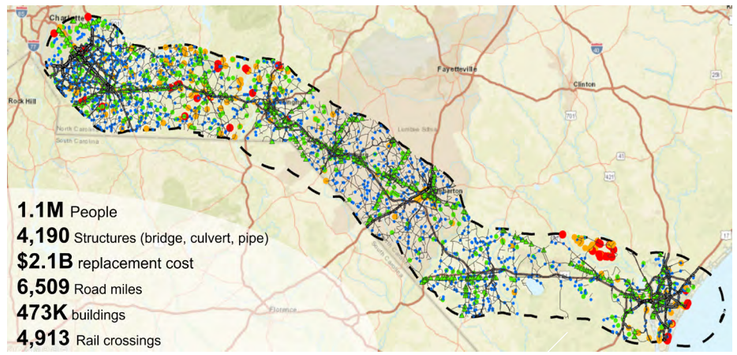

2.2 FUTURE SIMULATION IN A NESTED LOOP

Referring to the center diagram in Figure 1, the primary simulation algorithm works as a nested loop, running annually in the outer loop and daily in the inner over the 2020-2060 timeframe.

The annual loop simulates urbanization of the corridor. Beginning with a single-year projection of economic growth in the city based on growth in the past three years, it estimates a number of new commercial buildings that will be added over the next 12 months. Using an algorithm similar to GIS suitability analysis (Bourne, 2007), the commercial buildings are placed in the most highly likely development locations. Businesses and workers are added to the commercial buildings. Residential buildings to house the new workers are then added, also using the suitability analysis approach. The workers are then given families, spouses and child agents. Once placed on the landscape, road and utility networks are expanded to provide service to the new buildings. Then, impacts to the floodplains and ecosystems are evaluated. Carbon footprint is also evaluated, which includes greenhouse gas (GHG) emission estimates for vehicle travel and for building operations.

2.3 DAILY LOOP

Climate change-influenced events hitting the corridor are simulated in the daily loop, as are travel, work, commerce, and recreation activities. Driven by a projection of future weather created from general circulation models (GCM) rain and temperature projections, the loop integrates the climate change signal. These projections are created using a process called downscaling. Designed to blend the projected changes in climate with historical weather data, the process starts with UNIPCC CMIP5 monthly projections of rain and temperature from multiple models as an ensemble. The ensemble uses either the RCP4.5 or RCP8.5 GHG emission scenarios (NASA 2022), the former representing a globe that is trying to control GHG and the latter a globe that is operating as it does today, with no additional GHG control. Using historical data in addition to the GCM projections reflects both a realistic depiction of local micro-climates while also embedding the change in weather statistics that the GCM results project.

The daily loop checks for heatwave and flood events. If an event occurs, the tool identifies which assets in the digital twin are impacted. The severity of the event determines the duration that the asset is disabled and unusable by corridor residents (see Figure 3).

FIGURE 3

Process for estimating cost of damage to transportation infrastructure assets.

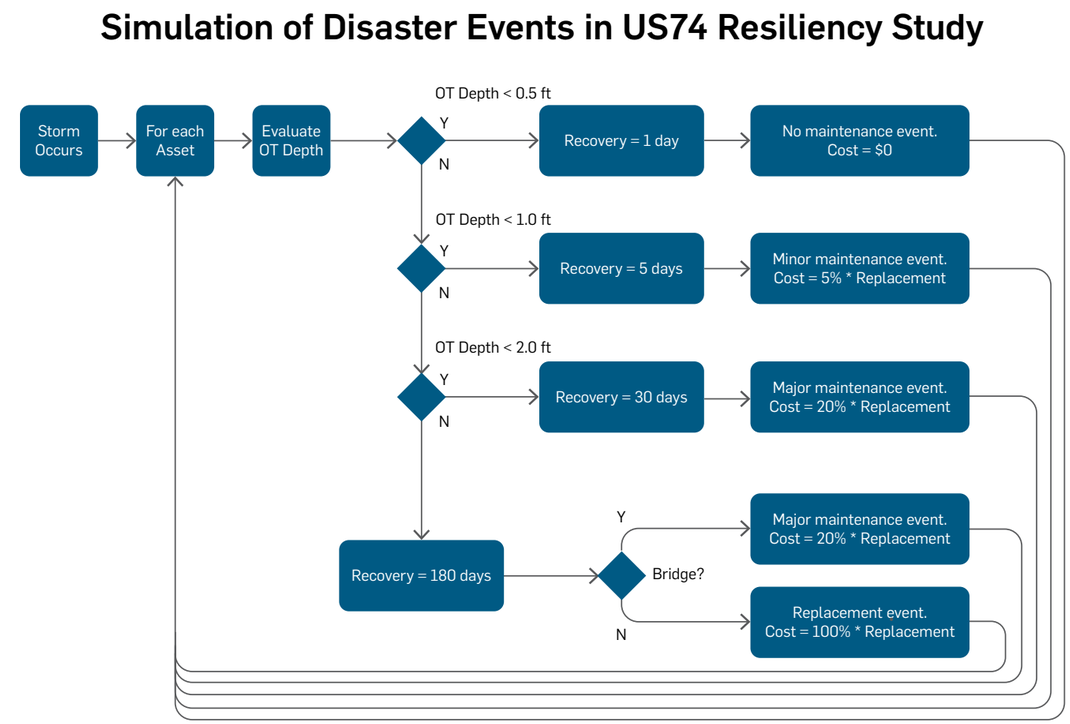

2.4 SIMULATING FLOOD EVENTS

FEMA HAZUS depth-damage curves are used to estimate the economic cost of building damage. For transportation assets, the level of overtopping at the road supported by a bridge, culvert, or drainpipe is translated into a level of damage. For example, six inches of overtopping may result in a simple stoppage of traffic with no monetary damage, while three feet of overtopping may be assumed to completely wash away the culvert and overlying road, resulting in a total replacement cost of the asset to restore transportation service.

When a building or transportation asset is damaged, a recovery period in days is assigned and the asset is removed from services for the course of the recovery period. For the prior example, six inches of overtopping may result in two days of impassability on the road, while three feet may result in 180 days where the road is unusable.

2.5 SIMULATING HEAT IMPACTS

Heat events are simulated similarly to flood events. The focus is on the so-called "flushing" phenomenon, which occurs over the typical 20-year lifespan of a road's asphalt wearing layer. When temperatures are high enough, the bitumen in the road loosens. When this occurs, the aggregate in the road becomes susceptible to being pulled out by over-riding vehicle tires. The result is a concentration of bitumen on the road surface, which reduces skid control. The result is a slowdown in traffic, which the simulator counts as a disruption to daily trips.

As flushing is a progressive phenomenon - happening over a period of years - the driving factor for flushing is heating degree days, as this factor measures cumulative exposure to heat. As an example, a year where maximum temperature is 100F every day would result in heating degree days of 100F × 365 days = 36,500 degree-days. Following the probabilistic model created for rail buckling events created by Chinowsky (2019), a simple model was developed that assumed that an average 20-year lifespan road would have non-zero probability of flushing condition at one third of its lifespan, or 6.67 years if the road was steadily subjected to an average maximum daily temperature of 85°F each day. This implies an approximately 200,000 heating degree day threshold for probability of flushing to move above zero. We further assumed that the probability of flushing would increase to approximately 20% by its 20-year lifespan if subjected to the same average maximum daily temperature. We used the following relationship to quantify the probability of flushing as heating degree days increase (see Figure 4).

FIGURE 4

Heat events are simulated in a probabilistic model that assigns exponentially increasing probability of a so-called flushing event as heating degree days exceed approximately 400,000.

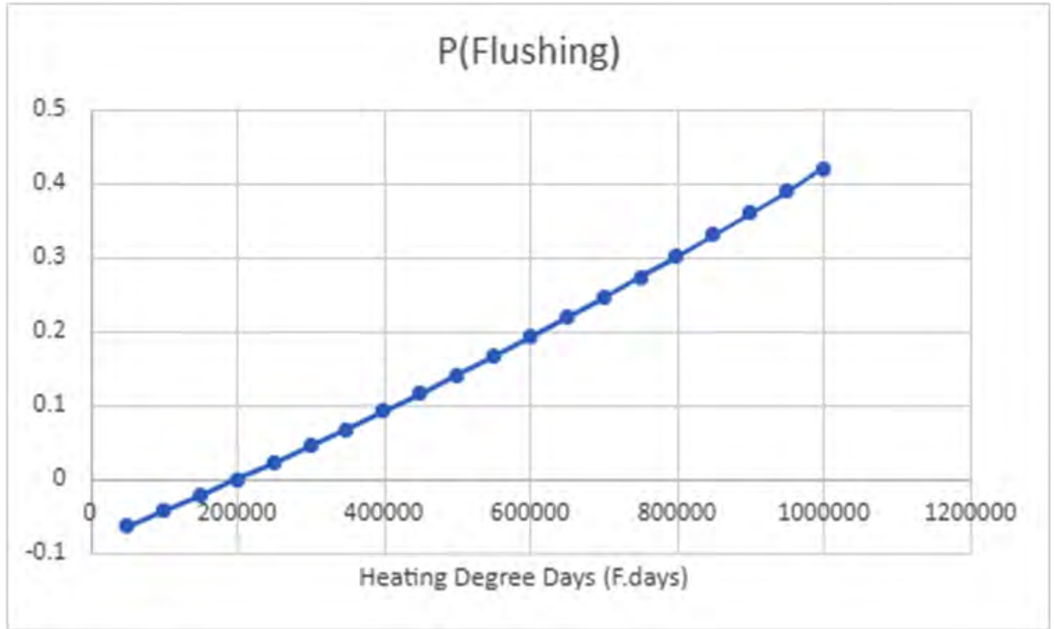

$$P(Flushing) = 33^{\frac{Heating\ Deg.Days - 100000}{100000}/25} - 1 \qquad (1)$$

During the simulation, each road in the system has a heating degree day accumulator, which sums the maximum temperature each day since the last road maintenance event. When heating degree days reaches the 200,000 degree-day threshold, the probability of flushing is estimated using Equation 1. A uniformly-distributed random number is then generated from 0 to 1. If the number is lower than the probability of flushing, flushing is assumed to be present on the road. When this occurs, a disruption event is recorded in the simulation. In reality, this disruption may range from no change in traffic speeds to a controlled slowdown with traffic directed to the sides of the road to avoid low-traction areas. For simplicity and performance needs, the simulation did not represent this range of eventualities, assuming any event where flushing is present is a disruption. Future enhancements may assume the level of disruption as a function of the heating degree days for the road, but calibration data will be required.

Intuitively, as maximum temperature increases with climate change, the simulation found an increase in flushing across the transportation corridor, with flushing occurring earlier in each road's lifespan moving into the future.

Other than flushing, heat has several other avenues for impacting transportation infrastructure. They include:

- **Blow-outs** – water trapped under asphalt roads may boil, causing the overlying asphalt to erode and crack.
- **Concrete Road Buckling** – when thermal expansion at temperatures beyond design temperature causes road sections to compress against each other and buckle.
- **Rail Buckling** – when thermal expansion at temperatures beyond design temperature causes rail sections to compress and buckle.

Each of these phenomena impact speed of traffic similarly and can be modeled with an exponentially increasing probabilistic model such as the asphalt flushing model described above. In this study, roads were assumed to all be asphalt construction and rail buckling was not simulated. Future studies may include these phenomena.

2.6 SIMULATING SEA LEVEL RISE

Mean sea level is projected to rise in Wilmington, NC between 1.28ft and 2.26ft relative to the current mean higher high water (MHHW) (National Oceanic and Atmospheric Administration (NOAA) Sea Level Rise Viewer). This will cause both chronic disruptions in the form of nuisance flooding during high tides and acute disruptions, as the impact of storm surges will be exacerbated by higher mean sea levels.

The rationale for modeling sea level rise in the simulation was to produce a daily projection of high and low tide levels and to estimate the impacts of both tidally-driven nuisance flooding and tidally influenced storm surges when these flooding events occur in the simulation.

The projection of tide was created by superposing: 1) projected mean sea level from NOAA, 2) predicted tide fluctuations from gravity effects from entities like the sun and moon, and 3) variations from predicted tide fluctuation caused by local phenomena like wind and river flows.

2.7 SIMULATING NUISANCE FLOODING

To simulate nuisance flooding events, each road segment was assessed against the projected high tide level each day in the simulation. When flooding did occur, a disruption was recorded for the asset impacted. Buildings were not assessed within the simulation, only road segments. Assessing impacts on individual buildings can be incorporated into future simulations if desired. A key measurement impacting the simulation was the elevation of the road segment above which overtopping, and road disruption occurs. To estimate this elevation, each road segment was measured for elevation at a 30m interval along the road centerline. The minimum elevation along the road segment was retained as the overtopping elevation of the road segment. Through this definition, the simulation implicitly assumes that if any part of the road segment overtops, then all trips along the road segment are disrupted. This may not be true as real trips may only use a portion of a road segment. The assumption was retained, however, to ensure that any level of disruption is captured in the simulation results.

Recognizing that high tide levels that do not overtop road segments can still have an impact by inundating the road structure with seawater, a so-called "freeboard flooding" metric was also introduced to the simulation. This metric essentially recorded disruptions in the same way as the overtopping metric but set the overtopping threshold as the road segment's overtopping threshold minus two feet. The simulation results present both the nuisance flooding metric and the freeboard flooding metric.

2.8 SIMULATING SEA LEVEL RISE IMPACT ON STORM SURGE

Acute impacts of rising sea levels will come in the form of storm surges sitting atop elevated mean sea levels. An ADCIRC model was combined with an EPA WHAFIS model to estimate the depth of flooding in the coastal region of the corridor for 10, 50, 100, 500, and 1,000-year events. The depth rasters produced for each return period were then sampled at the low points of each road segment to produce a return period to the overtopping depth curve for each road. When large storm events occur during the simulation, these curves were used to rapidly estimate overtopping depths at each road, and thereby estimate disrupted trips.

The ADIRC+WHAFIS model-based estimates are configured with the assumption of mean sea level in 2020 as a boundary condition. As the sea level rises, this assumption causes the estimates of inundation to become increasingly under-estimated. A more accurate estimate can be found by re-running the ADCIRC+WHAFIS models with a varying range of mean sea level and then using the appropriate version of the model based on the estimated mean sea level at the time of the future event. As running multiple ADCIRC+WHAFIS models was beyond the scope of this study, a more approximate method was used to estimate inundation during future storm surge events. Namely, in each year, the projected increase in mean sea level relative to mean sea level in 2020 was calculated. If a storm surge event occurred in that year, the depth of inundation in the flood response curve was augmented with the estimated sea level rise projection.

2.9 KEY PERFORMANCE METRICS

The 2020 – 2060 timeframe was selected by the study stakeholders because it aligned with existing master plans created by NCDOT as well as the municipal planning organizations (MPOs), counties, and local municipalities along the corridor. Stakeholders from these organizations, including multiple divisions from NCDOT, the FHWA, and the military, determined the key performance metrics to be used, which ensured the metrics would best inform existing stakeholder decision-making.

The metrics included:

- **Assets Disrupted** – this is the percentage of the transportation assets overtopped when a storm event occurs.
- **Lost Productivity** – this is the total salary not earned by agents because they are not able to make it to work because their home, workplace, or commute path are disabled from storm damage.
- **Storm Damage** – this is the dollar value required to repair assets (buildings or transportation assets) damaged by storms.
- **Asset Spending** – this is the spending on transportation assets (bridges, culverts, and drain pipes in the US74 study) for storm damage, regular maintenance, and master planned projects. The insertion of a maintenance event in the simulation was triggered by fitting each major asset with a decay curve, which projected the condition of the asset in each year. Using this approach, each asset in the system was replaced approximately every 75 years, with minor and major refurbishment events at 30 and 50 years. The cost of each minor and major refurbishment events was assumed to be a fraction of the replacement cost of the asset. The fractions were set using a ground-truthing calibration process, where total spending on storm damage, maintenance, and master planned projects was queried from the NCDOT asset management system for the corridor assets from 2010-2022. The fractions were set to ensure that on an annual average basis, there was a match in spending.
- **Asset Condition** – this metric was the number of assets within each of four condition categories, “good”, “fair”, “poor”, and “failing.” The assets would move from good to failing over the course of their lifespans as described in the asset spending metric above.
- **Disrupted Trips** – this metric was the number of commute and other trips disrupted by a transportation asset when a storm event or heat event occurs.

- **Disrupted Freight** – this metric was the tonnage of freight that was disrupted when a storm or heat event occurs. The tonnage was evaluated by simulating heavy trucks specifically and converting the number of trips to tonnage using a national average tonnage per truck. Rail freight was also evaluated, though tonnage of rail freight was considered a sensitive metric. As a result, this metric was replaced by the number of times rail crossing are inundated with flood.
- **Long Disruptions** – hurricanes Matthew and Florence showed NCDOT that extreme flood events can result in extremely long disruption events, which leave traffic disrupted for months. This metric measures the number of assets that experience 180-day or longer disruptions.
- **Disadvantage Population Accessibility** – A key focus in the study was on disadvantaged populations. Defined through NCDOT's Title IV specification as census block groups with high minority and poverty populations, the accessibility of agents within these areas to sustenance facilities like gas stations, shops, emergency care, and schools (assumed to be emergency shelters) was evaluated. This was done by identifying routes from these agents' homes to the sustenance facilities and assessing how often these routes will be disrupted by flood and heat events in the future.

Corridor-level metrics were evaluated on a daily or annual basis by summing the individual experiences of system agents. The metrics were initially evaluated as an annual time series, but to collapse to an annual average to compare one scenario to another.

2.10 EVALUATING ADAPTATION AND MITIGATION OPTIONS WITH A SCENARIO APPROACH

To enable measuring the resilience that adaptation and mitigation options will bring, a scenario-based approach was used.

The baseline scenario consisted of all projects in the current transportation master plan from 2020-2030. After 2030, it was assumed maintenance events driven by decay curve-based condition simulation accounted for all corridor upkeep projects. The scenario also included climate change-influenced projections of future storms and heat. The goal was to simulate how the corridor would be managed over the next forty years under current policies.

The resiliency scenario added mitigation and adaptation options to the baseline, adjusting requirements for regular maintenance events. For example, when a replacement event occurred, the subject asset would be elevated to the 2020 500-year flood level. Similarly, rail crossings were hardened to ensure that future overtopping disrupted rail for shorter periods of time in the future. The replacement was prioritized by working first on assets that cause the most future disruption. The additional cost was estimated for these resilience-focused projects and allowed for comparison of the scenarios.

3. Results

Multiple findings resulted from the simulation. As of the time of writing, the specific metric values are still under review, and are therefore not published here. General descriptions of the findings are listed below.

3.1 FINDINGS

1. A 42% increase in disrupted trips from heat, riverine and pluvial flood, and sea level rise flood, is expected across the corridor by 2060.
2. US74 has several locations that are vulnerable to future flood, though the highest vulnerability is in the road network connecting to US74.
3. Large storms have increased dramatically over the last several decades and will continue increasing into the future.
4. Maximum temperatures will rise steadily across the corridor, pushing the number of days above 90 degress F to more than three times higher than 2020. This will increase disruption to road and rail traffic.
5. I-95 and supporting roads are vulnerable to future floods close to US74.
6. In the coming 40 years, future floods are likely to disrupt millions of trips per year, causing millions of dollars in lost productivity among commuters each year.
7. Millions of tons of freight are likely to be disrupted by flood and heat each year.
8. Maintenance of the system of bridges, culverts, and pipes will cost approximately $4.5M per year across the corridor in the coming 40 years. Future floods will drive maintenance cost higher.
9. Coastal roads in Wilmington will be covered by sea water 60% more in 2060 than in 2020 on average.

3.2 IMPACTS OF FOCUSING ON RESILIENCE

The resilience-focused scenario both 1) adjusted existing planned projects like replacing interchanges and bridges to ensure the projects could handle up to the 500-year event, and 2) added resilience focused projects not yet envisioned in the master plan to manage the worst future disruptors in the transportation system. Though specific results are not available at of the time of writing, the reduction in disruption is expected to be significant, resulting in similar disruption levels across the 2020-2060 timeframe when compared to those experienced today.

4. Discussion

Creating a digital corridor and simulating it into the future with climate change resulted in a highly detailed and quantified dataset providing a depiction of what climate change impacts will be on each asset in the NCDOT system. The results showed that keeping the status quo in terms of current maintenance approaches will not keep up with disruption from climate change. A focus on resilience is needed that will require spending more on asset maintenance but will keep climate change impacts at bay.

References

- 2022 - NOAA - Sea Level Rise Technical Report: Download and FAQs (noaa.gov) https://oceanservice.noaa.gov/hazards/sealevelrise/sealevelrise-tech-report-sections.html
- 2018 – National Climate Assessment 4 – Vol II. Impacts, Risks, and Adaptation in the United States. https://www.globalchange.gov/nca4
- 2016 – Kipp, Max. Nationwide (USA) Pluvial Flood Modeling via Telemac2D https://www.nrc.gov/docs/ML2106/ML21064A445.pdf
- 2007 – Bourne, Stephen. Microsoft PowerPoint - ARC TAZ Disaggregator.ppt (ampo.org) https://www.ampo.org/assets/604_arctazdisaggregator.pdf
- 2022 – NASA SVS: CMIP5: 21st Century Temperature and Precipitation Scenarios (nasa.gov) https://svs.gsfc.nasa.gov/4110
- 2019 - Paul Chinowsky, Jacob Helman, Sahil Gulati, James Neumann, Jeremy Martinich. Impact of Climate Change on Operation of the US Rail System. Transport Policy, 2019.
- 2018 – Extreme heat causes pavement buckling issues across the state - Radio Iowa

Daniel Damov, M.Sc.A., P.Eng.
Senior Hydraulic Engineer
SNC-Lavalin Inc.
Montreal, QC, Canada

Joe Groeneveld, M.Eng., P.Eng.
Senior Hydraulic Engineer
Hatch
Calgary, AB, Canada

Greg Saunders
Manager, Marine Barriers
Revelstoke Design Services Limited
Winnipeg, MN, Canada

Clyde McLean, MASc, MBA, P.Eng.
Area Manager River Operations, Muskrat Falls Project
Lower Churchill Management Co.
St. John's, NL

Greg Snyder, FEC, P.Eng.
Engineering Manager, Muskrat Falls Project
SNC-Lavalin Inc
St. John's, NL, Canada.

05: Muskrat Falls River Ice Management During Construction: From Design to Implementation

Abstract

As part of the Lower Churchill Project (LCP), the Muskrat Falls Hydroelectric Development is located on the Churchill River, about 291km downstream of the Churchill Falls Hydroelectric Development which was developed in the early 1970's. The facility consists of a 824MW powerhouse located on the south side of the river, a gated spillway constructed adjacent to the powerhouse and a dam connecting to the north bank acting as an overflow spillway. Under natural conditions, a large ice dam was forming downstream of the Muskrat Falls. The considerable influx of frazil ice generated in the upstream reaches of the Lower Churchill River combined with a deep pool area immediately downstream of Muskrat Falls created conditions for ice accumulation and jamming. The flow restriction at the ice dam has an impact on the water level at the Muskrat Falls project site, with a backwater effect that can cause the water level upstream of the ice dam to rise significantly, in some years by more than 15metres, drowning out the Lower Falls and sometimes the Upper Falls as well. This paper presents the various aspects that were taken into consideration for successful ice river management at Muskrat Falls, from the initial pre-project desktop analyses to the conditions experienced during the first two years of river diversion. The challenges and constraints that were met during the implementation and optimization of the plan are also discussed in the paper.

KEYWORDS
Hydroelectricity; Dams; River ice management; Churchill River

1. Background

As part of the Lower Churchill Project (LCP), the Muskrat Falls Hydroelectric Development is located on the Churchill River, about 291km downstream of the Churchill Falls Hydroelectric Development which was developed in the early 1970's. The installed capacity of the Muskrat Falls facility will be 824MW (4 units of 206MW each). The facility consists of a powerhouse located on the south side of the river, a gated spillway constructed adjacent to the powerhouse and a dam connecting to the north bank acting as an overflow spillway.

Under natural conditions, the river reach upstream of the project site remained open all winter, and a large ice dam was forming immediately downstream of Muskrat Falls. The considerable influx of frazil ice generated in the upstream reaches of the Lower Churchill River combined with a deep pool area downstream the falls created conditions for ice accumulation and jamming. The formation of this ice dam has an impact on the water level at the Muskrat Falls project site. Under natural conditions it was creating a backwater effect causing the water level immediately downstream of the Lower Muskrat Falls (and between the falls) to rise by more than 15m.

A theoretical approach for managing river ice at the project site was studied which involved the creation of a pond upstream of the project site by raising the water level in this river reach. This increase in level reduced the velocity of the river flow and allowed a competent ice cover to form upstream of the project. The ice cover then limited the amount of ice generated in the upstream reach, and provided an upstream area for deposition and storage of the influx of frazil ice generated in upstream reaches. An exhaustive plan for the ice river management during construction prior to river closure was developed based on these analyses.

The diversion of the Churchill River at Muskrat Falls took place in the fall of 2016. Several additional project constraints forced the modification of the initial ice management plan, but an ice cover was successfully formed and it functioned as anticipated. The experience gained during the ice management in winter 2016-2017 confirmed the theoretical approach. It also provided insights for the optimization of the approach based on observations and data collected during that winter. Subsequently, an updated plan for river ice management for the 2017 2018 winter was developed and implemented.

This paper presents the various aspects that were taken into consideration for successful river ice management at Muskrat Falls, from the initial pre-project desktop analyses to the conditions experienced during the first two years of river diversion. The challenges and constraints that were met during the implementation and the optimization of the plan are also discussed in the paper.

2. Typical Mid-Winter Ice Conditions

The Churchill River varies along its length from very narrow channels with high velocity flow and super critical hydraulic regimes, to large lakes with relatively low flow velocities. During the winter, the narrow channels remain open with only a small amount of shore ice. In other areas, where velocities are low, shore ice, or border ice will grow to a significant extent each winter. The large lakes typically become ice covered and experience mechanically thickened ice accumulations (ice jams) at many of the inlets. Frazil ice generated in the open water area is responsible for the formation of these ice jams.

Frazil ice consists of very small ice crystals which are formed in super-cooled water (water temperature below 0°C). It is generated when open water comes into contact with cold air. This causes the temperature of the water to decrease rapidly and the water to become super-cooled.

There are two different types of frazil ice: active and passive. Active frazil ice is defined as freshly formed frazil ice crystals dispersed in super-cooled water and which are actively growing in size. In this condition, frazil ice will adhere to underwater objects such as intake trash racks or rocks. When the frazil ice is attached to the riverbed, it creates "anchor" ice.

Normally, frazil ice will remain active for a period of about 10 to 15 minutes after being submerged under an ice cover, i.e. the time required for the water to return to 0°C or slightly above. Active frazil ice, however, has also been observed after travelling for more than one hour under an ice cover.

FIGURE 1

Frazil ice observed on the Churchill River near Muskrat Falls in March, 2011

Passive frazil ice occurs once the temperature of the water returns to 0˚C or above and the frazil ice crystals stop growing; they become inactive (passive). Passive frazil ice loses most of its adhesive properties and is less troublesome than active frazil ice, but can still accumulate. Passive frazil ice will still grow into large pans and/or ice sheets at the surface of the river, and these large pans and sheets can be observed floating at the surface. River ice jams can be created by the migration downstream of these large ice volumes.

3. Theoretical Approach for Ice Management

3.1. ICE FORMATION AND ICE FORMATION CRITERIA

There are different types of ice cover and different criteria are required for the formation of each type. There have basically been two types of ice cover observed at the Muskrat Falls site – a thermal ice cover and a dynamic ice cover. Each are further described below.

3.1.1 THERMAL ICE COVER

A solid layer of ice will form very quickly over a water surface once the air temperature drops below 0˚C in areas with very low velocities (less than 0.2m/s). This solid ice cover will then grow vertically through a thermal process. The ice cover may also form through a process known as bridging, and then advance upstream through a process known as juxtaposition when the river velocity is low (less than 0.65m/s) and the Froude number is less than 0.08. Ice cover formation by bridging occurs at very low flow velocities and relatively high concentrations of surface ice when the incoming ice volumes spontaneously arch across the open width of the channel.

At the velocities and Froude numbers quoted above, the cover will form as a single layer of pans, which will quickly freeze together and begin to grow vertically downward through a thermal process. The advancing and thickening thermal ice cover will serve to cut off or greatly reduce the supply of frazil ice from upstream reaches. Frazil ice does not normally form when a thermal ice cover is present due to the insulation properties of the cover which separates the water from the cold air.

3.1.2 DYNAMIC ICE COVER

When the velocity of flow is greater than 0.65m/s, more dynamic ice processes will begin to occur. This can include ice cover formation via shoving or deposition in a hanging ice dam.

Ice formation via shoving can occur at a wide range of flow velocities. The ice cover will collapse in the downstream direction and becomes thicker as the forces acting on it exceed its ability to withstand those forces. The strength of an ice cover formed from many separate pieces of ice increases with its thickness, so that when shoving takes place, the strength of the ice cover is increased. An ice cover may repeatedly shove and thicken as it progresses upstream.

Ice dams often form at the base of a set of natural rapids, where velocities and Froude numbers in the channel are too high to allow the ice cover to progress upstream. In these situations the ice accumulates in a very large ice dam at the base of the rapids, constricting the channel and leading to significant backwater level increases. This will continue to occur until the resultant staging that it creates is sufficient to allow the cover to progress through the upstream high velocity area.

The large ice dam that forms each year below Muskrat Falls forms through a process of deposition and shoving. As shown in Figure 2 below, the river remains open upstream of the falls for a considerable distance upstream, and ice generated in the long open water reach passes through Muskrat Falls and accumulates at the base of the falls in a pool that is up to 60m deep. This leads to the formation of a massive ice dam each winter (Figure 2).

FIGURE 2

Site of Muskrat Falls with location of ice dam, March 2011

3.2 PROPOSED ICE MANAGEMENT APPROACH

The ice management approach adopted to reduce (and eventually eliminate) ice dam formation downstream of the Muskrat Falls project consists of cutting off and trapping the frazil being generated in the upstream reaches of the Churchill River. This can be achieved by creating an ice storage capacity upstream of Muskrat Falls, along with a stable ice cover that will reduce the length of frazil generating reaches. The combined impacts of ice storage and ice generation reduction will help to ensure that no ice will be transported into the downstream reach, reducing potential stage increases. By raising and controlling the reservoir level upstream of the project site, flow velocities are reduced and it will promote the formation of a stable upstream ice cover.

3.3 ICE STUDY

An ice study to establish the required headpond water elevation was carried out using a one dimensional ice simulation model. The model was used to analyse this complex phenomenon by simulating two separate river reaches of the Lower Churchill River. The upstream model (between the outlet of Lake Winokapau and the outlet of Gull Lake) was used to develop conservative estimates of the total volume of ice that could be generated in this very long reach, and the volume expected to pass through Gull Lake down into Sandy Lake. Because of its deep invert, Gull Lake will quickly form a surface cover each winter, and then acts as an efficient repository for any ice generated upstream of Gull Island Rapids. It was determined that a significant volume of ice is not passed through Gull Lake until partway through the winter (approximately mid to late January). Prior to this, the ice tends to collect within Gull Lake, and it does so until the lake's ability to "store" ice has been exceeded. The estimated volume of ice passing through Gull Lake, as determined from the upstream model, was then used as input to the downstream model which extended from the outlet of Gull Lake (or just upstream of Sandy Lake) to the Muskrat Falls cofferdam. Any ice passed from the upstream reach was provided as an incoming ice volume to the downstream model, and was allowed to accumulate and contribute to the downstream ice cover.

The 1:20 annual exceedance probability (AEP) monthly flows were simulated for a severe climate winter (1972-73), and for this case the downstream water level was iteratively increased to determine the minimum required water level at the Muskrat Falls cofferdam to initiate a stable ice cover upstream. This water level was determined to be 25m and is governed by a constricted hydraulic condition in the approach channel just upstream of the cofferdam, and not by the total volume of ice generated. Figure 3 presents the simulated end of March ice cover profile along the modeled reach for the winter of 1972-73. As shown, the profile includes a significant accumulation of ice at the upstream end of the reach (upstream of approximate chainage 70km).

FIGURE 3

End of March profile:
25m forebay level, severe
winter (1972-73)

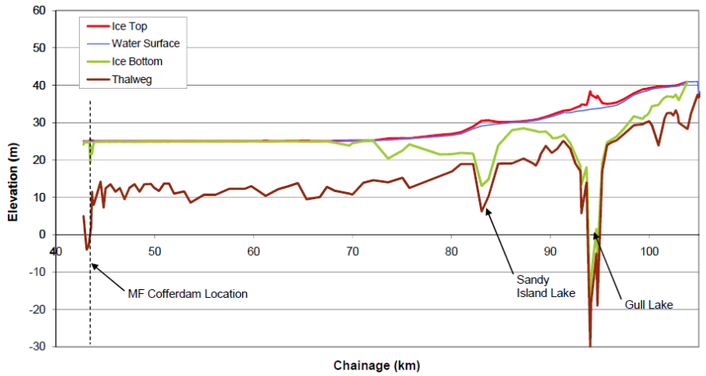

It should be noted that for that winter, the model predicts a small accumulation of ice appearing just upstream of the construction site, at the narrowing of the river at Upper Muskrat Falls (approximate chainage 44km). The constriction is created by the physical narrowing of the river channel just upstream of the project structures. This narrow channel increases the velocity through this short reach, and this in turn increases the hydrodynamic forces applied to the cover and also increases the Froude number of the section.

At this location some shoving and telescoping of the ice cover may occur with the effect of raising water levels and reducing velocities to the point that the ice cover can progress upstream. If the accumulation is deemed to be a concern, the forebay level could be raised to el. 26m, and/or an ice boom could be installed just upstream of this location to ensure a stable cover is initiated in the upstream river reach. Figure 4 presents the ice profile for a el. 26m forebay level. As shown, the accumulation of ice upstream of the cofferdam is significantly smaller in this case.

FIGURE 4

End of March profile:
26m forebay level, severe
winter (1972-73)

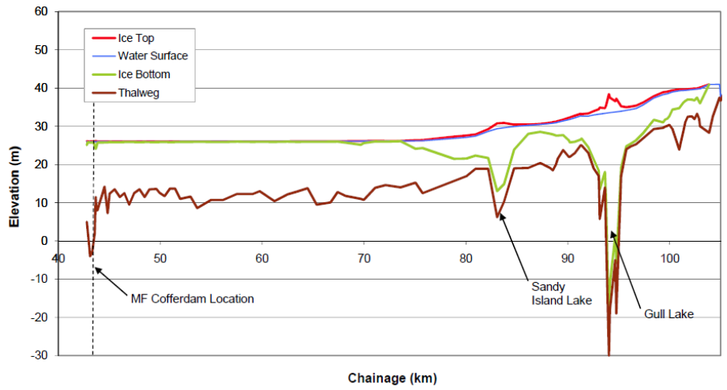

The results of the ice modeling study were verified using a hydraulic 1D simulation. The objective was to assess the velocity and the Froude number in the river channel. With a water level of the headpond at el. 25m and a discharge of 2,200m³/s (maximum flow observed between 1973-2011), the simulation shows that stable ice conditions can be maintained for over 20km upstream of Muskrat Falls, however there would be no ice cover maintained between the falls as both the flow velocity and Froude's number would be greater than that required to maintain a thermal ice cover. Also, at this water level, it is indicated that a stable ice cover would not be maintained at two narrow sections further upstream where rapids conditions are present as well as between Sandy Lake and Gull Lake (Figure 5).

FIGURE 5

Thermal ice assessment
at Lower Churchill
River – Muskrat Falls
headpond at el. 25.0m

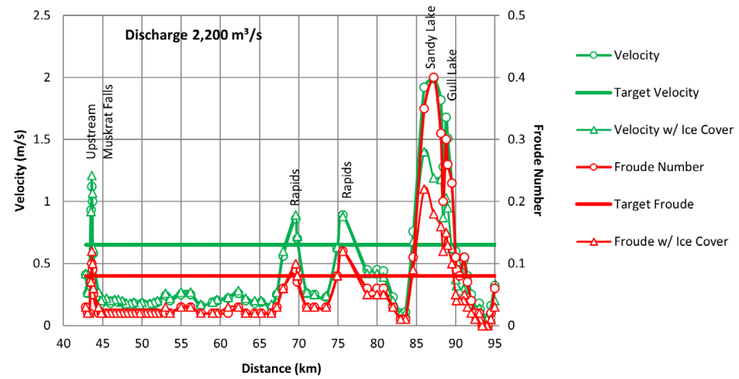

Based on the analyses, an upstream winter water level of 25m was retained for the construction stage of the project. Hydraulic Study for Ice Boom Location Positioning.

3.4 HYDRAULIC STUDY FOR ICE BOOM LOCATION POSITIONING

The Muskrat Falls gated spillway was built on the south side of the river between the powerhouse and the North Dam. It consists of five bays, each 10.5m wide, with vertical gates on rollways having a sill elevation of 18.0m. Initially, the bays were without rollways to allow river closure, with the rollways progressively constructed during the diversion period.

During the construction stage, the water level upstream of the spillway would be raised to a planned elevation of 25.0m in order to drown the Upper Muskrat Falls and decrease the quantity of frazil produced.

The construction of the North Dam would take place during this period behind the main cofferdam, with water level controlled using the spillway gates. An ice boom would be installed upstream of the Upper Muskrat Falls to serve as a precaution to help in stable ice formation (Figure 6). It is noted that the boom is a multi-purpose year-round boom to aid with ice cover formation, collect river debris and for public safety protection.

FIGURE 6

Plan View of Muskrat Falls Facilities during Construction and Location of Boom

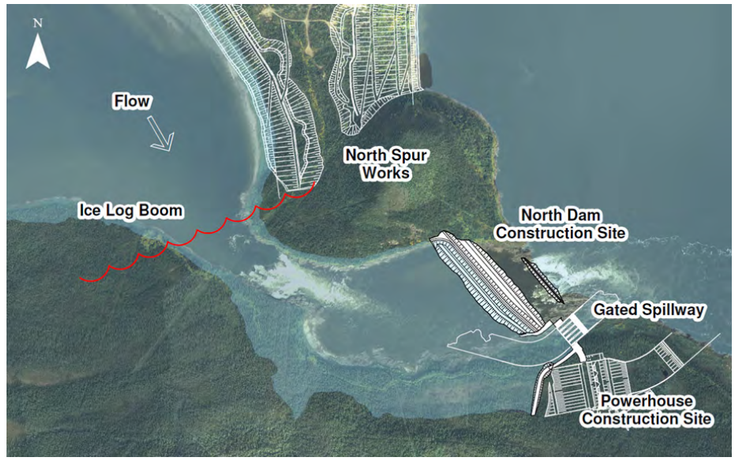

Figure 7 shows a comparison of the surface velocity profile in natural conditions and with the water level raised to el. 25.0m. These results were obtained with 2D hydraulic modeling. It can be seen that the flow velocities upstream of Upper Muskrat Falls have been significantly reduced with the raised water level, even though the flow for that simulation was higher and corresponded to the 20-year return period winter flood. This allows positioning the ice boom at the location with maximum flow velocities averaging 1.0m/s (Figure 7) during ice formation periods. Since Upper Muskrat Falls is completely drowned and the headpond is covered with ice, frazil production would no longer be expected in that area. Some frazil ice would still be produced between the ice boom and spillway but the total quantity would not be sufficient to create an ice dam.

FIGURE 7

Velocity profile in natural conditions and with the water level at el. 25m

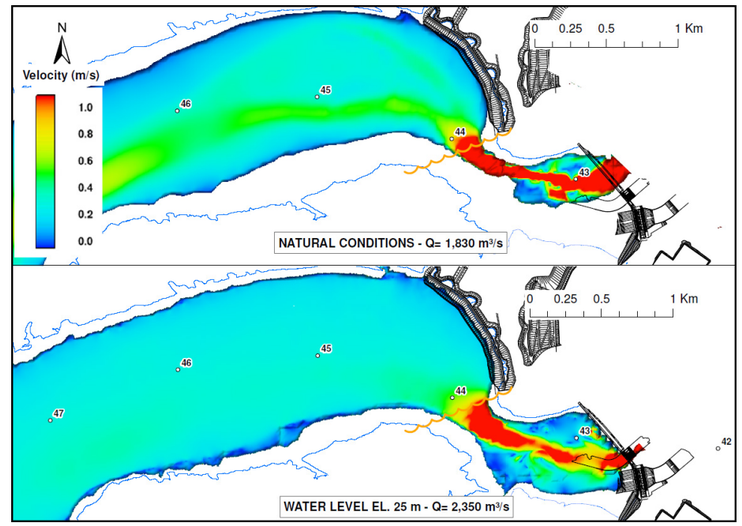

4. Ice Management in Winter 2016-2017

The plan for ice management going into the winter 2016-2017 was to have the river cofferdams and spillway ready to allow the rise of the headpond water level to elevation 25.0m. Moreover, the ice boom had to be installed prior to river freeze-up. However, various constraints occurred that prevented full implementation of the ice management plan. Primarily, these constraints led to a delay of impoundment and limitation of the headpond maximum water level rise to el. 22.0m instead of the planned el. 25.0m. The resulting flow velocities in the headpond for the range of anticipated winter inflows were higher than the recommended conditions from the design studies although, according to the 2D hydraulic assessment, still in the range allowing for stable ice formation upstream of the Upper Muskrat Falls for normal inflows (Figure 8).

The delayed impoundment and the resulting high flow velocities at the location of the planned ice boom prevented its installation. Therefore, the challenge in the river ice management was the initiation of the ice cover formation in the headpond upstream of the Upper Muskrat Falls and the reduced storage capacity for frazil ice capture arriving from the upstream reaches of the Lower Churchill River.

FIGURE 8

Velocity profile with the water level at el. 21.5m

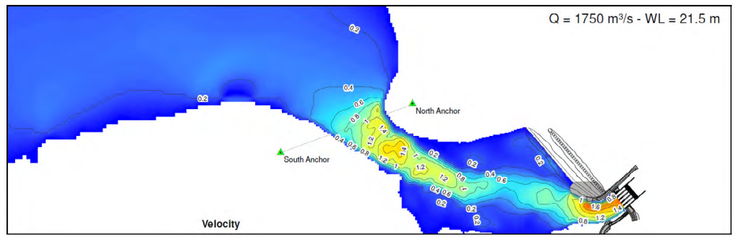

The delayed impoundment and the resulting high flow velocities at the location of the planned ice boom prevented its installation. Therefore, the challenge in the river ice management was the initiation of the ice cover formation in the headpond upstream of the Upper Muskrat Falls and the reduced storage capacity for frazil ice capture arriving from the upstream reaches of the Lower Churchill River.

4.1 2016/17 FREEZE-UP

Ice formation on the river began in early December 2016, however impoundment was delayed until late January 2017 due to constraints from ongoing construction activities. By early February partial thermal ice covers had formed under natural conditions upstream of Muskrat Falls along each bank, but frazil ice generation was in full progress and an ice dam had formed immediately downstream of Muskrat Falls (Figure 9).

FIGURE 9

View of ice accumulation downstream of Muskrat Falls Spillway (February 14)

By mid-February water levels upstream of Muskrat Falls had been increased from el. 17m to el. 20m to help promote the formation of an upstream cover. During this mid-winter impoundment the ice conditions in the upstream reservoir were being monitored closely for cracks and any movement of the existing ice cover. As expected cracks formed in border ice along the shorelines and some small pans of competent border ice and grounded ice (on sandbars) began to move. Border ice growth in the mid pool also progressed at the higher water levels.

On February 14th, with the water levels upstream of Muskrat Falls at el. 20.2m and a flow of 2000m³/s and the advancement of border ice growth at upper falls location, a large competent sheet of ice jammed/grounded across the upper falls location. This initiated an upstream cover, and within 6-8 hours the ice front progressed 10km upstream of the upper falls (Figure 10).

FIGURE 10

Looking upstream from upper Muskrat Falls location (February 14)

With this event, frazil ice generation in the 20km reach upstream of the project was cut off, and the frazil ice trap was in place for ice generated in the river upstream of the Gull Rapids site. The ice cover continued to advance upstream over the following days. No frazil ice was observed between the upper falls and Spillway once the ice cover formed upstream. With a lack of frazil ice supply, the ice dam immediately downstream of Muskrat Falls gradually deteriorated and by February 15th water levels downstream of Muskrat Falls had began to drop (Figure 11). By February 18th the open water downstream of Muskrat Falls increased (Figure 12) and downstream water levels had dropped from el. 7.0m to less than 5.5m.

Water levels upstream of the Muskrat Falls were gradually increased to el. 21.5m by February 18th and were held at that elevation until end of March at which point they were increased to el. 22.5m.

FIGURE 11

Water level downstream of Cofferdam

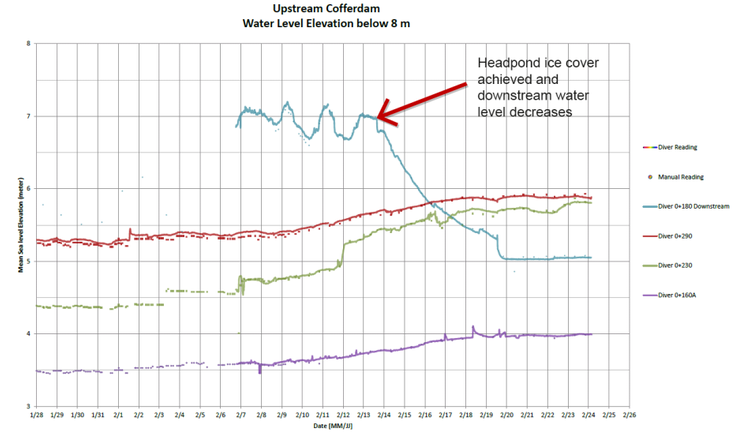

FIGURE 12

Change in open water downstream of Cofferdam (Feb 1st vs. Feb 18th)

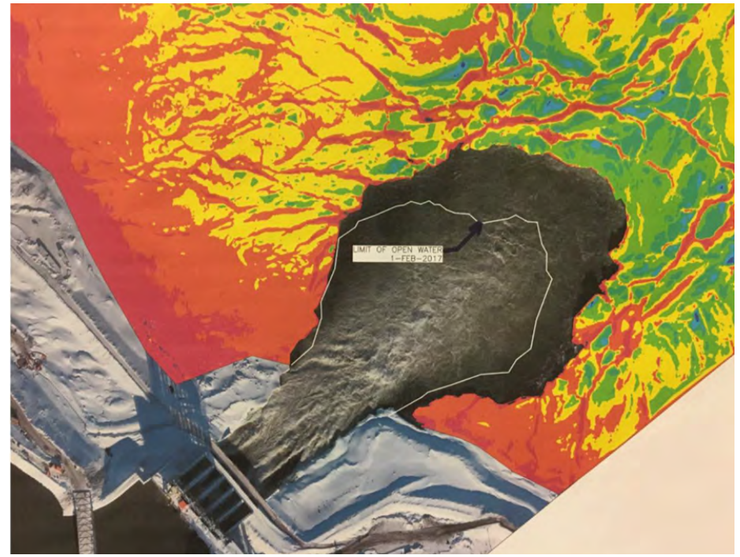

4.2 2017 ICE BREAKUP

In preparation for spring runoff and ice breakup water levels upstream of Muskrat Falls were lowered from el. 22.5m to el. 21.5m in early May. Ice thicknesses upstream of Muskrat Falls varied, with early winter border ice estimated at 1.0-1.2m and late winter mid channel ice estimated at 0.15-0.3m. On May 11th the flows at Muskrat Falls were 2160m³/s and rising due to the melting snow from increased temperatures.

Solar radiation and warming temperatures quickly deteriorated the mid winter ice cover (Figure 13). The spring melt was very rapid with flows at Muskrat Falls increasing from 2000 to 4560m³/s between May 10th and 17th. The higher flows and increased river velocities quickly flushed the weaker mid channel ice on May 12 and 13th, before flows reached 3000m³/s.

FIGURE 13

Looking upstream from the upper Muskrat Falls (May 12th)

Border ice below Sandy Lake had mostly flushed through by the afternoon of May 14th when flows were at 3440m³/s. During the ice run, there were frequent accumulations of ice in the mid-pool that would gradually flush through the spillway. Flows reached 3970m³/s on May 15th and peaked at 4560m³/s on May 17th (Figure 14).

FIGURE 14

Looking upstream towards the Upper Falls (May 14th)

Reservoir ice that had passed through the spillway then accumulated in the large ice dam downstream of the project. As in previous years, the large ice dam below Muskrat Falls remained in place until well after the 2017 spring peak flows were observed (Figure 15).

FIGURE 15

Looking upstream towards the Upper Falls (May 14th)

5. Ice Management in Winter 2017-2018

The ice management planning and the experience gained during the winter of 2016-2017 allowed the project team to revisit the requirements for the various aspects constituting the plan. The initial approach was based on a headpond water level at el. 25.0m based on theoretical analyses. The reasons were as follows:

- Prevention of an ice dam from forming downstream;
- Expert review confirmed el. 25.0m as recommended level to minimize risk related to ice cover formation in the upstream reservoir;
- If the headpond is lower than el. 25.0m, there is risk that reservoir ice cover may take longer to form, and therefore would not be as effective in preventing formation of the ice dam, with potential for elevated water levels downstream;
- Facilitating operation of gates in winter (less ice buildup on gates);
- Minimizing risk of ice damage to gates and Spillway structure; and
- Ice boom optimal performance is at el. 25.0m.

The cover formation with a water level at el. 21.5m and without an ice boom, as occurred in winter 2016-2017, was considered to be a fortunate event (competent ice sheet jam/grounding at upper falls) but could not be relied on to occur again. Therefore, the plan for winter diversion in 2017-2018 was revisited. There are two periods that are critical for the ice management at Muskrat Falls. The first relates to the ice cover formation at the beginning of winter which allows the control of the frazil ice and the potential backwater effect at the construction site from a downstream ice dam. The second one relates to the management of the ice during the spring freshet when the flow and the flow velocity increase while river is still not free of ice.

The operating ice management experience gained in winter 2016-2017 allowed for an improvement in the theoretical ice management plan. It has showed that an ice cover should be capable of forming at lower water levels, particularly with an ice boom in place. This was also supported with the results from a 2D flow and velocity hydraulic analysis. It was found that the boom should still be effective over much of its length in trapping migrating ice, and thereby facilitating ice formation for headpond levels in the range of el. 22.0m to 25.0m.

Several project risks were identified and a balance was struck between the risk and consequences and the benefits associated with operation at a lower elevation. This strategy was employed in the preparation of the updated ice management plan. These risks were related to: the geotechnical stability of the cofferdam structure; the integrity of the ice boom; the formation of ice cover; and the available capacity at the Spillway.

The geotechnical risk at the cofferdam, which had not been exposed to water levels higher than el. 22.5m, was reduced by adding backpressure on the downstream side of the structure. The addition of this backpressure allowed the team to safely raise the water level higher than this elevation. A detailed procedure for management of the cofferdam was put in place. According to this procedure, increases in the water level, if required, should be moderate and temporary. Any increase in water level would only be considered in tandem with careful observation of instruments and a plan to lower it quickly if required.

There was also a risk that ice boom failure (release of ice/debris) could occur in spring if the boom were to be overloaded. However, the consequences of this were considered to be low due to the sufficient flushing capacity of the Spillway. The critical velocity for the integrity of the ice boom was estimated to be 1.6m/s. Should there be flow velocities greater than that while the boom is still retaining ice, fuse links incorporated at one end of each boom span would fail and release the retained ice, but would prevent complete loss of the boom. These velocities could be achieved only in the spring time during the routing of the spring freshet. There was determined to be no risk related to the ice boom during the freeze-up period when operating at these lower elevations.

The design criteria of the temporary diversion is to safely route the 1:40 year flood. The capacity for handling such floods with all five spillway bays available is achieved with the headpond water level above el. 22.5m.

The comparison of the headpond water level requirements related to each one of these risks is as follows:

- **Geotechnical** – keep the headpond water level as low as possible and preferably around el. 22.5m;
- **Ice boom** – keep the headpond water level as high as possible and around el. 24.0m - 25.0m;
- **Ice cover formation** – keep the headpond water level in the range el. 22.0m - 25.0m and create an ice hinge at as high an elevation as possible (el. 23.5m);
- **Spill capacity** – keep the headpond water level at el. 22.5m or higher.

From this analysis, it was recommended that the winter water level should be at least el. 22.5m. Procedures for ice management during the period of freeze-up and break-up were prepared on this basis.

5.1 WINTER 2017-2018 FREEZE-UP PROCEDURE

The plan that was put together for the freeze-up procedure was as follows:

Starting Water Level:

- Recommended starting level is el. 22.0m

Implementation:

- A team was in place to monitor and assess cover formation and recommend action if required
- Monitoring of instruments and cameras to refine our approach to potential cover formation
- Daily assessment and reporting
- Determine if an increase in level is required

One technique considered to promote ice cover formation was to temporarily raise the water level to increase conveyance, temporarily lower flows, and consequently lower the flow velocity. Hydraulic analyses in support of this approach were carried out (Figure 16). This indicated that the ice boom will double its effectiveness for the period of transition (velocity < 0.7m/s).

FIGURE 16

Velocity profile for 1800m³/s and 1500m³/s (during filling)

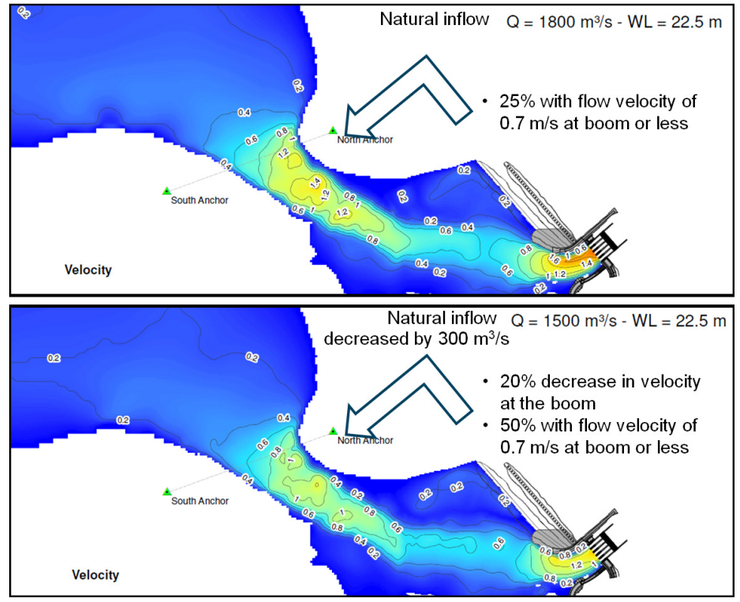

The maneuver to raise the water level would be carried out if the cover failed to form when expected. To aid in this, the weather forecast would be monitored for a cold spell, and the increase in level would be timed to coincide with this. The strategy was as follows:

- Raise the forebay level by 0.5m overnight to reduce velocity and promote cover formation
- Raise the level when the forecast is favorable for cover formation (cold nights)
- Hold the level for 2 days to assess effects
- Evaluate whether to raise or lower for next attempt if needed

The following findings were identified in the preparation of a plan for the development of a successful cover:

- The phenomenon was weather dependent: cannot predict when it will form but likely before 3rd week December
- The ice cover initiation should occur by bridging at or upstream of boom
- The cover will consist of frazil and large pans in the river when it occurs
- Once bridging occurs, the cover will progress upstream and solidify
- Must allow 1 to 2 weeks for the ice cover to stabilize before changing water level
- The winter headpond water level should be el. 22.5m

In order to help mitigate the risk to ice movement during the spring breakup, it was recommended by the ice experts that steps be undertaken to form an ice hinge at el. 23.5m. This would need to be done in early winter when the weather was cold enough for rapid ice formation as the water level rose. The plan was to raise the water level by 0.5m, wait 2 days for the ice at the shoreline to re-form before raising it again until el. 23.5m was reached. Then, after a further 2 weeks, the level could be returned to the starting water level at which the ice cover had first formed (el. 22.5m).

5.2 SPRING 2018 BREAK-UP PROCEDURE

In order to minimize the risk of mobilizing the upstream cover prematurely, any increase in stage on the upstream reservoir levels should be limited. This will allow the bond between the banks and the ice cover to be maintained as long as possible, letting the cover remain in place and encouraging a thermal melt to occur. However, there is a headloss across the upper falls that will increase with flow. If the interim headpond operating level at the spillway is el. 22.5m, this means that when passing the 1:40 year spring flood event (peak flow 6500m^3/s), the head loss will be in excess of 0.5m. Levels upstream of the boom will therefore rise to el. 23m, likely breaking the bank/cover bond. This will increase the risk that the cover may mobilize. To mitigate this risk operation of a slightly higher headpond water level (el. 23.0m) is required.

This rise would provide the system with the capacity to prevent any surcharge on the upstream levels while passing even the 1:40 year flood, allowing the ice to soften and degrade thermally for as long as possible. The sole requirement to handle successfully the spring 2018 break-up is to maintain the headpond water level at el. 23.0m.

To evaluate the proposed approach in ice management during spring freshet, hydraulic analyses were carried out. The water profile for various river flows was computed with a headpond water level at el. 22.5m at Spillway. A relationship between the flow velocity at the location of the ice boom and the river discharge was established. Figure 17 presents velocity and water level profiles for river flow of 3000m^3/s and Figure 18 shows the relationship. Relationships relating the head loss across the upper falls to flow discharge were also generated and used to manage spillway operations.

FIGURE 17

Velocity and water level profiles for 3000m^3/s and headpond at el. 22.5m

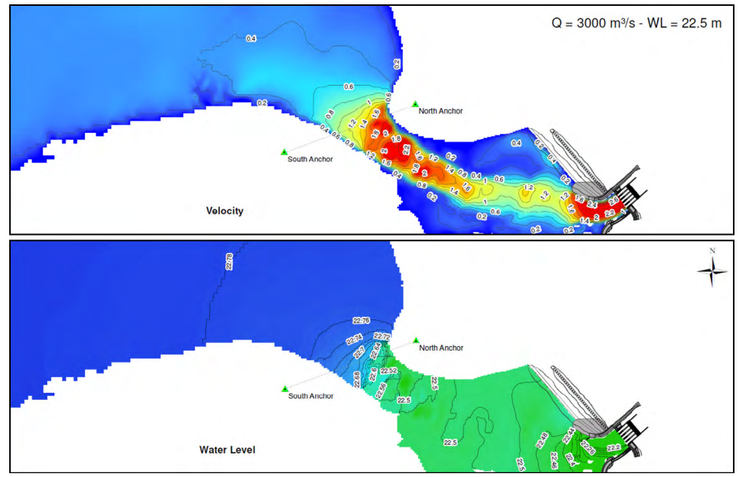

From the established relationship, the critical velocity at the ice boom of 1.6m/s would be reached under 2700m³/s when the headpond is at el. 22.5m measured in the mid pool upstream of the spillway (Figure 18).

FIGURE 18

Flow Velocity vs. Discharge at the Ice Boom

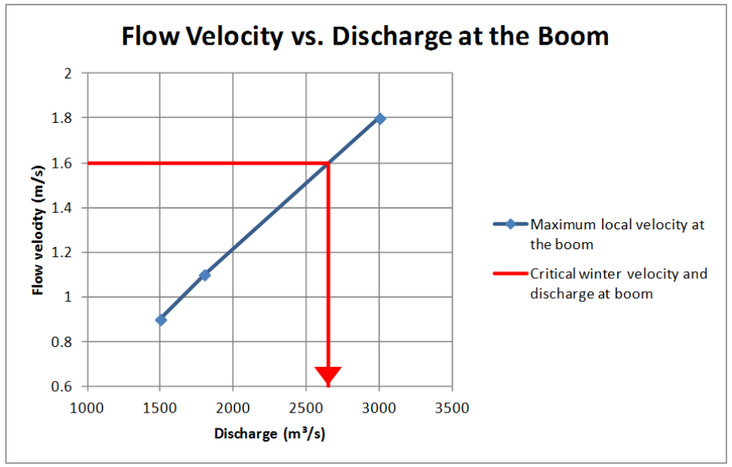

Analysis of the historical spring floods and heating degree-days of spring above zero temperatures indicated that (Figure 19):

- Flood arrives, on average, when 40 heating degree-days in average are accumulated;
- Critical discharge is attained when 100 heating degree-days in average are accumulated;
- There are 14 days on average between the beginning of the flood and the critical discharge of 2700m³/s.

FIGURE 19

Spring Flood Freshet vs. Degree-days Temperature

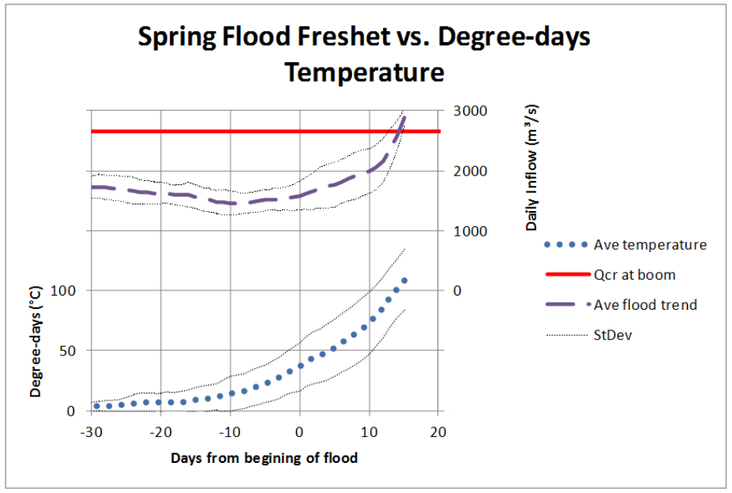

Based on the hydraulic analysis results, historical spring floods and heating degree-days temperature, it is highly likely that the ice cover will be sufficiently eroded, melted to a significant degree in place and perhaps flushed by the time the critical ice boom flow and velocity are attained. This in turn confirms the viability of the spring 2018 break-up procedure.

5.3 WINTER 2017-2018 ICE FREEZE-UP

Headpond water levels heading into late November were increased to el. 22.0m. The ice boom was now in place to aid with the formation of the upstream ice cover. Average daily temperatures fluctuated in November from +3 to -9°C and gradually cooled the water temperatures in the Churchill River. However it wasn't until November 21st that average temperatures stayed below 0°C and frazil ice formation began. The water level was increased to el. 22.5m at that time to facilitate ice cover formation.

By late afternoon on November 28th ice pans began to accumulate and progress upstream of boom while Churchill River flows were at 2,130m^3/s and headpond el. 22.5m (Figure 20). Ice pans had accumulated along 90% of the headpond with some open water in the ice cover and along the boom span near the North Spur where velocities were higher. The upstream frazil ice trap was in place early in the winter season which stopped the formation of the natural ice dam downstream of Muskrat Falls almost immediately. Observations from an ice survey on January 11th showed no ice dam and significant open water immediately downstream of Muskrat Falls (Figure 21).

FIGURE 20

Ice accumulation at boom and ice cover looking upstream from North Spur (November 29th)

FIGURE 21

Looking at area downstream of Muskrat Falls where ice dam previously formed (January 11th)

In January, after the upstream ice cover had strengthened the water levels were gradually increased to form an ice hinge along the shoreline at el. 23.5m. The ice hinge would help lock the ice cover in place during the spring runoff and allow the ice to mostly melt in place and avoid the heavy ice floe similar to what was observed in spring 2017. By January 11th, the water levels were at the target elevation and held there for 2 weeks to allow the ice hinge to form. Water levels in the headpond were then lowered to el. 23.0m for the remainder of the winter.

No significant ice floes were observed at the Spillway structure during the winter of 2017/18. A thermal ice cover developed in the headpond and over the winter ice measurements recorded ice thicknesses of 0.8m - 0.9m at end of the winter. The ice dam did not form downstream of Muskrat Falls as it did in previous years and significant open water remained immediately downstream of the Spillway for the winter period.

5.4 2018 ICE BREAKUP

Temperatures began to warm up on April 23rd however, the overnight lows generally were below 0°C until around May 28th. During this period there would be a few days with day time highs in the teens followed by cooler temperatures. This resulted in a slow melt of the snowpack. Some snow on the ice cover began to melt in April and this help to degrade the ice cover (Figure 22).

FIGURE 22

Looking downstream at Muskrat Falls (April 25th)

By early May the solar radiation and warmer water temperatures underneath the ice cover began to rapidly degrade the ice cover. An ice survey conducted on May 11th showed the ice cover was melting in place and that it had deteriorated significantly with open water areas scattered throughout the ice cover (Figure 23). Higher velocities and westerly winds worked on the upstream ice front which began to recede toward Muskrat Falls (Figure 24). Similar conditions were being observed downstream of Muskrat Falls and much of the thermal ice cover immediately below Muskrat Falls had also melted in place by mid-May (Figure 25).

FIGURE 23

Looking upstream from approximately 6km above Muskrat Falls (May 11th)

FIGURE 24

Looking upstream from approximately 7km above Muskrat Falls (May 13th)

FIGURE 25

Looking south at Spillway discharge (May 13th)

Due to the slow melt of the snowpack, the flows on the Churchill River remained below 2,300m^3/s while the ice covers melted in place. The only ice remaining upstream of Muskrat Falls reservoir area by the end of May was the ice cover in Sandy Lake and Gull Lake and this ice did not mobilize until the higher flows were observed in last few days of May and early June (peak flows of 5,150m^3/s were observed on June 2nd).

No massive ice floes were observed at the Muskrat Falls Spillway during the 2018 spring breakup. With the exception of the ice from Sandy Lake and Gull Lake ice that was observed passing through the Spillway was very weak degraded ice compared to ice floe observed in spring 2017.

6. Conclusions

The paper has provided an overview of the design and implementation of the ice management program for Muskrat Falls. It has shown that the level effort that went into the understanding of the issues, analysis of alternatives, understanding of the risks and development of plans allowed for a robust program that was able to adapt to changing circumstances that occurred during construction.

The successful implementation of this program in the 2016-2017 ice season allowed a better understanding of the processes and an optimization of the program for the 2017-2018 ice season. The theoretical basis for the program, in forming a headpond to reduce the frazil ice supply and reduce or eliminate the formation of the a hanging ice dam was clearly demonstrated, and was successful in mitigating the risk of flooding of the Muskrat Falls construction site from high backwater levels.

Acknowledgements

This paper was previously presented at the Canadian Dam Association 2018 Annual Conference, Québec, QC, Canada (Oct 15-17, 2018).

Joseph Conlon
Graduate Engineer
Engineering Services – Transportation UK
London, UK

Andrew Love
Head of Train Control and Signalling
Engineering Services – Transportation UK
London, UK

Rail Safety

06: Quantifying Collision Risk with Simulation

Abstract

When upgrading the rolling stock used on an existing railway, it is important that the potentially higher maximum attainable speeds from faster accelerating trains are considered, and the associated risk they pose in conjunction with existing infrastructure is assessed. For certain track assets (i.e. switches that guide a train onto another line, or a buffer stop that protects the end of the track) overspeeds from erroneous acceleration could result in derailment, or even the catastrophic event of a train crashing into a station concourse. Newer, more modern trains have high acceleration rates, and hence a section of track that may previously have been declared within tolerable levels of safety could now pose a hazard. This paper looks at work undertaken by SNC-Lavalin Atkins' Rail Consulting Practice in simulating train performance using a MATLAB model to inform quantitative risk assessments looking at the probability and magnitude of "hyper-acceleration" events leading to potential derailment over switches, or high-speed buffer stop impacts. The result of this work was a recommendation that existing buffer stops may be unsuitable in light of the superior performance of new rolling stock, and that they should be upgraded to reduce risk.

KEYWORDS

Buffer stops; Quantitative Risk Analysis; Signalling; Automatic Train Protection; Driverless

1. Introduction

The final approach of a train into a terminal station at the end of the line can be a dangerous part of the passenger's journey. Automatic Train Protection (ATP) systems that can intervene in the event that unsafe circumstances arise are becoming increasingly common. Such systems are capable of autonomously applying a train's brakes in the event that permitted linespeeds are is exceeded by certain margins, or if it determines that the driver has not interacted with the train in a sufficient time period, which could be indicative of driver incapacitation or error. However, in the event of non-automated railways, concentration, skill, and precision are required on the driver's behalf to diligently operate the vehicle. A train must approach the terminus at an appropriate speed, reach the correct stopping position, respect the limits of any ATP system, and, of course, do all this within the allowances of the timetable governing the railway.

Major civils assets and stations are often finalised before the nuanced requirements of railway signalling systems are fully understood. This can be down to inadequate communication between signalling engineers and station designers, or a result of brownfield railway projects where substantial rework is unavoidable. The resulting spatial constraints at terminal stations mean that buffer stops can sometimes be sited just a few metres after a train's intended stopping position, and just a few metres ahead of the end of the track (which can often be a literal concrete wall). There are cases like the original London Underground (LU) Victoria Line which was designed with Automatic Train Operation (ATO) and ATP already in place, but the gentle curves and generous overruns arising from such informed design are by and large the exception to the rule.

With two buffer stop impacts at speeds significant enough to cause extensive damage and injury occurring at Enfield and Kirby Stations in just a matter of months this past year, the choice of appropriate platform end protection is still evidently a vital concern. A less forgiving buffer stop rated for higher magnitude impacts means unnecessary damage and injury will be caused during low magnitude collisions; a lower rated buffer means that potentially a train is not contained during an incident, and possibly breaches the remit of the track. With the proximity of station concourses or other densely populated urban developments, an incorrect choice of buffer stop could have dire consequences extending beyond the train's immediate passengers.

2. Quantitative Risk Assessment

2.1. AUTOMATIC TRAIN PROTECTION

Increasingly commonly, speed restrictions imposed on buffer stop approaches are enforced via ATP, or a variant of some such system. As previously mentioned, this detects overspeeds above a prespecified margin and will enforce a corrective action depending on the magnitude of said exceedance. The nature of intervention varies from system to system, but will typically be automated traction cut-off, and possibly activation of the service or emergency brakes if the speed violation continues unchecked. A flowchart of events leading to an ATP Emergency Brake (EB) intervention for a generic light rail system is presented within Figure 1.

Speeding on approach to a buffer stop can be attributed to several factors, from poor judgement through to a driver being rendered incapacitated by a medical issue such as a heart attack or stroke. Speeding could even be indicative of something more insidious, such as a malicious act by a driver with the nefarious goal of inflicting damage and death. In many instances, the root cause can never be ascertained (for example the 1975 LU crash at Moorgate). Regardless of the reason for the collision however, the magnitude of overspeeds from all causes should be considered.

The Rail Safety and Standards Board (RSSB) Safety Risk Model (RSSB, n.d.) provides real-world statistics for several situations where a train could strike a buffer stop with "potential for a high-speed impact." This database uses historic, empirical figures, detailing collisions attributed to a driver misjudging braking, losing concentration, inexperience, an underlying medical condition, and several others. Combined, these amount to more than 13 individual buffer stop collisions annually on the entire UK mainline network and predict a fatality from these events every 40 years. Of course, real life neither observes nor exclusively adheres to statistics, so it is very conceivable that a fatality caused by a collision with a buffer stop could well occur within the operational life of a railway. It should also be noted that these statistics average out historical data to determine fatality rates. In reality, a train accelerating into a buffer stop at sufficient velocity to be fatal to an individual will likely kill or seriously injure many more.

FIGURE 1

Automatic train protection logic

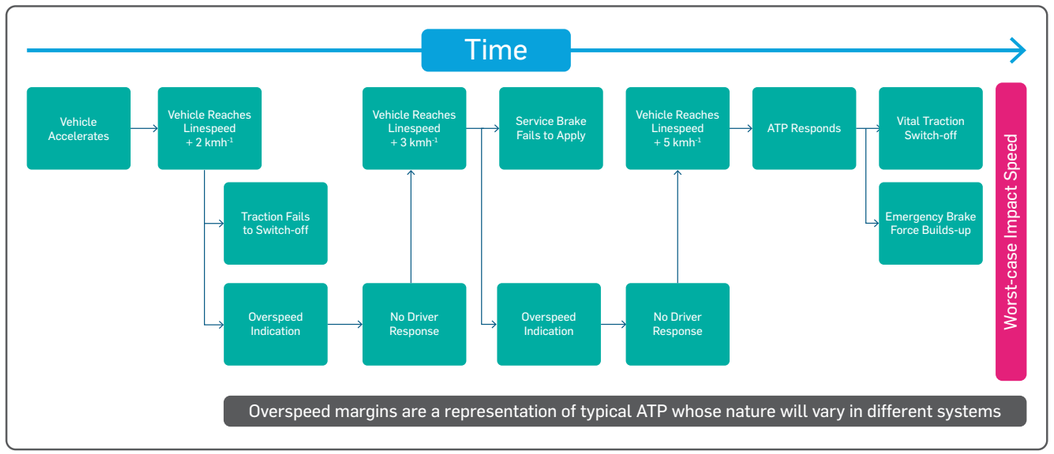

Figure 1 depicts the high-level logic followed by a generic ATP system resulting in an EB intervention. We can see several indications are presented to the driver, which all must be ignored for the emergency brake to be commanded. The scenario also depicts the failure of both the "non-vital" Traction Cut-out (TCO) functionality and Service Brake (SB). Whilst not the case for all vehicles, often the SB is actuated before the EB to minimise "jerk" experienced by passenger – the utilisation of Magnetic Track Brakes (MTBs) during emergency braking invokes a high rate of change of acceleration, which causes a secondary issue of damaging rails by "track burn." The non-vital TCO in this example refers to an ATP-initiated traction switch-off, commanded once an overspeed tolerance is exceeded. The "vital traction switch-off" refers to a "vehicle-initiated" TCO, which generally occurs once a sensor in the brake cylinder detects a rise in pressure indicative of the brake being activated, preventing a train being subjected to acceleration and braking at the same time. Specific system architecture and integration of this vital function may vary from train-to-train (and there is the more dire possibility of an EB failure) but this example is chosen to show the procedure that ATP integrated on a light railway may follow.

2.2. HYPER-ACCELERATION

An erroneous or intentional application of traction when a train should be braking is actually a well-documented phenomenon, with the concept of "runaway acceleration" (or more colloquially, "hyper-acceleration") being documented extensively within standards such as IEEE 1698 (IEEE, 2009). As an example, whilst an arbitrary ATP system may be designed to apply the brakes once a train exceeds linespeed by 5kmh^{-1}, the time taken for the system to send the command, combined with the times for traction to be cut-out and the brake cylinder pressure to build up is non-negligible. The supplier-quoted response times for many ATP systems are upwards of half a second, and in tandem with nigh one-second TCO times and the multiple seconds required for brake force to build to sufficient levels to start slowing the train effectively means that there could be several seconds of a vehicle accelerating when it should be braking, all the while gaining speed when it should be losing it.

Hyper-acceleration may be less of a concern on larger trains, but for smaller units maximum acceleration rates regularly approach 1ms^{-2} (and modern rolling stock now exceeds this value in many circumstances (Robert, 2022)). When we consider there could be multiple full seconds of a train accelerating at its maximum rate, we can understand how a less massive train could surpass its ATP threshold by an additional 5, 10 or even more kmh^{-1} before braking begins in earnest. Furthermore, a train will naturally be travelling slower on approach to a buffer stop, and hence the instantaneous acceleration rate will not only be greater at this low speed, but the significance of a 10+ kmh^{-1} overspeed is far more notable. Empirical test data from maximum acceleration testing conducted on a moderately sized and loaded Diesel Multiple Unit (DMU) in 2014 revealed that the maximum rate of acceleration is almost twice as fast at 25kmh^{-1} than at 50kmh^{-1}. When we factor in the risk of failure of the service brake or traction switch-off function, we realise how important it is to both quantify the magnitude of maximum possible approach speeds, and the probability of these speeds occurring. This allows the selection of a buffer stop with an appropriate amount of "give" that will not be unduly harsh and cause a train to telescope under its own momentum, yet will provide enough resistance to prevent a catastrophic breach at the end of the track in the event of unusual but credibly high impact speeds.

Many trains have a driver safety device acting as an "engineering control" to mitigate the effects of driver incapacitation. These vigilance systems, also referred to as a "dead man's switch" or "pedal" are designed to require an action from the driver to continue operating the train, or else they automatically arrest the vehicle. Whilst these systems allow a train to "fail-safe" in theory, the timescales required for some devices to activate means that a hyper-acceleration event is not sufficiently mitigated by the system (if at all). A typical vigilance device will require modulation of a switch, handle or pedal within a time period, or else an alarm sequence is initiated, either instantaneously or after a slight delay. If a countdown is started, it can be reset by acknowledging the alarm in this period, but regardless, there is the potential for tens-of-seconds to elapse from the point at which a driver could have been medically incapacitated and slump comatose against the traction controller through to the point at which the brakes actually automatically apply. A severe impact may only require a few seconds of maximum acceleration initiated at the worst possible location on approach to a buffer stop to result in a potentially fatal incident. As such, whilst a dead man's switch is an effective control to mitigate prolonged acceleration on long sections of track, it cannot be counted as assurance to alleviate a buffer stop collision to acceptable levels of severity nor probability. What's more, as with any system requiring human input, inherent fallibility is present, and there exists a temptation for personnel to circumnavigate designed procedures and take shortcuts (if not prevented by appropriate technical measures).

2.3. PROBABILISTIC ANALYSIS

The assessment of error induced buffer stop collisions also requires the quantification of human error rates when performing (or failing to perform) the prerequisite actions necessary to adhere to linespeed. Because human factor considerations of ATP systems and their ergonomic integration on a given train varies widely, there is no "one size fits all" value for erroneous acceleration. Some trains may require a driver to depress a spring-loaded lever to increase speed, which is less likely to result in unintentional, prolonged hyper-acceleration than a driver inadvertently hitting a non-spring-loaded control. Human error may also be location specific; a driver will be far less likely to accelerate towards a buffer stop within a station where there is an abundance of visual cues such as passengers, platforms, and Victorian arched infrastructure compared to a siding or pocket track, where the surroundings are generally uniform.

Conducting a Railway Action Reliability Assessment (RARA (RSSB, 2012)) is a sound approach to determine the probabilities underpinning human error rates in various situations. RARA is a subset of HEART (the Human Error Assessment and Reduction Technique) which provides a framework for estimating a human's reliability—or lack thereof—when performing a certain action or sequence of actions. A "Generic Task Type" is assigned, which is then multiplied by relevant factors called "Error Producing Conditions" which scale this value to reflect the specific process or procedure being considered. The result is an upper and lower bound for unreliability (corresponding to the 5th and 95th percentiles) and a nominal "Human Error Probability" (equivalent to the median). We can then undertake event tree analysis or a similar technique and, using the human "failure" rates we derived alongside system failure rates informed by standards or documentation, can elicit an estimate of each eventuality considered under our analysis.

2.4. DETERMINATION OF SEVERITY

We now start to see how the risk profile representing hyper-acceleration and a subsequent buffer stop impact is a vital input into the selection of appropriate end-of-track protection. But whilst the probability of discrete impact speeds arising from different combinations of failures and/or errors is easily determined, quantifying the risk severity component is not as simple. There is a myriad of factors that can influence a train's maximum attainable speed, such as adhesion, gradient, loading, and odometric uncertainty, to name but a few. Additional factors that cannot be reliably predicted such as wind and temperature will also have a notable (albeit diminished) effect on possible collision speeds.

Whilst a simple yet sound approach would be to assume the combined worst-case for every possible condition and factor, this evolves pessimistic and conservative speeds. Due to the astronomically improbable combination of preceding circumstances (all required to occur in tandem) these speeds are so unlikely they will likely never happen during the operational life of the railway. Furthermore, the impact speeds calculated assuming worst-case conditions may be so restrictively high that it would be extremely impracticable from both a commercial and operational perspective to safely mitigate the hazard posed to an acceptable level of severity. So, further analysis looking into the likelihood of distinct events can yield a distribution of various speeds, each occurring with a discrete probability.

The outcome is that end-of-track protection can be selected that is resilient to impact speeds corresponding to a level of risk that the operator is willing to accept. A buffer stop can then be chosen accordingly that is capable of dissipating the associated kinetic energy of the vehicle when factoring in the expected loading conditions and train mass.

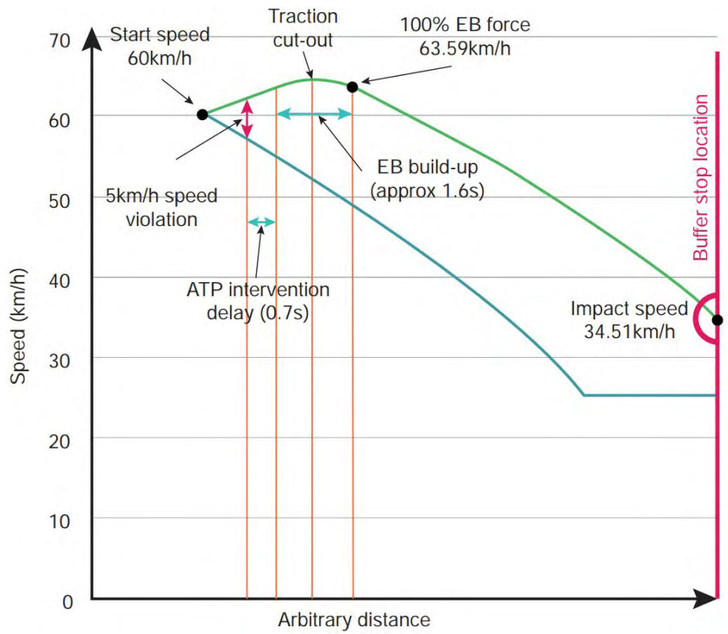

FIGURE 2

Speed-distance graph of train performance

Figure 2 depicts a speed-distance graph using a step-based MATLAB model to simulate an unladen diesel-electric train striking a buffer stop. The blue line represents the service braking curve enforced by "continuous" supervision ATP, calculated using the equations documented within the system's safe braking model. The light green line represents the overspeed arising from hyper-acceleration in unfavourable conditions, in tandem with a SB failure. The pink vertical line represents the buffer stop location.

The scenario depicted in Figure 2 pertains to sequential failures of the ATP-initiated service brake and traction cut-out function before an eventual EB intervention once linespeed is exceeded by 5kmh^{-1}.

This delta is reached once the braking curve has dropped to approximately 57kmh^{-1}, and vehicle speed has increased to 62kmh^{-1}. The ATP response time is a typical 0.7 seconds, at which point the vehicle has continued accelerating up to almost 64kmh^{-1}, whilst the permitted linespeed has dropped to 55kmh^{-1}. Only now does the EB start to activate, with the brake cylinder pressure (roughly analogous to the braking force experienced at the wheels) starting to build. Assuming non-vital traction switch-off fails, a sensor reads the increasing pressure, and traction is deactivated via a high-integrity intervention. Top speed is reached the moment before the traction cuts out, whilst the brakes are only applying approximately 50% of their maximum potential force. The consequence of this series of events is a train impacting a buffer stop at almost 35kmh^{-1}.

A release speed of 25kmh^{-1} for the final approach is present in the above example, extending up to the buffing face. This gives the driver discretion to operate the train at any speed up to this value. One rationale supporting implementing a release speed is that as the enforced driving profile decreases to a standstill it becomes increasingly difficult to adhere to, due to the poor handling characteristics of a large, heavy train. Release speeds also protect against positional uncertainty arising from microslip occurring at the wheels used for odometry. Microslip can make the ATP believe the train is travelling faster than it actually is, which can result in an erroneous brake application. Usually microslip is not a hazard in and of itself, but when operating within the tight tolerances of a platform its presence becomes far more significant. A release speed can permit a faster approach and later braking, reducing overall transit times and improving operational performance and reliability. Undesirable ATP intervention can cause a train to stop prior to the platform and rack up delay minutes, and upon resetting the train after such an application a potentially dangerous situation has evolved where the vehicle must now accelerate towards the buffer to reach the stopping point. In addition to this hazard, passengers on the platform are likely now pressing door-open buttons, and passengers onboard will be confused as to why the doors have not yet been unlocked.

Whilst the example depicted in Figure 2 is somewhat embellished by the high release speed, it does highlight the potential that exists for catastrophe when unsuitable speed profiles are integrated into the signalling design. Station layouts could mean only suboptimal placement of buffer stops are possible, with just a few metres between buffing faces, and a concrete wall, or precipitous drop from a viaduct that may follow. Capacity and performance demands can incentivise signalling and system designers to squeeze every possible second out of each journey. This may result in speed profiles being pushed closer to the buffer stop, which reduces the margin for error that would otherwise mitigate an unlikely but potentially severe collision.

3. Results

By conducting event tree analysis, we can produce discrete maximum impact speeds where each branch of the "tree" corresponds to a different combination of precursor events. As an example, the branch corresponding to a driver ignoring an initial overspeed indication but subsequently actuating the service brake upon hearing a secondary alarm will have a lower maximum attainable speed when compared to the scenario of a driver ignoring all overspeed indications, the ATP system failing to cut-out traction, and the service brake system failing, requiring autonomous intervention of the emergency brake via ATP. Whilst the former scenario is far more probable than the latter due to the smaller required number of consecutive, concurrent failures and lapses necessary, all tree branches should be analysed to conduct a full risk assessment and allow due consideration of all scenarios that could credibly arise as per best practice outlined in standards such as EN 62502 (British Standards, 2011).

Ideally, there needs to be an identification of safety targets prior to undertaking this risk assessment, so the relevant personnel can compare results objectively and determine if they are workable, or whether implementation of further mitigations or controls is necessary. This may involve looking at how much kinetic energy a particular buffer stop is capable of dissipating, and whether this is adequate when factoring in a trainset's mass and potential impact speeds at the probabilities being considered. Typically, the severity of buffer stop impacts is recorded in Fatalities and Weighted Injuries (FWI) over an extrapolated one-hundred-year period, which considers the risk to both the passengers and workforce on the train, and to the public and staff behind the buffer stop. Risk is weighted considering daily approaches, passenger loading, the area behind the buffer in question, and factors to account for other characteristics of the site such as the end wall, train buffing face and overall potential for collision. Mitigations following the results of a Quantitative Risk Assessment for a particular scheme could entail limitations on approach speeds towards buffer stops, screening of driver distractions, adherence to mandated intervals between inspections of the end-of-track protection, measures to improve adhesion, and possible assessment of illumination on final approach. For pessimistic results, the distance from the normal stopping position to the buffer stop could be increased, end walls optimised for impact dissipation, and any retail units/offices in the area behind the buffer stop possibly being relocated.

TABLE 1:

Sample output of a Quantitative Risk Assessment of buffer stop collisions attributed to hyper-acceleration

1st Alarm Ignored	TCO Fails	2nd Alarm Ignored	SB Fails	EB Fails	Impact Speed	Probability (per approach)
Yes	No				N/A	~ $2x10^{-10}$
Yes		No			$5kmh^{-1}$	~ $2x10^{-12}$
Yes			No		$10kmh^{-1}$	~ $4x10^{-14}$
Yes				No	$15kmh^{-1}$	~ $4x10^{-16}$
Yes					$20kmh^{-1}$	~ $4x10^{-20}$

The worst-case impact speeds for the prerequisite combination of failures and/or errors are shown, alongside the probability of an impact occurring up to the specified impact speed every time a train approaches the buffer stop. Note: the figures contained within Table 1 are fabricated and should NOT be used for design nor assurance purposes.

4. Discussion

The RSSB's FWI measures are, of course, only guidelines, and the decision if the risk of a buffer stop impact is tolerable or not is dependent on numerous factors such as crashworthiness, train loading, compatibility between train and buffer stop height, seating arrangements and the external environment. A rudimentary calculation converting probability to "number of years per event" may well reveal a collision at an unacceptable speed could occur too frequently to be signed off, and conversations will need to be had about altering approach profiles, lowering release speeds, or upgrading to a buffer stop capable of handling an impact at such a speed if it were to occur.

There are certain operational and engineering controls we can implement to mitigate the risk of a buffer stop collision. Often a high-magnitude impact may result from a train hyper-accelerating from a far higher speed (as shown in Figure 2), right before the profile drops to enforce the train's deceleration on the final approach. Whilst an ATP intervention at high speed should take the same time as one occurring at a lower speed, a far greater distance will be covered in this period, meaning that whilst the train may start braking well before the buffer, the driver will essentially "run out of track" and hit it anyway. We can deal with this by lowering the release speed, moving the higher preceding speed profile back a distance that correlates to an impact speed that is acceptable, or by implementing a "step-down" speed profile where the enforced speed drops incrementally. This has the benefit of permitting additional resolution and control compared to a continuous service braking curve, which will likely have to adhere to an equation defined in the safe braking model governing the network. As aforementioned, often the EB system will include a magnetic track brake (MTB); this is commonly inactive during high-speed braking and on many trains will only apply if the EB is initiated at speeds below $20kmh^{-1}$,or a comparable low-speed figure. Hence, a secondary benefit of an optimised approach profile is that the MTB may now be permitted, which has a marked effect on the overall deceleration rate.

Frictional buffer stops are fixed to the track and designed to slide—some up to almost 10 metres. Hence a key consideration for safe installation and effective performance of end-of-track protection is communication between the station designer and signalling team to ensure that sufficient track length can be provided for a buffer stop to be situated where it has adequate distance to suitably mitigate collision hazards appropriately. Even on greenfield projects, all too often this is an afterthought, and consideration is omitted until issues crop up at a later stage of the project where an ingenious signalling solution is now required to ensure safe operation whilst delivering a workable timetable to the operator.

5. Conclusion

In this paper, we have outlined the risk of buffer stop collisions, and how protection systems such as ATP and driver vigilance devices may not actually mitigate impact risk effectively. We have shown that in exceptional circumstances, hyper-acceleration can cause a train to impact end-of-track protection at a speed significantly greater than a buffer stop's design speed. Operational or engineering controls such as invoking step-down speed profiles or station design considerations allowing a buffer stop to be placed further forward with a greater distance to arrest train movement before the physical end of track can prove more effective solutions. Where this is not possible, for example on brownfield sites, due diligence and rigorous and robust risk assessment processes should be followed to ensure that the residual risk of a buffer stop collision is reduced to as low as reasonably practicable.

References

- British Standards, 2011. Analysis techniques for dependability - Event tree analysis (ETA) - EN 62502:2011, s.l.: BSI Standards Publication.
- IEEE, 2009. IEEE Guide for the Calculation of Braking Distances for Rail Transit Vehicles, s.l.: IEEE.
- Robert, R. C. a. R., 2022. Simulating Performance, s.l.: IRSE News.
- RSSB, 2012. Railway Action Reliability Assessment user manual - A technique for the quantification of human error in the rail industry, s.l.: RSSB.
- RSSB, n.d. Safety Risk Model v8.5.02, s.l.: s.n.

Bharath Kumar Amaranath
Senior Group Engineer
Engineering Services – Global Technology Center
Bangalore, India

Tiju Zachariah
Associate Technical Director
Engineering Services – Global Technology Center
Bangalore, India

Chris Hendy
Technical Director, Atkins Fellow, Professional Head of Bridge Engineering & Transportation
Engineering Services – Transportation – UK
Epsom, UK

Zhao Lei, Zhao Shikang
CHEC Port City Colombo Pvt Ltd.
Sri Lanka

Bridge Engineering

07: Design Consideration Including Construction Stage Analysis for the Cable Stayed Bridge (FB01-Marina Bridge) in Port City Colombo Project, Sri Lanka

Abstract

Port City Colombo developed by CHEC Port City Colombo (Pvt) Ltd through China Harbour Engineering Company (CHEC) is a pristine city development in Colombo, Sri Lanka, spanning 269 hectares. Port City Colombo, built as an extension of Sri Lanka's vibrant capital city Colombo, once completed, would be South Asia's premiere residential, retail and business destination. Atkins, a member of the SNC Lavalin Group, was appointed by CHEC Port City Colombo (Private) Limited to provide Consultancy Services for the design of all Infrastructure and Landscape works, public realm, and associated infrastructure in Colombo Port City. This paper discusses the design criteria of the marina cable stayed foot bridge (FB01) in depth including the construction stage and service stage analysis and design checks.

KEYWORDS

Fixed Arch Bridge; Cable Stay; Pedestrian Footbridge; Steel Orthotropic Deck; Long Span; Tuned Mass Dampers; Cable Tuning Analysis

1. Introduction

The approved masterplan of Colombo Port City Project requires a very attractive pedestrian footbridge near the mouth of the canal entering the Port city. This is depicted in Figure 1.

FIGURE 1

Master plan of Port City Colombo

The aesthetic parameters of the foot bridge include an in-plan curved deck with a radius of 120m, spanning 137m between the abutments, and supported by an inclined steel tubular arch and stay cable supports.

This paper discusses in detail the various options that were considered to meet the aesthetic requirements, the design criteria considered, including the construction stage analysis, and few challenges involved. The paper also gives an insight into the mathematical model developed to understand the dynamic behaviour of the bridge and inspecting the bridge for (i) any pedestrian induced deck excitation and (ii) the susceptibility of the footbridge to any wind induced excitation. The use of tuned mass dampers for eliminating residual deck excitation, if any, is also studied. Further, the paper highlights the choice of cable supports and the importance of cable tuning analysis for the construction sequencing used for this foot bridge.

The article concludes with the learning experience of the design and construction teams during the design and construction phase of the footbridge. A few site photographs showing construction stages of the footbridge are depicted in Figure 2.

FIGURE 2

Construction photos of FB01 bridge

2. Concept Design

The design intended in the masterplan needed several options to be studied as this bridge was strategically proposed to be located at the “mouth” of the canal and was meant to be used for several occasions including lighting shows during Sri Lanka’s national day celebrations.

With the above requirements in mind, it was agreed that the basic form of the bridge required a deck curved in plan, supported by cables connected to a steel arch leaning backwards. A few other option studies conducted along with the finalised option are described below.

2.1 OPTION STUDIES

The options study for the bridge included a footbridge with

1. In-plan curved orthotopic deck supported by cables connected to a leaning single pylon as depicted in Figure 3.
2. Curved orthotropic steel deck supported by a twin pylon and cable stay support arrangement as depicted in Figure 4.
3. Fixed double arch with stay cables supporting curved deck as shown in Figure 5. Alternate forms of the arch support studied in this sub option included (i) a 3-dimensional space framed arch and (ii) a tubular section with varying diameter of both arches as depicted in Figure 5.

FIGURE 3

Option study – Single pylon cable stayed

FIGURE 4

Option study – Twin pylon cable stayed

FIGURE 5

Option study – Twin arch cable stayed

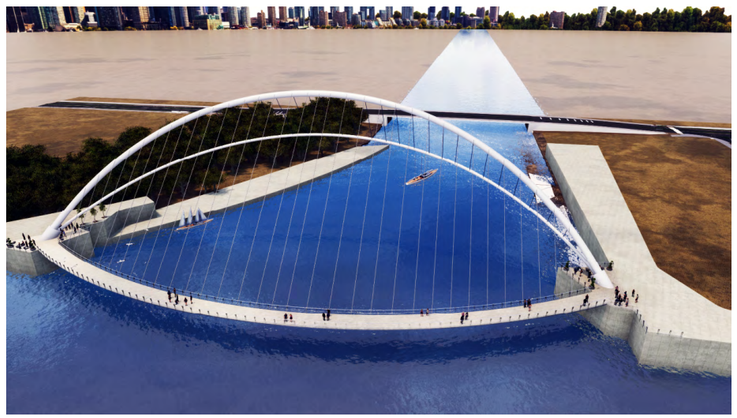

2.2 FINAL STRUCTURAL FORM

The option with a single backward leaning arch was concluded as the one providing better structural efficiency with optimal material usage, and easier to fabricate and assemble at site. Most importantly, it does not require any support inside the creek. Figures 6, 7, and 8 show the final form of the bridge.

FIGURE 6

Plan of bridge

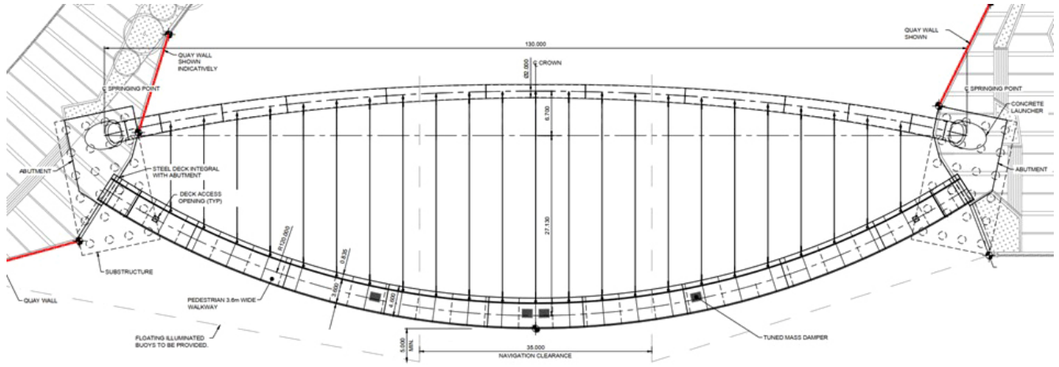

FIGURE 7

Elevation of bridge

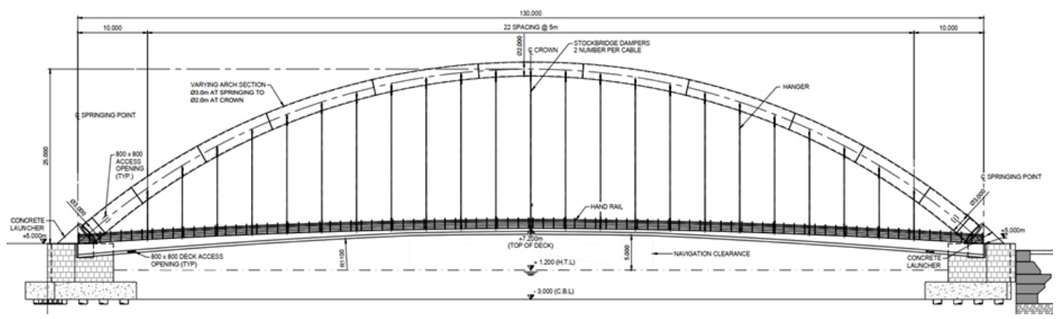

FIGURE 8

Typical cross section of bridge

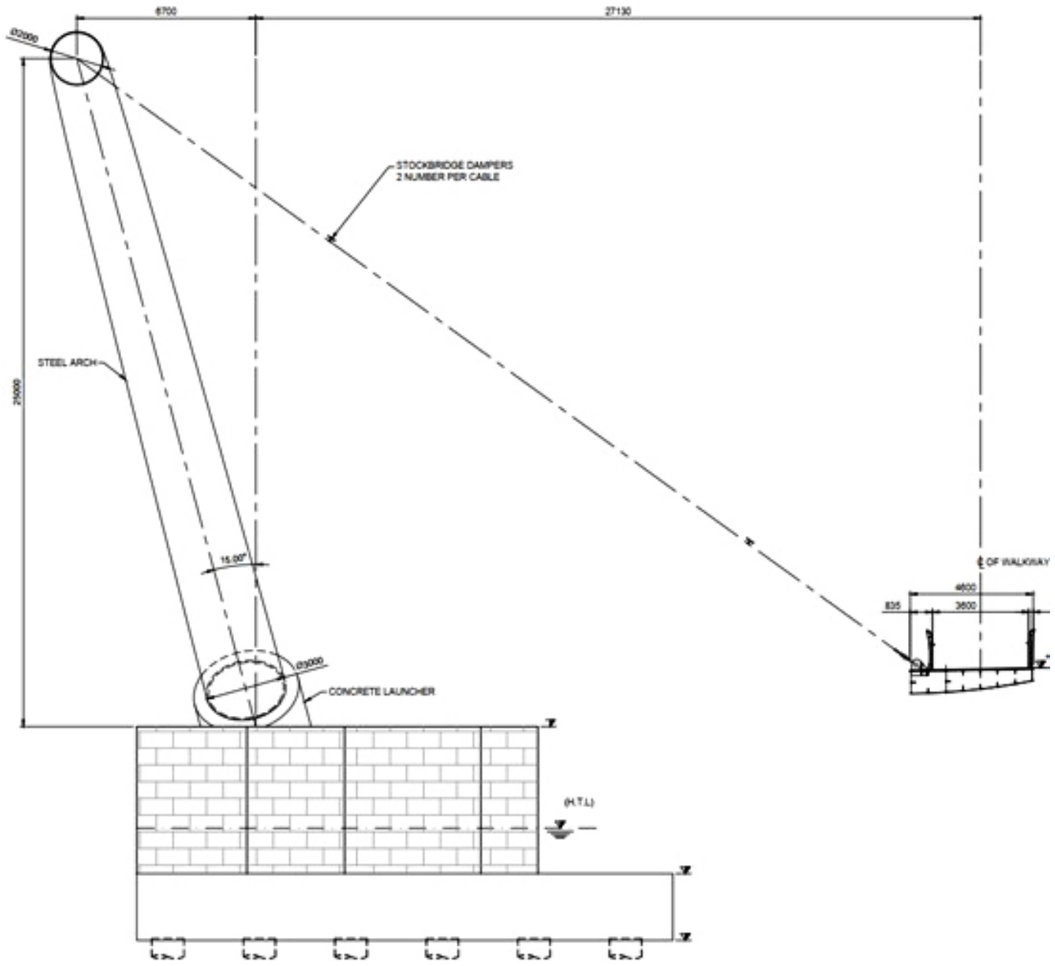

3. Detail Design

3.1 FOUNDATION AND SUBSTRUCTURE

The geometry of the deck curved in plan with an offset/eccentricity with respect to the line of abutment supports, as large as 18m, posed a unique challenge for designing the huge out-of-balance moments to be restrained at the supports.

To counter this problem, the arch was inclined at an angle of 15 degrees about the vertical axis, leaning away from the deck, which resulted in countering the moments in the opposite direction. It was also advantageous to make the steel orthotropic deck integral with the abutments to limit the effects of thermal expansion and contraction as well as to satisfy the dynamic characteristics of the entire structural system for both wind and pedestrian induced effects.

Figure 9 depicts the plan view of the abutment structure. The size of the abutment is 6m (width) x 9m (length) x 4.5m (depth) and are supported on pile foundation. The orientation of the abutment and pile foundation were chosen such that it reduced the secondary moments generated from eccentricity for thrusting actions from the arch and deck.

The rigid support arrangement provided a robust mechanism for the transfer of relatively huge axial thrust forces generated from arch and deck.

The geotechnical interpretative report mentions soil layer classifications as follows:

- Reclaimed soil fill
- Very loose silty sand
- Stiff sandy clay
- Highly weathered gneiss
- Moderately weathered gneiss

As the site was on reclaimed land, foundations had to be deep with 1.2m diameter piles anchored into the medium weathered gneiss rock.

The length of the pile foundation was about 17m with maximum pile capacities of 7250kN calculated, considering end-bearing capacity and shaft friction capacity contribution for the portion of the pile socketed inside the rock strata.

Pile capacities were calculated based on the following equations with a factor of safety of 3:

Shaft resistance in rock socket: $Q_s = f_s \times \pi \times d \times L_s$

Base resistance in rock socket: $Q_b = q_b \times \pi \times d \times d/4$

where,

Q_s = Friction capacity, kN

Q_b = Base capacity, kN

f_s = Ultimate unit shaft resistance, kPa

q_b = Ultimate unit base resistance, kPa

d = Diameter of pile, m

L_s = Length of the pile, m

The Srilanka Bridge design manual, along with British standards, were used for design of piles.

FIGURE 9

Plan showing bridge abutment and foundations

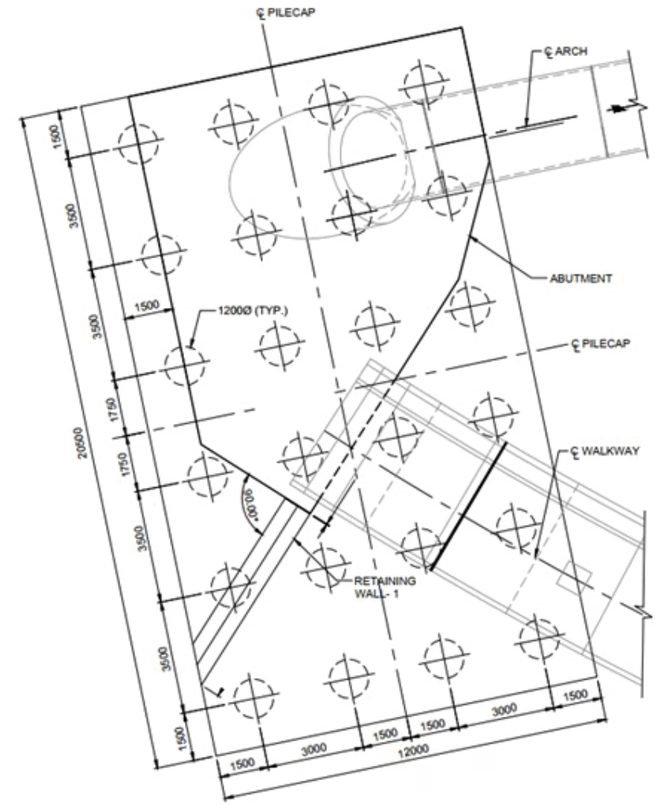

3.2 ORTHOTROPIC DECK DESIGN

The deck is curved in plan with a radius of 120m. In addition to this, a vertical profile of radius 110m radius was required to facilitate adequate vertical clearances for vessel movement underneath the bridge. The deck cross section varies from 0.8m at centre to 2.0m at support section.

The deck was cast into abutment with steel integral connections and reinforced concrete launcher, which connects the steel arch with fixed end condition to the abutment.

Since the deck was supported only by cables on the inner side, as shown in Figure 10, the geometry of the deck needed careful consideration with regards to the location of its shear centre and line of forces from cable.

FIGURE 10

Typical cross section of bridge

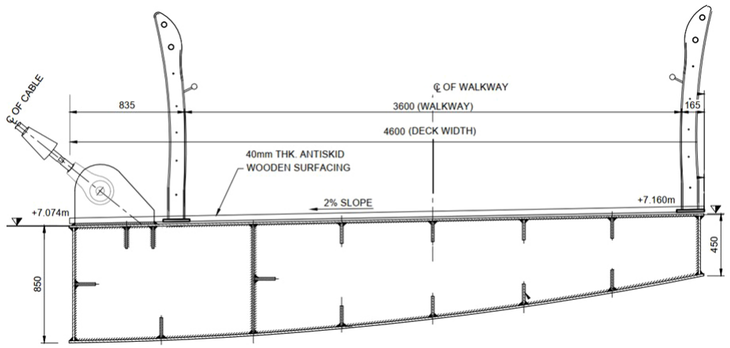

The plan curvature of the deck provided torsional rigidity and stiffness to lateral bending about longitudinal bridge axis.

The deck steel sections were verified for (i) combined bending and shear representing bending action and (ii) combined axial and bending for axial compression forces as per clause 9.9.3, 9.9.4, and 10.6.2 as per BS 5400-3. Plate sections were also checked for yielding criterion of combined effects as per the equation given below and limited to yield stress of the material:

$$\sigma_{1e}^2 + \sigma_2^2 - \sigma_{1e}\sigma_2 + 3\tau^2 \leq \left(\frac{\sigma_{yw}}{\gamma_m \gamma_{f3}}\right)^2$$

where,

σ_1 and σ_2 = Principal stress in two planes

τ = Shear stress

σ_{yw} = Yield stress of material

γ_m, γ_{f3} = Partial safety factors

A detailed Finite Element Model was developed in Lusas software, representing each element of the deck such as top flange, bottom flange, stiffeners, top diaphragm, and end plates, and was verified for Von Moises stress verifications.

FIGURE 11

Lusas Model - FB01 bridge

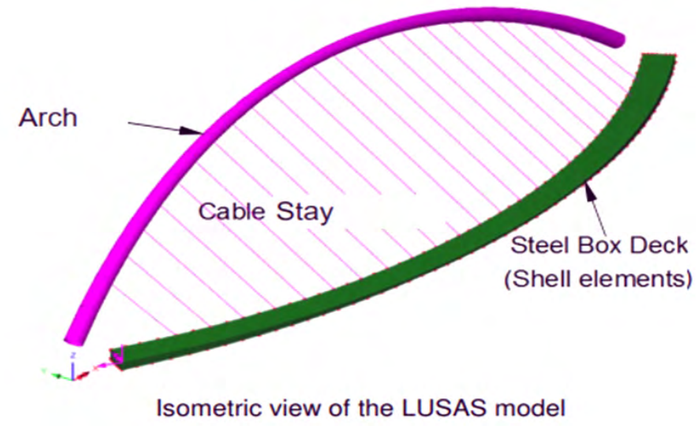

FIGURE 12

Finite Element Model - Deck of bridge

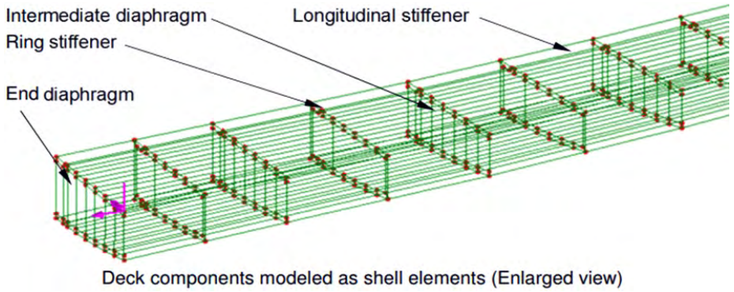

The steel decks were made integral with the abutments to provide rigid supports. This was achieved by providing end plate, anchor plates, and stiffeners connections that transferred the tensile force from top flange to reinforcement slotted in the holes of anchor plates. The forces from reinforcement transferred to concrete through shear transfer. Figure 13 depicts the above-mentioned arrangement.

FIGURE 13

Deck Integral Connection
- Cross section

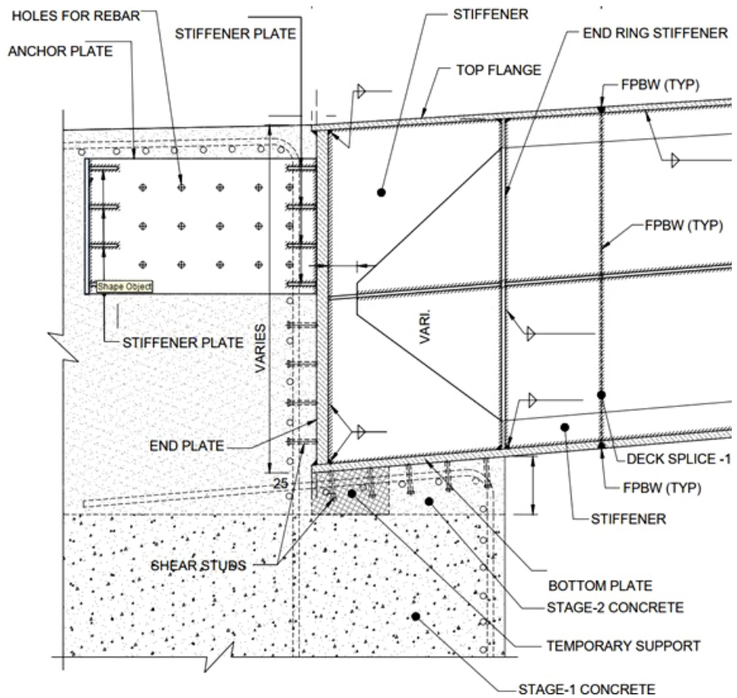

The cable connection points on the deck were chosen at a constant spacing of 5m along the length of the bridge. Due to plan curvature of deck and the backward inclination of the arch, the angle of inclination of each cable at its connection points also varies, resulting in varying forces to be considered for the connection designs.

3.3 ARCH

Arch height from springing to crown is 25m with inclination of 15 deg leaning away from the deck which gives a lateral offset of 6.9m at the crown. Some of the critical design considerations for cable stay bridges, such as this bridge, include the following:

- cross section to provide maximum lateral stiffness to support deck.
- minimal resistance to wind induced excitations.
- angle of the cables connecting the deck (refer to Figure 8).
- buildability of the arch structure in terms of shape, optimised segment length, ease of fabrication, etc.

The diameter of the steel tubular arch section varied from 3.0m at the springing support to 2.0m at the crown as shown in Figure 14. The arch was split into 13 segments to limit segment weight to 75 tonnes to facilitate ease of fabrication, segment transportation and assembly at site.

FIGURE 14

Arch – Elevation – Half view

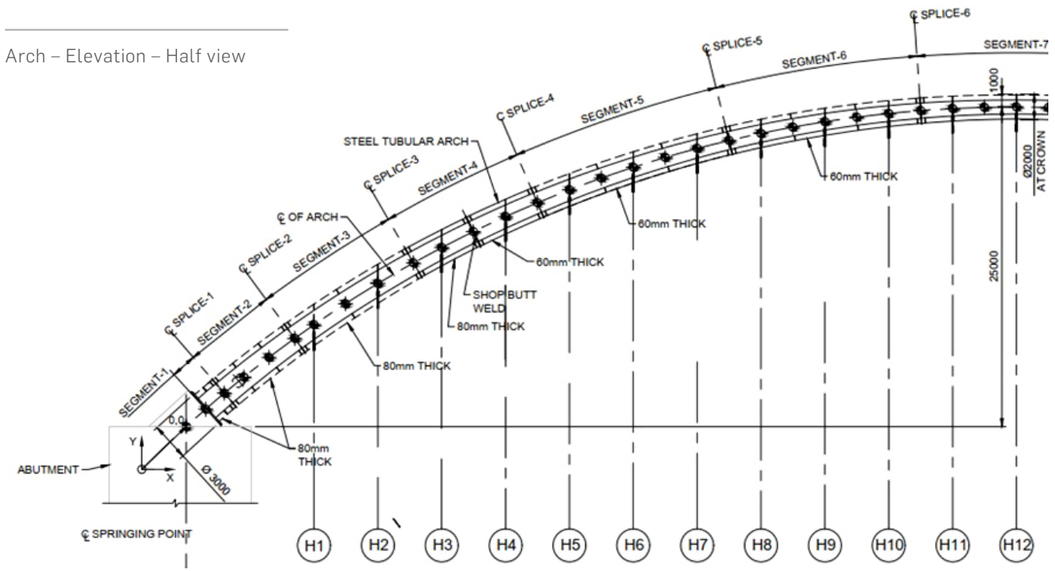

FIGURE 15

Arch – Cross section at diaphragm

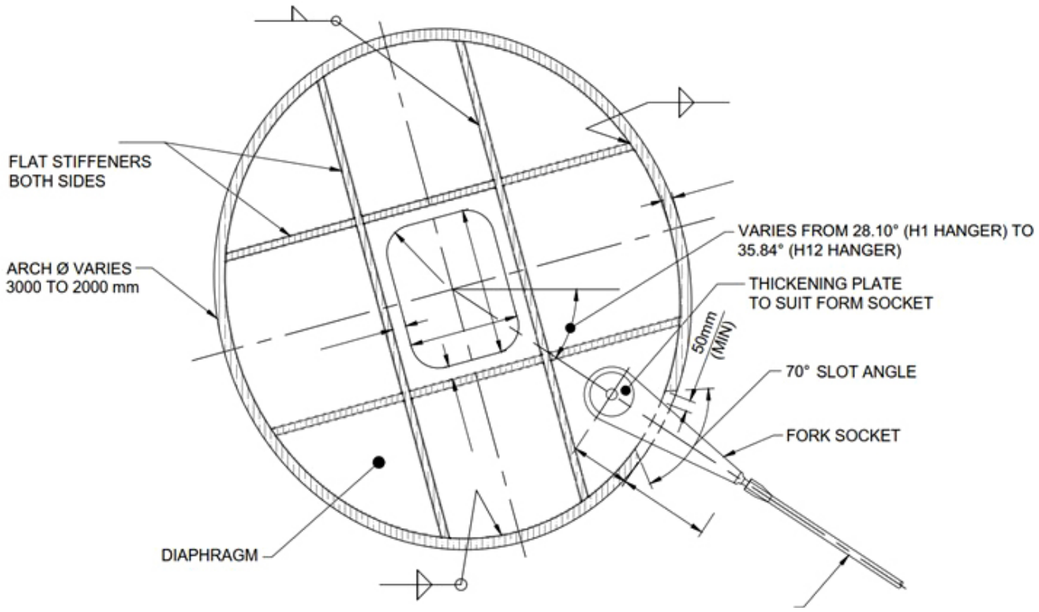

The connection of the fixed arch with the concrete launcher and substructure were achieved by post tensioning system comprising of 24 bars of 75mm diameter Macalloy 1030 bars.

Reinforced concrete launchers, as depicted in Figure 16, were provided for the supports and were designed considering the large axial thrust and bursting forces developed from the arch on the reinforced launcher.

The arch sections were also verified for (i) combined bending and shear along with (ii) combined axial and bending as per clause 10.6.1, 9.9.1, 9.9.2, and 10.6.2 as per BS 5400-3 with corresponding buckling factors. Plate sections were also checked for yielding criterion of combined effects as per the equations provided in section 3.2 and limited to yield stress of the material.

$$\frac{P_{\max.}}{P_{\mathrm{D}}} + \frac{M_{\mathrm{x,max.}}}{M_{\mathrm{Dxc}}} + \frac{M_{\mathrm{y,max.}}}{M_{\mathrm{Dyc}}} \leq 1.0$$

where, $P_{max,}$ $M_{x,max}$ & $M_{y,max}$ are maximum axial loads and bending moments corresponding direction.

$P_{D,}$ M_{Dxc} & M_{Dyc} are maximum axial and bending moments capacities corresponding direction.

FIGURE 16

Cross section through concrete launcher

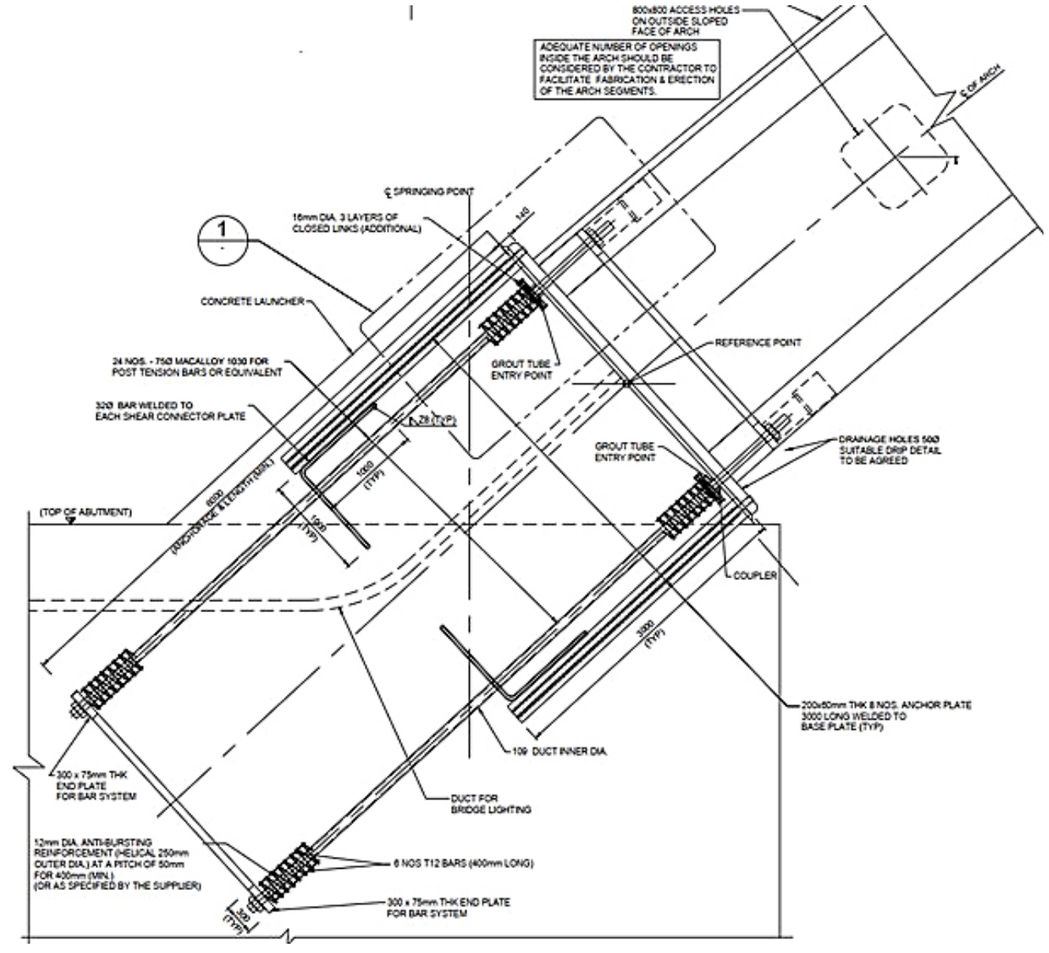

3.4 CABLE STAY

The cable stay system comprises of OVM parallel wire strands with socket, connecting sleeve, and forks at the ends as shown in Figure 17.

The fork socket with pin at ends is provided to connect the cable to the deck and arch ends. The connection is made using a gusset plate which is connected to the top of the deck and arch diaphragms. The connecting sleeve helps to connect the cable to the fork socket and also in adjusting the tolerance of cable lengths during the construction stage.

The cables were designed for SLS, ULS and Fatigue limit states. In general, the stresses in the cable would be limited based on the fatigue design requirements. The cables are designed in such a way so as to take into consideration any accidental snapping and the temporary redistribution of the forces to the adjacent cable stays.

Additionally, each cable was provided with Stockbridge damper to mitigate any wind induced vibrations of the cable.

FIGURE 17

Cross section through concrete launcher

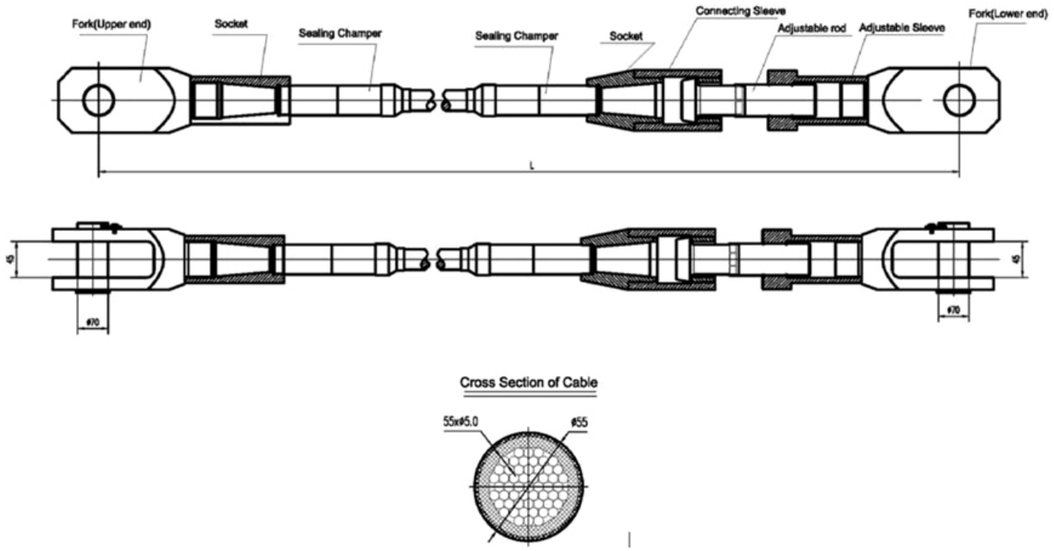

3.5 MATERIAL SPECIFICATION AND MAINTENANCE

As the bridge was in the coastal region and over the sea water, careful considerations had to be made in the choice of the material used for the bridge's components.

The substructure and foundation were provided with M40 grade concrete with adequate cover to the reinforcements along with protective coating over the finished concrete surfaces as well as to the exposed surfaces of the steel superstructure deck and arch.

Weathering steel was extensively used with additional allowance for corrosion effects during the service life of the foot bridge.

The inside of the arch section is made accessible with access openings closer to the springing location of the arch so that maintenance and inspection can be easily carried out.

Both the Arch and deck were provided with drainage holes inside so that any condensation or leakage of rainwater inside the deck could be drained out easily.

3.6 BUCKLING ANALYSIS

The slenderness for arch buckling analysis was carried out in Lusas to find global buckling mode shape of the structure.

All the loads were lumped into a single load and observations were made over first 100 modes for the global buckling mode, which had first arch buckling mode with single curvature as shown in Figure 17.

FIGURE 18

Global buckling mode from Lusas

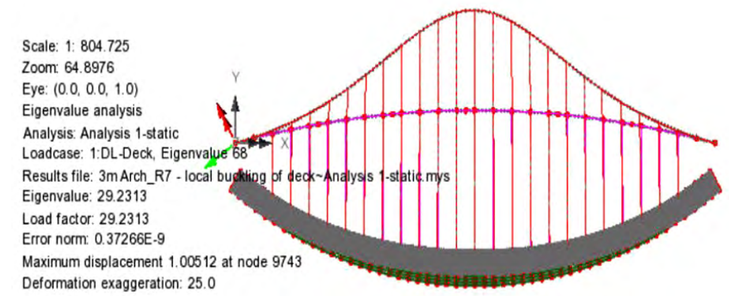

Results from the buckling analysis revealed that the critical buckling factor is about 30, thus indicating adequate margin of safety for buckling in arches. The results from Lusas was also compared with manual calculations using Euler buckling formulas and was found to be comparable with the detailed analytical model.

3.7 DYNAMIC ANALYSIS

The slender form of the bridge necessitated complete dynamic analysis to be carried out, both pedestrian dynamics and aerodynamics checks. Mitigation measures were provided by specifying tuned mass dampers (TMD) on the deck.

Using Finite Element model in Lusas, natural frequency of the bridge was verified and found to be having the first mode of vibration in the vertical direction with a frequency of 0.85Hz single curvature between supports – vertical mode, 1.82Hz double curvature between supports – vertical mode and 2.88Hz single curvature in middle third portion only – vertical mode, which were less than the frequency of 5Hz specified in Eurocodes. The potential modes of deck and arch system are shown in Figures 19, 20, and 21, respectively.

Pedestrian-induced dynamic checks were also studied in detail for walking, jogging, and crowd loading as per BS EN 1991-2 using Finite element analysis. Accelerations of the bridge were verified using Lusas and Dynamassit software. Sample accelerations for the bridge for crowd loading is shown below in Figure 22. As per clause BS EN 1991-2 and NA 2.44, accelerations limited to 1m/sec^2.

The deck accelerations were close to limiting values and hence, as a precautionary measure, tuned mass dampers were specified for different potential modes of vibration with parameters specified in Figure 19, 20, and 21 which were beneficial for wind excitations, as well.

FIGURE 19

Mode 1 with NF 0.853Hz

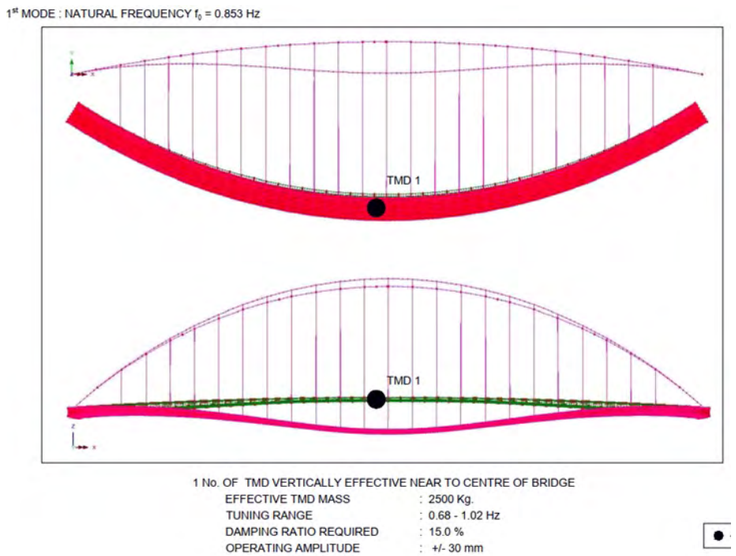

FIGURE 20

Mode 2 with NF 1.822Hz

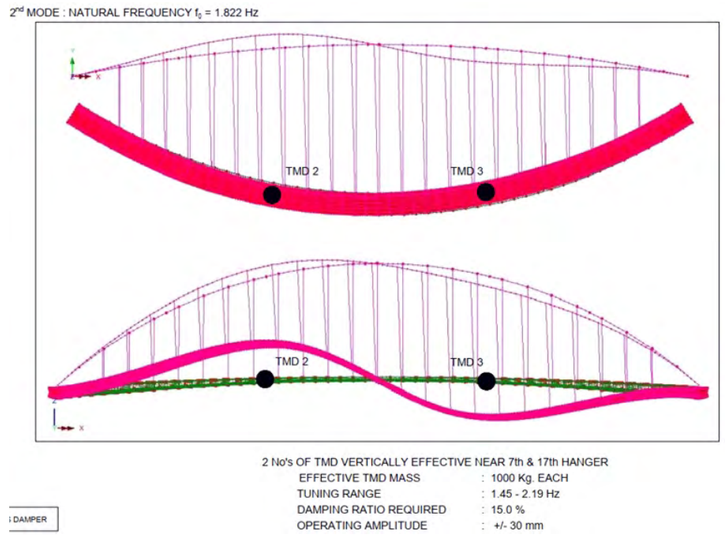

FIGURE 21

Mode 4 with NF 2.788Hz

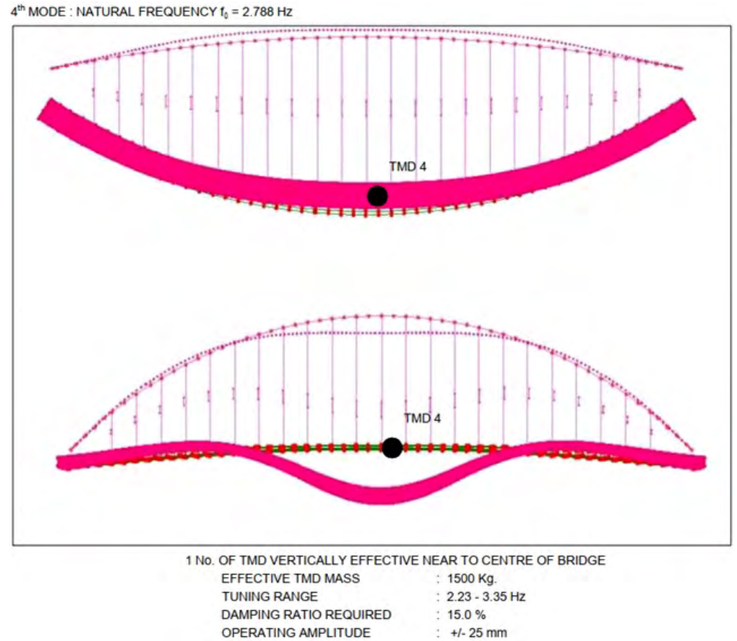

FIGURE 22

Acceleration graphs for Mode 1

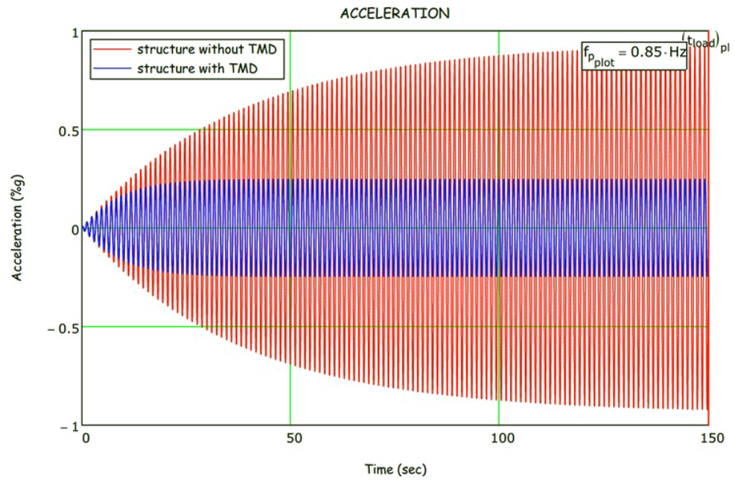

Tunes mass damper were chosen with different weights and damping ratios to give an effective damping ratio for the structure. Different combinations were verified and the one that gives the better behaviour and least accelerations were chosen.

Aerodynamic checks were carried out using BS BD49/01. The aerodynamic susceptibility factor P_b was checked as per clause 2.1 for the applicability of bridge for wind excitations and further verifications.

$$P_b = \left(\frac{\rho b^2}{m}\right)\left(\frac{16V_r^2}{bLf_B^2}\right)$$

where,

r = The density of air
b = Overall width of the bridge deck
m = Mass per unit length of the bridge
V_r = Hourly mean wind speed
L = Length of the relevant maximum span of the bridge
f_B = Natural frequency in bending

The bridge deck's susceptibility to vortex excitations, galloping, and stall flutter were checked as per clauses 2.2.1, 3.1, 2.1.2, and 2.1.3 in detail and found to be within acceptable limits specified in code.

Critical speed for Vortex excitation is calculated using following equations as provided in clause 2.1.1.2 of BD49/01:

$$V_{cr} = 6.5\ fd$$

where,

f = Natural frequency of corresponding mode
d = Depth of the bridge deck

Critical speed for galloping and stall flutter to be calculated as per equations given below:

a) Vertical motion

$$V_g = V_{Rg} f_B d_4$$

(b) Torsional mode

$$V_g = 5 f_T b$$

Critical wind speed for stall flutter is given by:

$$V_{Rf} = \frac{V_f}{f_T b}$$

where,

f_B = Natural frequency in bending mode
f_T = Natural frequency in torsional mode
d_4 = Depth of the bridge deck
b = Width of the bridge deck

3.8 CONSTRUCTION STAGE ANALYSIS

A detailed construction stage analysis was carried out based on inputs from the construction team. The initial design assumption was to tension the cables after the arch was lowered from the trestle support. A detailed cable tuning analysis in the Lusas software was carried out to arrive at the cable forces in each cable stay for different cable sequencing and achieving deck at proposed finished level.

However, further discussions with the construction team on the feasibility to construct onsite required the following sequencing:

- Arch and deck segments to be erected on the trestle supports with pre-cambering.
- Once the arch and deck splicing were completed, the cables from the arch were connected to the deck and provided with minimum preloads/tensioning to ensure no slack.
- The deck and arch were lowered gradually and simultaneously to provide tensing in the cables by self-weight of the structure.

The construction sequence as seen in Figure 23 dictated the design of cables and deck structure.

FIGURE 23

Construction sequence

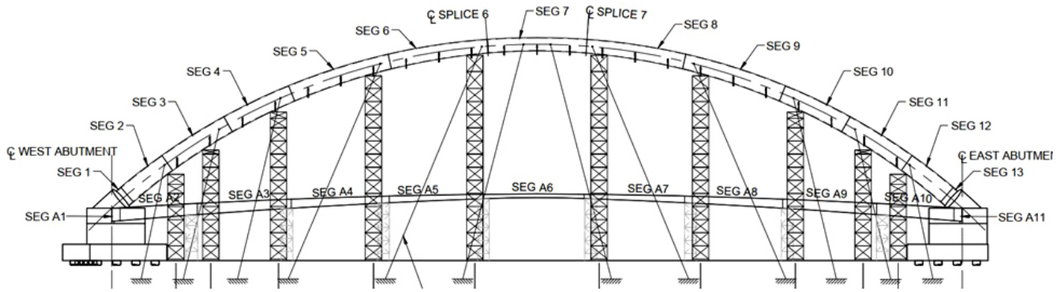

4. Conclusion

This paper describes the evolution of the foot bridge design from concept design stage to construction stage. A discussion of the analysis and design of the chosen structural form is presented in this paper. This paper also details the importance of choosing the apt structural form, choice of suitable materials, importance of detailing for ease of fabrication, and assembly at site, etc. Critical design checks such as that for wind – and pedestrian-induced vibrations and the associated mitigation measures are also presented. The construction of Marina Cable Stayed footbridge bridge is completed at site and will soon be opened for public. This footbridge brings to light the harmony between the bridge's intended purpose, the aesthetic requirements, and the optimal use of material, making it a construction marvel.

Acknowledgements

This paper was originally presented at IABSE Congress Nanjing 2022, Bridges and Structures: Connection, Integration and Harmonisation; September 21-23, 2022, Nanjing, China.

References

1. Chris R Hendy David A Smith Manuela Chiarello Walton bridge - A new arch bridge over the River Thames, UK ICE proceedings Vol 170 issue BE2
2. Chris R Hendy Designer Guide to EN 1993-2 Eurocode 3: Design of steel structures part 2: steel bridges
3. Chris R Hendy Designer Guide to EN 1992-2 Eurocode 2: Design of concrete structures part 2: Concrete bridges
4. Ian Ward Modal Maths- Formulas for structural Dynamic Issue 3.
5. Z A Blandford A Critical Analysis of the Gateshead millennium bridge
6. Butterworth, K. Carr, D. Kassabian, P., 2003. Gateshead Millennium Bridge, UK: fabrication, assembly and erection, Proceedings- Institution of Civil Engineers Bridge Engineering, Vol. 156, No.1, pp.11-20
7. BS EN 1991-2 Eurocode 1 Actions on structures – Part 2: Traffic loads on bridges
8. DMRB BD 49/01 Design rules for Aerodynamic effects on bridges
9. BS EN 1993-1-5 Eurocode 3 Design of steel structure Part 1-5 Plated structural elements
10. PD 6688-1-4 Background information to the National Annex to BS EN 1991-1-4 and additional guidance.

Stuart Archer
Principal Engineering Geologist
Engineering Services - Infrastructure UK
Cardiff, Wales, UK

Iain McKenzie
Principal Geotechnical Engineer
Welsh Government - Transportation Department
Wales, UK

Ground Engineering

08: Structural Culvert Subsidence: An Evidence-Based Assessment of Failure Mechanisms at a Site in South Wales

Abstract

Since installation in the mid-1980s, the culvert carrying the Nant y Coedcae watercourse beneath the A40 Trunk Road in Carmarthenshire, west Wales, has shown signs of movement. Initial indications of movement included minor cracking to the reinforced concrete box sections, but current movement is noticeable as subsidence. The highways agent manages the subsidence through regular carriageway resurfacing when there are concerns over road safety. The trigger for intervention is not easy to define, but the Overseeing Organisation considers that the ongoing asset management mitigation (regular resurfacing) may be exacerbating the problem and cannot go on in perpetuity. An investigation was commissioned because the serviceability limits of the culvert and the road are rapidly being reached and an alternative strategy is required. Ground investigation (GI) proved an absence of compressible soil beneath the culvert and therefore ruled out the initial hypothesis of consolidation settlement as the cause for subsidence. A free-draining granular backfill was used around the culvert and this was shown to be loose within a zone above and below water levels recorded during the investigation. Installation of monitoring equipment identified that subsidence event(s) were occurring following periods of high groundwater. The failure mechanism postulated as a result of the investigation and monitoring was “suffusion,” which is defined as “seepage-induced internal instability… whereby fine particles are transported from a non-plastic soil” (Fannin and Slangen, 2014). Soils experiencing suffosion are expected to have lower relative densities.

In this instance, subsidence of the culvert and carriageway above could result from a reduction in volume of the supporting granular fill, which could be expected to occur once groundwater levels normalise following peak periods. It is hoped that this finding could assist programming of resurfacing work and that it should inform backfill selection in future culvert design.

KEYWORDS
Engineering geology; Culvert; Subsidence; Monitoring; Prediction; Suffusion

1. Introduction

The A40 trunk road (A40), officially referred to as the London to Fishguard Trunk Road, was the main east-west link between London and south Wales prior to the construction of the motorway network. The route has been superseded by the motorway network in much of England and Wales. It remains a key route on the strategic highway network in south Wales, linking Fishguard in the west to Monmouth in the east via a number of significant employment and residential settlements across the region. The route is regionally and nationally important as it provides links between St Clears and onward to the key strategic ferry ports in Pembrokeshire, important regional population centres such as Haverfordwest in the west and Carmarthen in the east, and links to the A48, and subsequently the M4.

Sections of the trunk road still follow the route of the Roman road, particularly through Carmarthenshire along the northern flank of the Towy valley, while other sections have since been re-routed or upgraded to meet current demands. The area of interest is part of a dual-carriageway section between Carmarthen and St Clears in Carmarthenshire built around Bancyfelin to eliminate a bend under the railway bridge where, since being constructed in the 1980s, there have been signs of deterioration that are localised around a reinforced concrete box culvert carrying the Nant y Coedcae beneath the A40 near Bancyfelin. The culvert is referred to as the Nant y Coedcae culvert. This paper outlines the construction, inspection and maintenance history, and recent investigations undertaken, and discusses the interpretations made and recommendations put forward to avoid similar instances in future highway construction.

The study relates to work undertaken by Atkins for the South Wales Trunk Road Agent (SWTRA) who act on behalf of the Welsh Government (WG) to maintain the strategic highway network in south Wales, UK.

2. Background

2.1. CONSTRUCTION

Construction of the culvert was completed in 1984. Available as-built drawings show the box culvert external dimensions as being 4.85m wide and 3.4m high. The culvert is orientated east to west whilst the carriageway at this location is aligned northeast to southwest; the culvert is therefore oblique to the carriageway orientation and extends to a length of 55m.

The culvert is bedded on 75mm of blinding concrete on top of 1m of "Granular Fill." Granular Fill is also shown on the as-built drawings as backfill to the culvert. No further details are available to indicate the characteristics of the Granular Fill. The blinding and mass concrete used within the structure is recorded as "Class E." The reinforced concrete structure is noted to have been constructed using Class 30/20 concrete, which uses concrete with a compressive strength of 30N/mm^2 once cured for 28 days in a mixture where the maximum aggregate particle size is 20mm.

All faces of buried reinforced concrete were painted with two coats of bitumen paint up to a level of 150mm below finished ground level to provide some form of waterproofing to the structure.

The reinforcement used within the structure is steel rebar at diameters of 12 to 25mm. The reinforcement generally has a minimum cover of 40mm. The minimum overlap of individual reinforcement bars is given as 41mm, with the minimum lap of reinforced mesh fabric stipulated as not less than 300mm in any direction.

The base of the culvert is recorded to have been filled with 600mm of "Type B Granular Material" to replicate the bed of the Nant y Coedcae watercourse. At the western end of the culvert, gabion baskets were constructed to prevent bank erosion. The geometry of the individual gabions is given as 2x1x1m and the wire for the baskets is PVC coated.

2.2. INSPECTION AND MAINTENANCE ON BEHALF OF THE TRUNK ROAD AGENT

Routine structural surveys and inspections have taken place since the construction of the culvert and the A40. Reference to early inspection records completed in 1984 (year of construction) and 1988 record evidence of some cracking within the concrete of the culvert walls (at construction joints) and aprons between the culvert and earthwork interface.

The most recent Principal Structural Inspection was completed on behalf of SWTRA in August 2014. The main feature identified is a large vertical crack, which is described in the report as follows: "There is a large vertical crack to the culvert which runs from the base of the sidewall all the way round to the base of the opposite side wall. The crack is 15mm wide at the base of both walls and reduces to 0.25mm at the soffit. The crack is located 16.9m and 24m in from the downstream end on the eastern and western abutments respectively."

The history of the large vertical crack has been reconstructed from the available structural inspection reports in Table 1 with maximum dimensions plotted over time in Figure 1. The aforementioned distances for the crack location suggest a northwest to southeast orientation below lane 2 (overtaking lane) of the eastbound carriageway and extending into the central reserve.

TABLE 1:

Timeline of changes in main culvert cracking

Year	Type of inspection	Main crack dimensions (mm)	Comments (verbatim from inspections reports)
1988	Structural General Inspection	Not recorded	Minor cracks in abutment walls and slab soffit.
1992	Structural Principal Inspection	0.2	Cracking and significant leaching on the soffit and walls. Also, a suggestion of damage to waterproofing which is leading to the significant leaching.
1996	Structural General Inspection	Not recorded	3No. cracks in upstream concrete boxes with leaching from cracks and joints suggest failed waterproofing.
1998	Structural Principal Inspection	0.2 to 0.25	Cracks continuous around both abutment walls and soffit. Leaching in the soffit and top half of both abutment walls.
2002	Structural General Inspection	Not recorded	Cracking with leachate through abutment and soffit.
2004	Structural Principal Inspection	0.25	Cracking in abutments and concrete slab with significant leachate staining. Cracks are not greater than 0.25mm in width. Associated dampness and leaching is indicative of failure of waterproofing system.
2006	Structural General Inspection	3.0	Large crack 3mm to both abutments, 17m from downstream end. Numerous cracks with calcite staining, some full width on concrete slab. Evidence of water entering the structure through cracks.
2008	Structural General Inspection	0.1 to 10	Severe crack 10mm wide with calcite staining at base reducing to 0.1mm at top of both abutments. Numerous cracks with calcite staining, some full width on concrete slab. Evidence of water entering the structure through cracks. Settlement to lane 1 eastbound above culvert.
2010	Structural General Inspection	0.1 to 10	Severe crack 10mm wide with calcite staining at base reducing to 0.1mm at top of both abutments. Evidence of water entering the structure through cracks. Numerous cracks with calcite staining, some full width on concrete slab. Depression in westbound carriageway slow lane.
2012	Structural General Inspection	0.1 to 10	10mm wide with heavy calcite staining at base of abutments reducing to 0.1mm at top. Numerous cracks with calcite staining, some full width on concrete slab. Evidence of water entering the structure through cracks. Slight depression in east and westbound carriageway lane 1 & 2 (surfacing reapplied).
2014	Structural Principal Inspection	0.25 to 15	Large vertical crack which runs all the way around from the base of each abutment. Crack is 15mm wide at base of both abutment walls and reduces to 0.25mm at soffit. Significant leachate staining.
2016	Structural General Inspection	0.25 to 15	Large vertical crack to both abutments 0.25 to 15mm. Numerous transverse cracks with significant calcite staining in Primary Deck Element (roof of structure). Extensive calcareous deposits at crack locations.
2018	Structural General Inspection	0.25 to 15	Large vertical crack to both abutments 0.25 to 15mm. Numerous transverse cracks with significant calcite staining in Primary Deck Element (roof of structure). Extensive leaching deposits at crack locations.

FIGURE 1

Main culvert crack: maximum recorded width from structural inspection records

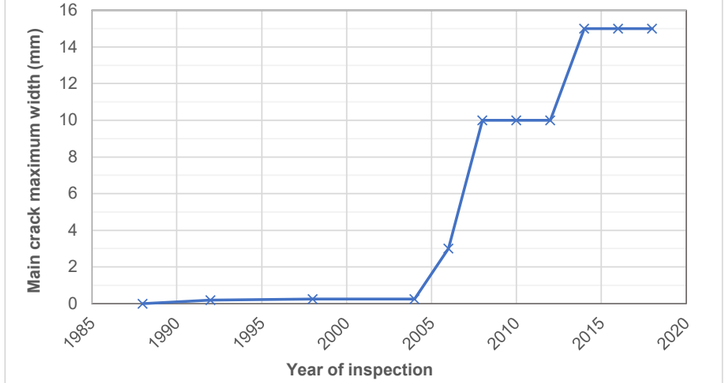

There is early evidence from a Principal Structural Inspection in 1992 of leachate in upstream boxes (beneath westbound carriageway) suggesting a failure of the waterproofing. It is not known whether the ongoing subsidence has led to defects in the waterproofing beneath the road construction layers, or if the waterproofing has failed for other reasons.

However, the inspection observations in Table 1 suggest that the subsidence and failed waterproofing may have been ongoing since construction and certainly since 1992 (eight years after construction).

The most recent structural record available is for an inspection that was completed in July 2018. The inspection noted numerous cracks within different elements of the structure. This included numerous transverse cracks with significant calcite staining in parts of the structure that are visible from inside the culvert (walls and roof). The inspection also confirms the 2014 inspection findings of a large crack present in the west and east walls measuring up to 15mm wide at the floor but reducing to 0.25mm at the soffit (roof). At the location of the cracks there are also extensive leaching deposits noted, which suggests damage to the waterproofing of the structure.

Principal Structural Inspections state that the culvert is designed to carry full HA loading and 45 units of HB loading. HA loading is a formula loading representing normal traffic in Great Britain. HB loading is an abnormal vehicle unit loading. SWTRA confirmed that the structure has not formed part of any assessment programme, and the condition surveys have not triggered re-assessment of the load carrying capacity; therefore, the original load rating is considered to remain current.

An inspection to assess scour at either end of the culvert was completed in September 2013. A Scour Risk Rating of 5 was assigned following the inspection. This is considered to be the lowest risk rating. Comments from the assessment identify the presence of three gravel bars within the culvert. It was also noted that the banks on either side of the entrance and exit of the culvert are stable with well-established vegetation.

3. Investigating the Cause of Carriageway Subsidence

3.1. DESK-BASED REVIEW

The superficial geology of the region varies, based on the British Geological Survey (BGS) mapping, Alluvium and Glacial Till are anticipated to underlie the A40 carriageway in the study area (British Geological Survey, n.d.). The strength and stiffness of these materials can be highly variable, with the fabric of the material affecting the engineering properties.

Historical exploratory holes located to the north of the site boundary record Glacial Till at approximately 1.4m below ground level (bgl), whilst exploratory holes to the south record Tidal Flat Deposits (with peat) at approximately 1.6m bgl.

The carriageway of the A40 Trunk Road at this location is supported by small embankments and at grade earthworks, which are likely to be comprised of Engineered Fill. It was anticipated that Engineered Fill is likely to reflect a general fill in composition and comprise reworked natural materials.

Based on available records, the bedrock comprises Ordovician shales of the Tetragraptus Beds (Arenig Series). The underlying geology of the road may be heavily folded and, as such, material characteristics and depth of weathering have the potential to vary significantly over short distances.

A summary ground model based on the factual report for the A40 Carmarthen to St Clears Trunk Road improvement works (Tarmac Construction Limited. Geotechnical Division, circa 1972 (exact date not provided)) is provided in Table 2 with an adapted extract of as-built cross section B-B in Figure 2. The investigation was conducted in 1972 prior to the construction of the A40 bypass diverting the route away from the village of Bancyfelin. One borehole (BH64) from the study relates specifically to the Nant y Coedcae culvert.

TABLE 2:

Factual report (Tarmac Construction Limited. Geotechnical Division, circa 1972 (exact date not provided)) findings at Nant y Coedcae culvert

Ground Conditions					Groundwater
Strata*	Thickness (m)	Depth (m bgl)	Elevation (m AOD)	Description^	
Alluvium / Tidal Flats Deposits (CH)	1.15	0 – 1.15	20.1 – 18.95	Soft organic gravelly clay of high plasticity	Groundwater strike at 1.5m below the existing ground level (18.6m AOD).
Alluvium (CL)	1.45	1.15 – 2.6	18.95 – 17.5	Firm alluvial silty clay of low plasticity with gravel	Highest recorded standing groundwater during drilling was at ground level (20.1m AOD)
River Terrace Deposits (GP)	4.0	2.6 – 6.6	17.5 – 13.5	Dense poorly sorted alluvial gravels and cobbles	
Glacial Till (CI)	2.5	6.6 – 9.1	13.5 – 11.0	Stiff boulder clay of intermediate plasticity	
Tetragraptus Beds (Shale)	Not proven	> 9.1	< 11.0		

Notes:

*strata inferred from description and correlation with geological maps, summary log soil classifications in brackets, e.g. (CH);
^descriptions from Factual Report (Tarmac Construction Limited. Geotechnical Division, circa 1972 (exact date not provided))

AOD = above Ordnance Datum

FIGURE 2

Cross section B-B (central reserve location) from as-built general arrangement with superimposed BH64 (BGS exploratory hole reference: SN31NW20) summary log (note: scale is approximate)

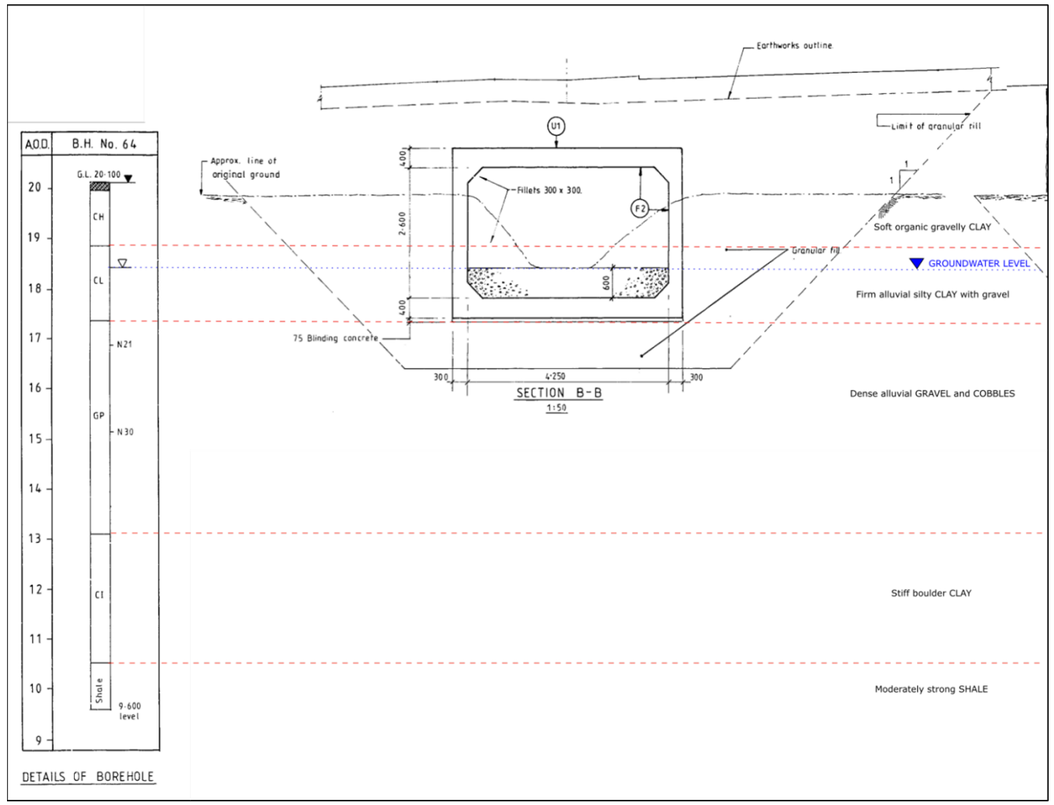

Groundwater was encountered in all three historic exploratory holes available from the BGS (British Geological Survey, n.d.). Groundwater was typically encountered at a shallow depth of between ground level and 2.45m bgl (20.1m and 16.95m above Ordnance Datum [AOD]). Reference to the as-built drawings shows that the base of the culvert is located at 17.55m AOD with carriageway level at 21.25m AOD, and this highlights that groundwater was anticipated close to the base of the culvert. Evidence from BGS exploratory hole SN31NW20 (identified as "BH64" from historical factual report (Tarmac Construction Limited. Geotechnical Division, circa 1972 (exact date not provided))) at the location of the culvert identifies seepages at 1.5m bgl and a more significant groundwater strike at 5m bgl (15.1m AOD), which quickly rose to ground level (20.1m AOD). Interpretation of the borehole log shows that the significant groundwater strike was encountered in material interpreted to be River Terrace Deposits.

Based on the aforementioned information, the primary cause was considered to be due to the presence and ongoing settlement of compressible material (alluvium) beneath the culvert. No settlement monitoring data was available to constrain or predict the likely remaining magnitude and duration to the practical completion of settlement. It is also possible that the cracking provides a conduit for water to enter the formation, which could lead to softening or washout of material supporting the structure.

3.2. GROUND INVESTIGATIONS AND THE ENGINEERING GEOLOGICAL GROUND MODEL

A Ground investigation (GI) was carried out in accordance with BS EN 1997-2 in order to determine the ground and groundwater conditions of the strata underlying the highway and associated earthworks.

The investigation commenced with a Ground Penetrating Radar (GPR) survey to mark out the extents of the culvert and identify buried services. Five boreholes were then carried out from carriageway level by a combination of rotary core drilling and dynamic windowless sampling to approximately 15m bgl. Standard Penetration Testing (SPT) was undertaken in all boreholes. The aim was to ensure one borehole location per running lane spanning the width of the culvert and targeting the location of the main crack within the culvert structure (lane 2 eastbound and central reserve areas). A Flood Risk Activity Permit (FRAP) was required for the boreholes as they were within 8m of a designated Main River. A groundwater monitoring standpipe was installed in BH01 and fitted with a data logger. A magnet extensometer was installed in BH04 to monitor settlement at different depths. Inclinometer casing was selected for the access tube of the extensometer in order to allow for future monitoring of lateral movement if required / desired. Sampling of materials, groundwater, and surface water was used for geoenvironmental and geotechnical laboratory testing.

The interpreted engineering geological ground model is presented as a cross section along the length of the culvert (Figure 3).

FIGURE 3

Engineering geological ground model cross section A-A (along culvert length)

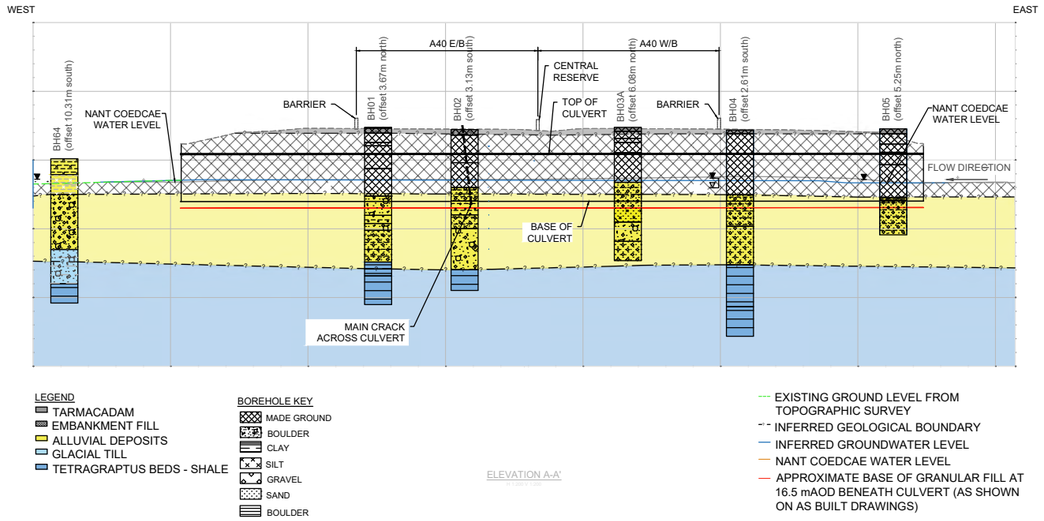

3.3. GEOTECHNICAL MONITORING

Groundwater was struck in two of the exploratory holes, BH04 and BH05, at depths of 4.20m bgl and 3.68m bgl, respectively. Groundwater was likely to have been encountered in all boreholes. However, due to the addition of water to aid drilling, it was difficult to identify a groundwater strike in every borehole during the investigation.

Groundwater data collected up to 11 January 2022 is plotted on Figure 4 along with groundwater strikes during the GI. Also plotted for comparison are the Nant y Coedcae river levels recorded during the topographic survey on 14 April 2021, the rainfall records from the nearest gauge at Tavernspite (16 km southwest), and the level of the River Cynin at St Clears (5.7 km southwest). The data suggest that the groundwater level is comparable to the Nant y Coedcae river levels and that both are responsive to rainfall. The high rainfall recorded in May 2021 corresponds to periods when Natural Resources Wales (NRW) flood warnings were issued and therefore may represent a period when groundwater and river levels are close to their highest known levels. Over the monitoring period, the groundwater level was between approximately 2.5m and 3.8m bgl (19.88m and 18.58m AOD) and be within the Embankment Fill. Rainfall (Tavernspite) and river levels (River Cynin) up to 6 March 2022 have been included. Groundwater monitoring data has yet to be retrieved for the period 11 January to 6 March 2022. It is anticipated that the same relationship shown between rainfall and river levels will be recorded in the groundwater levels at BH01.

FIGURE 4

Groundwater monitoring plot showing nearest river levels and rainfall volumes

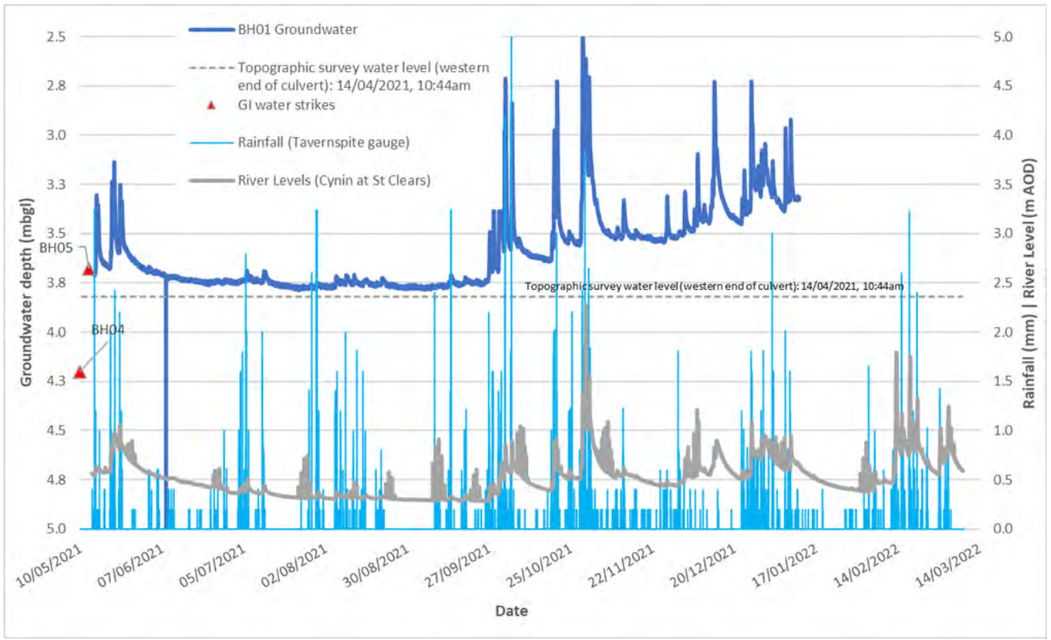

Magnet extensometer monitoring data are plotted in Figure 5. After the initial settlement recorded between installation and the first monitoring visit, only minor changes are recorded in three of the four magnets. However, at Magnet 3, cumulative settlement of 190mm was recorded over a period of 10 months. The initial changes recorded between the installation and first return visit are believed to be a result of the grout around the extensometer tube setting or minor grout loss before hardening. For Magnet 3, very little change was identified between installation and the September visit. However, significant changes were measured in the subsequent three monitoring visits in November 2021, January 2022, and March 2022. Magnet 3 is positioned 2.3m bgl at approximately the centre of the Embankment Fill layer (including pavement construction). The groundwater levels over the same period were all below the level of Magnet 3. The top of the culvert was approximately 1.5 to 1.7m bgl and the base of the culvert was approximately 5.3m bgl. Extensometer data constrains the settlement to be predominantly within the Embankment Fill.

FIGURE 5

Extensometer monitoring plot with groundwater monitoring data from BH01 (up to most recent date of data collection)

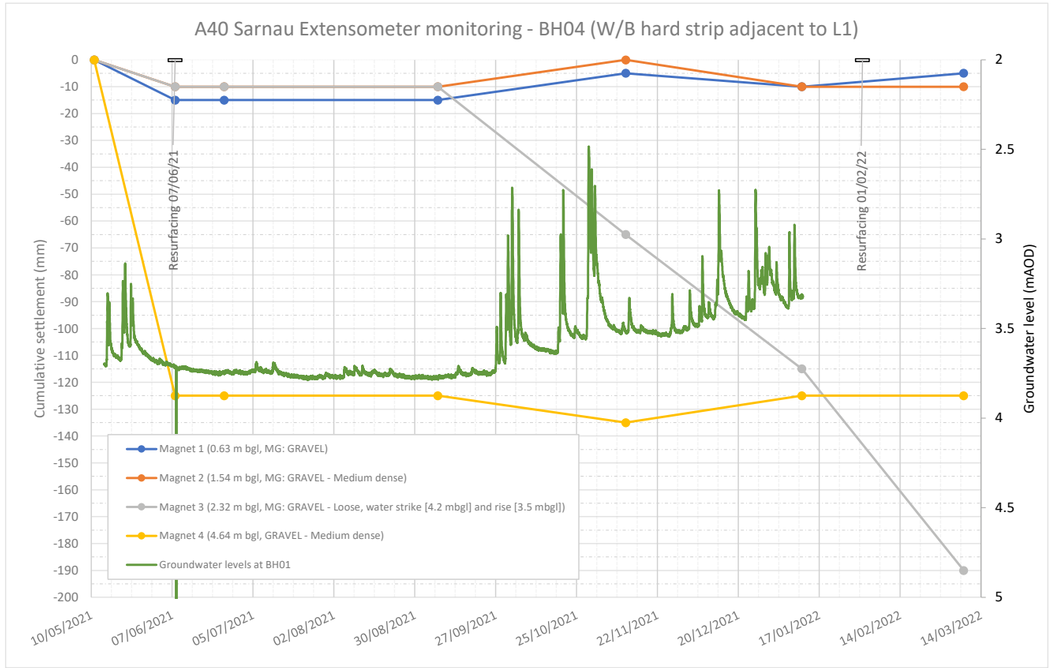

4. Interpretation of the Failure Mechanism

Following the desk-based review, the primary cause of the subsidence was believed to be due to the presence and ongoing settlement of compressible material (alluvium) beneath the culvert. The GI, however, did not identify a significant quantity of compressible material in any of the boreholes with between 0.60m and 1.05m of clayey silt or clay (alluvium) encountered in BH01, BH02, BH03A, and BH05. Two SPTs were wholly within this stratum and the blow counts (N-values) were recorded as 23 (BH02, 5.2m bgl) and 33 (BH03A, 6.0m bgl) with consistency described as stiff and empirically derived undrained shear strength values in the range 45 to 75 kPa. Natural moisture content for the stratum were also below the plastic limit, which is indicative of an over-consolidated soil. It should be noted that none of the boreholes were advanced through the base of the culvert and were instead positioned as close as possible to the outside wall. This was considered necessary, amongst other reasons, due to the steel reinforcement within the culvert structure.

The principal soil type for all other natural ground above the mudstone bedrock was granular (sand, gravel, cobbles). However, the ground conditions, particularly around the groundwater level, led to poor sample recovery. Therefore, inferences and assumptions have been made when deriving the ground model. Cohesive alluvial deposits were encountered in four of the exploratory holes between 4.20m bgl and 6.40m bgl (15.98 – 18.06m AOD) with recorded thicknesses of 0.60m to 1.05m). The material was described as stiff dark grey silty clay. The mass of sample recovered was insufficient for laboratory plasticity testing. However, due to poor recovery near to the groundwater level, it is likely that the material is of low plasticity. Saturated, low plasticity cohesive soils are considered difficult to recover using dynamic sampling geotechnical drilling methods. In addition, historical exploratory hole SN31NW20 (also referred to as BH64) identified similar material described as firm alluvial silty clay of low plasticity with gravel between 18.95m and 17.50m AOD (~3m to 4.5m below existing carriageway level). The cohesive alluvium encountered is located between the base of the granular fill and approximately 2m below the excavation used to create the culvert formation. This suggests that the failure mechanism causing subsidence is not linked to consolidation settlement / material compressibility.

The base of the Embankment Fill was recorded in the boreholes to be at between 4m and 5m below carriageway level. The as-built General Arrangement and Details drawing suggests that the natural ground beneath and on either side of the culvert was replaced with approximately 1m of granular fill (assumed to be the same as with Embankment Fill).

This would be approximately equivalent to an elevation of 16.5m AOD (5.7 to 5.9m below carriageway level). The base of the Embankment Fill recorded in the GI appears broadly consistent with the as-built records when considering the offset of the borehole locations from the centreline of the culvert and the 1V:1H indicative angle of the granular fill around the culvert.

4.1. SUFFOSION

The process of suffosion is believed to explain the failure mechanism within the underlying soils and would account for the observed subsidence of the culvert (as indicated by defects such as dips in the carriageway surface). Fannin and Slangen (2014) state that "seepage-induced internal instability is a phenomenon whereby fine particles are transported from a non-plastic soil. A distinction can readily be made between a washed-out soil structure that remains intact and one in which some form of destruction or collapse of the structure accompanies the migration of fine particles. The three variables of a measured value of mass loss, a measured value of volume change and a value of change in hydraulic conductivity (deduced from measurements of hydraulic gradient and flow rate), are sufficient to quantify, and hence distinguish between, seepage-induced internal instability phenomena. The term suffusion is advocated to describe the non-destructive response, which may be quantified by a mass loss, no change in volume and an increase in hydraulic conductivity. The term suffosion is recommended to describe the instability phenomenon whereby the transport of fine particles by seepage flow is accompanied by a collapse of the soil structure."

Soils that have undergone or are undergoing suffosion are expected, therefore, to have lower densities than the surrounding ground. As the process is progressive, the distribution of lower density zones is unlikely to be uniform or predictable even in a relatively homogeneous material. Changes in seepage forces, and consequently the rate of suffosion, are therefore allied to groundwater and / or river levels. In this instance, subsidence of the culvert and carriageway above could result from a change (reduction) in volume of the supporting granular material (predominantly Embankment Fill, but also the upper granular alluvium) caused by suffosion, which could be expected to occur once groundwater levels have normalised following peak periods (i.e., high groundwater and / or surface water levels). High groundwater and surface water levels would be expected to follow periods of heavy and / or prolonged rainfall.

Reviewing the ground model with the above in mind, it is possible to identify a horizon of lower density material within the granular Embankment Fill that is within ±0.4m of the groundwater levels recorded in both the historic GI (1972) and the current GI (2021). A suggested "active zone of suffosion" is shown on Figure 6, which has been based on the interpreted ground model, measured groundwater levels, and the suffosion process as described above. Although there is a well-defined horizon of lower density material within the Embankment Fill, the zone of suffosion is shown extending into the Alluvium (Figure 6). There are two reasons for this: 1) some SPT N values (labelled on the figure) within the granular Alluvium are lower than values above and below within the same borehole, and 2) Embankment Fill is shown beneath the culvert on the as-built General Arrangement and Details drawing (ref. B501AC) and this material would be expected to be vulnerable to the same processes.

FIGURE 6

Suggested zone of suffosion based on SPT N values, groundwater levels, and the engineering geological ground model

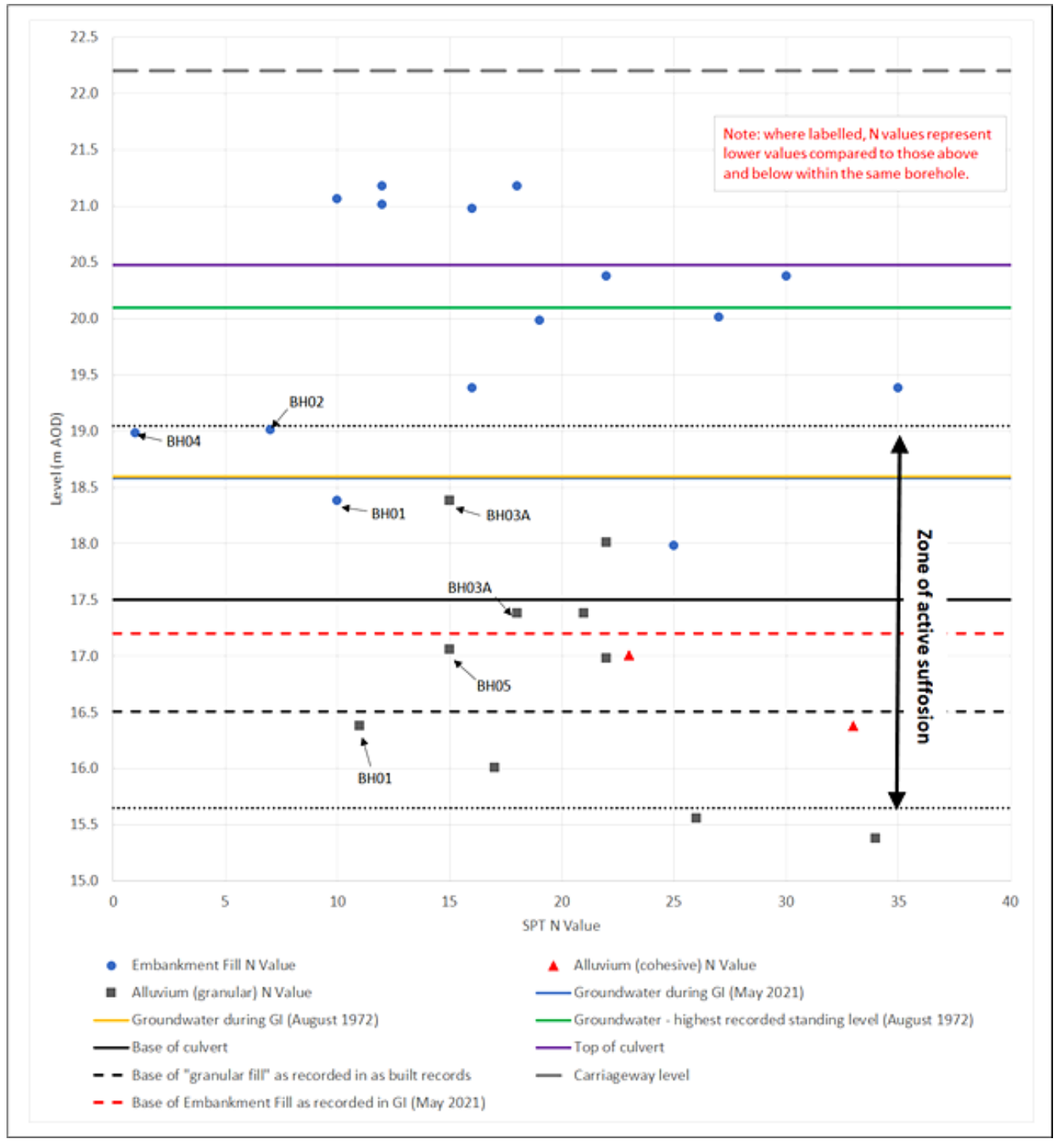

In support of the conclusion that suffosion is the failure mechanism, the ongoing extensometer monitoring has identified approximately 180mm of subsidence in the material between 2.3 and 4.6m below carriageway level between September 2021 and March 2022. This subsidence occurs following large changes in groundwater levels supporting the idea of seepage-induced washout of fine particles within the principally granular material. Ongoing monitoring has been recommended to further validate the interpreted failure mechanism.

5. Recommendations

The evidence gathered thus far has highlighted a link between periods of high river levels (and corresponding groundwater levels) and carriageway subsidence. The interpreted failure mechanism, defined as suffosion, provides a theoretical basis for connecting the two observed phenomena, and therefore identification of a solution(s) to avoid similar occurrences on other projects would need to achieve one of the following outcomes:

1. Lowering groundwater levels below the structural fill surrounding a culvert.
2. Eliminate / reduce washout of fine particles within the structural fill surrounding a culvert.
3. Support to the carriageway across a watercourse.

Outcome 1 above is technically and practically difficult to achieve. Outcome 3 would be resolved by the use of a bridge/structure to span the watercourse, but costs are likely to make this option unrealistic. Outcome 2 could be achieved by specifying fill types that are not susceptible to washout of fines, i.e., a material with less than 5% fines and where internal stability of the material is reliant on particle to particle contact such as Class 6A fill as defined in the Manual of Contract Documents for Highway Works, Volume 1 Specification for Highway Works: Series 600 Earthworks.

Where a carriageway above an existing culvert is showing signs of subsidence, but the end of structural design life of the culvert has not been deemed to have been reached, the use of monitoring should be considered to enable efficient programming of maintenance work. This study highlights the benefits of using automated remote monitoring to ensure targeted intervention for maintenance in order to extend the service life of existing assets.

Acknowledgements

To the SNC-Lavalin Inc. SWTRA team involved in the project, specifically Josh Hyde, Elizabeth Simmonds, Jon Robinson and Rich Morris.

To SWTRA and Welsh Government, specifically Hywel Davies and Iain McKenzie.

References

› British Geological Survey. (n.d.). GeoIndex. (British Geological Survey) Retrieved 2020, from http://mapapps2.bgs.ac.uk/geoindex/home.html

› Fannin, R. J., & Slangen, P. (2014). On the distinct phenomena of suffusion and suffosion. Géotechnique Letters, 4(4), 289-294.

› South Wales Trunk Road Agent. (2014). A40 850 - Nant-y-Coedcae Culvert, Principal Inspection Report.

› South Wales Trunk Road Agent. (2020). A40 Sarnau Culvert Bancyfelin Subsidence, Preliminary Sources Study Report.

› Tarmac Construction Limited. Geotechnical Division. (circa 1972 (exact date not provided)). London - Fishguard Trunk Road (A40); Carmarthen - St. Clears Improvement; Soil Survey - Factual Report (HAGDMS report ref. 3630).

SNC·LAVALIN

snclavalin.com

Contact Information
Dorothy Gartner
Librarian, Knowledge Management
dorothy.gartner@snclavalin.com